

Aus der Lasermikroskopischen Division, Institut für Mikroskopische
Anatomie/Anatomie II der Medizinischen Fakultät
Friedrich-Schiller Universität Jena

**Multiphotonen-Mikroskopie und Laser-
Nanochirurgie der Kornea mittels Naher-Infrarot
Nanojoule Femtosekunden Laserpulse**

Dissertation

Zur Erlangung des akademischen Grades

Doctor medicinae (Dr. Med.)

Vorgelegt dem Rat der Medizinischen Fakultät der Friedrich Schiller Universität Jena

Von

Bao-Gui Wang

geboren am 12 März, 1973, in Shan Dong, China



**Friedrich-Schiller Universität Jena
2006**

Dekan der Medizinischen Fakultät: **Prof. Dr. med. habil. Heinrich Sauer**

Vorsitzende der Promotionskommission: **PD Dr. habil. Frank Richter**

Wissenschaftliche Betreuung:

1. Prof. Dr. med. habil. Karl-Jürgen Halbhuber

2. Prof. Dr. rer. nat. habil. Karsten König

Gutachter:

1. PD Dr. rer. nat. habil. Dietrich Schweitzer

2. Prof. Dr. med. Dr. med. habil. Chris P. Lohmann

Datum der Promotion (Disputation): 04 Juli, 2006

Dedicated to

My parents
My wife Shuping

Introduction

1. History and advances in laser refractive surgery

The era of laser refractive surgery with the excimer laser was heralded by the United States' Food and Drug Administration's approval (FDA) in 1995. Since then, other advances in refractive surgery have spurred great public interest and enthusiasm. Actually, surgical correction for myopia has been attempted for almost 100 years (Waring *et al.* 1996).

Among the four basic types of visual error including myopia (nearsightedness), hyperopia (farsightedness), presbyopia (probable loss of elasticity of the lens with aging), and astigmatism (induced by irregular oval-shaped cornea or lens or both), all but presbyopia respond well to the laser surgical correction. As more and more patients are drawn to the idea of surgical correction of visual error, it is here necessary to appreciate the benefits and risks involved in each procedure firstly in this work.

1.1 Radial keratotomy (RK)

Between the late 1970s and begin of the 1990s, the most popular procedure for vision correction was radial keratotomy involving in making deep incisions in cornea with mechanical blade (Fig.1). It corrects myopia by flattening the central cornea and also corrects astigmatism by making the cornea more regular. Long-term follow-up studies show that radial keratotomy is not a suitable procedure for patients with high degrees of myopia and astigmatism.

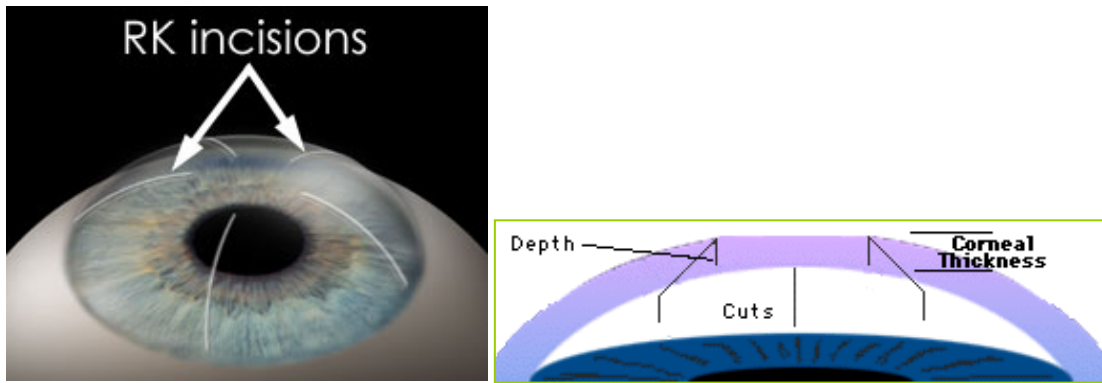


Fig.1 Diagrams illustrating radial keratotomy (RK). **Left:** RK incisions performed with mechanical blade; **Right:** Demonstration of the deep RK-cuts (www.eyemdlink.com).

Advantages of RK: satisfied results in low degree of myopia; the least expensive.

Disadvantages: weakened cornea; unpredictable results (high rate of re-operation up to 30%); regression; hyperopic shift*; fluctuation of vision and sensitivity to glare (Waring *et al.* 1985 and Grimmer *et al.* 1996). The facts that the cornea is seriously weakened and continues to change shape with time, are the major detriments to recommending the standard RK. Lasers have been used to make these cuts in procedure of RK but with little improvement in results (http://www.pacificyecare.com/eyecare/prk_qa.htm#RK).

*Most people who had radial keratotomy (RK) surgery gradually become more farsighted for at least 8 to 10 years after surgery. This is called the hyperopic shift. It is not yet clear what causes the shift, how long it may continue, or how significant it may become.

1.2 Excimer laser-assisted photorefractive keratectomy (PRK)

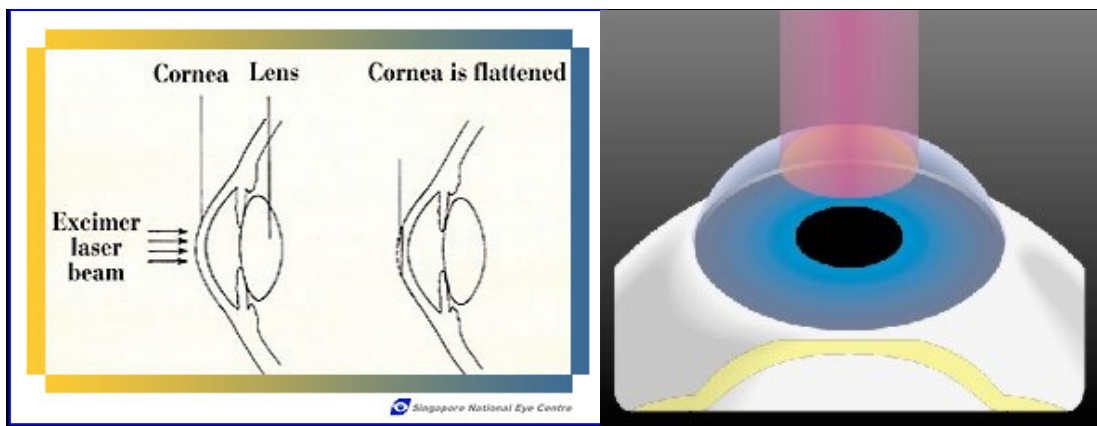


Fig.2 Diagrams illustrating PRK. In this procedure, the epithelium, Bowman's layer and ventral part of stroma are ablated by laser pulses (www.snec.com.sg/).

With the advent of the excimer laser, photorefractive keratectomy (Fig.2) became one of the most popular refractive procedures in the middle 1990s and almost replaced RK for visual correction completely since then. Excimer stands for “excited dimer”. The first excimer laser to have received Food and Drug Administration (FDA) approval for

treatment of myopia and astigmatism (up to about 12 D of myopia and 4 D of astigmatism) were made by Summit Technology, Massachusetts, and VISX, California (Bowman *et al.* 1997).

The excimer laser uses light in the ultraviolet spectrum at 193 nm (UVC) to ablate the entire corneal tissue including epithelium, Bowman's membrane and ventral part of stroma, and thereby to reshape and flatten the central cornea (Fig.2). Its interaction is primarily photochemical and non-thermal. The advantage of this laser is that it dissipates a minimum amount of heat, thus limiting coagulative tissue damages. The laser beams are driven by computer-controlling and each pulse of the laser removes approximately 0.25 micrometers of tissue (Munnerlyn *et al.* 1988)

Advantages of PRK: It does not involve deep cuts into cornea and therefore does not weaken the treated cornea; Good results for low and moderate myopia and astigmatism; Less re-operation than with RK; Less hyperopic shift and regression than with RK; Less intraocular infection (non-contact operation) (Talley *et al.* 1994 and Bowman *et al.* 1997).

Disadvantages: A big disadvantage of PRK is elimination of Bowman's layer. It is well known that this layer of human cornea is non-regeneratable after impairment and plays a big role in maintaining the stability and curvature of human cornea. Disturbance of Bowman's layer may lead to increased incidence of corneal haze and scarring. In a few patients, especially those with high degrees of myopia, decreased visual acuity has been reported. In addition, PRK has longer recovery time and more postoperative discomfort than LASIK due to epithelial abrasion. Other complications including halos and ghost images, decentred ablation, and elevated intraocular pressure have been also recorded (Pallikaris *et al.* 1994 and El-Agha *et al.* 2000).

1.3 Laser epithelial keratomileusis (LASEK) and Epi-LASIK

LASEK (Fig.3) is a relatively new procedure that is technically a variation of PRK. This procedure is used mostly for people with corneas which are too thin or too flat for LASIK. This method was pioneered by Italian surgeon, Massimo Camellin in 1999.

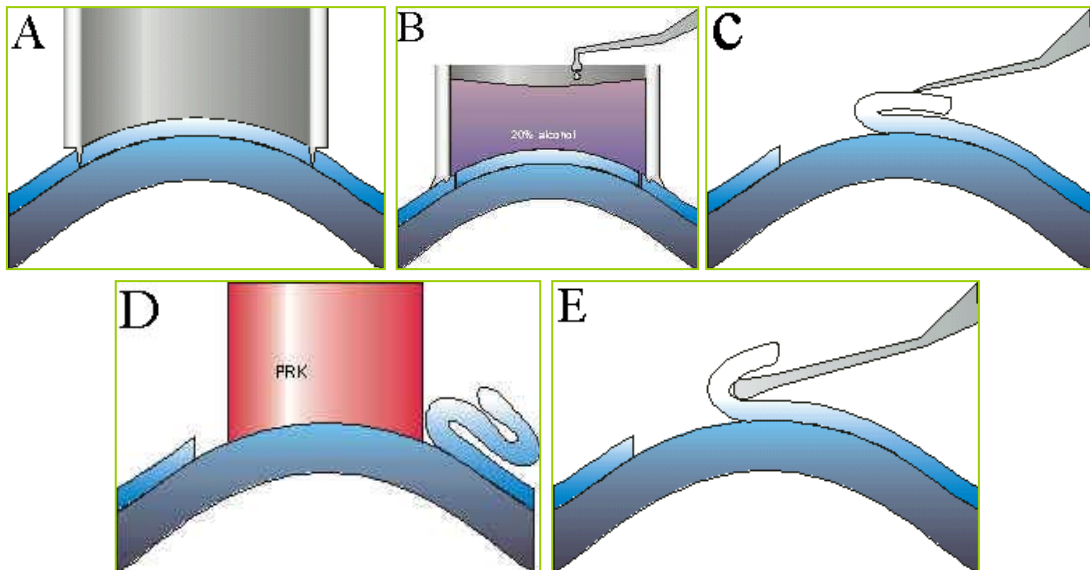


Fig.3 Procedures of LASEK. **A.** Epithelial incision with trephine; **B.** Epithelial immersion with alcohol solution; **C.** Epithelial lifting with a hoe; **D.** Corneal ablation with excimer lasers; **E.** Put-back of epithelial flap (www.augenklinik-mri.de).

In term of the procedure, the epithelium is cut not with the microkeratome, which is used as cutting tool in LASIK, but with a finer blade called a trephine in the first step of LASEK (Fig.3). Thereafter, the eye is covered with diluted alcohol solution (approximately one part alcohol and four parts sterile water) for around 30 seconds. The solution loosens the edges of the epithelium from Bowman's membrane. After sponging the alcohol solution, a tiny hoe is used to lift the edge of the epithelial flap and to gently fold it back out of the way for laser ablation. Then an excimer laser is employed, with the same procedure as in LASIK, to ablate the underlying corneal tissue (only Bowman's membrane and stromal tissue). Finally, the epithelial flap is repositioned again with a kind of spatula.

Advantages: Epithelium is not ablated in LASEK. Visual recovery after LASEK is generally faster than in PRK but slower than in LASIK.

■ **Epi-LASIK:** an improved procedure of LASEK.

The epithelial flap of Epi-LASIK (Fig.4) created only with a special Epi-LASIK-keratome need no assistance of alcohol solution.

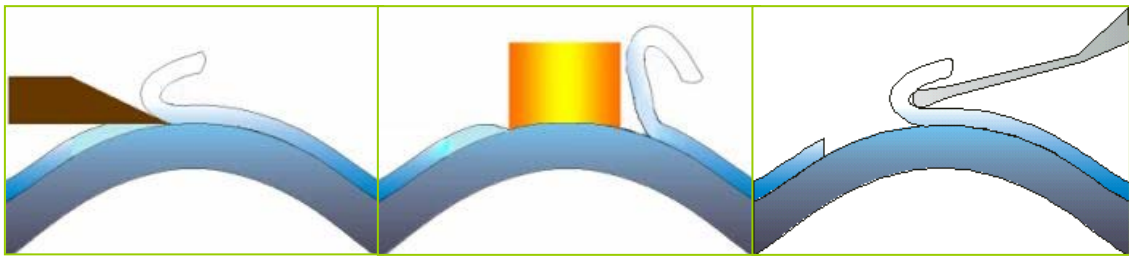


Fig.4 Procedures of Epi-LASIK performed in the Eye Clinic Rechts der Isar of TU Munich (operation supervisor: Professor Chris P. Lohmann in Eye Clinic Rechts der Isar). **Left:** Generation of epithelial flap with a special LASEK-keratome; **Middle:** Laser ablation; **Right:** Replacing of epi-flap (www.augenklinik-mri.de).

The flap generated with the special keratome comprising only epithelium has been evidenced by histological cross-sections (Fig.4_1L). Fig.4_2R shows the laser-ablated corneal bed in Epi-LASIK.

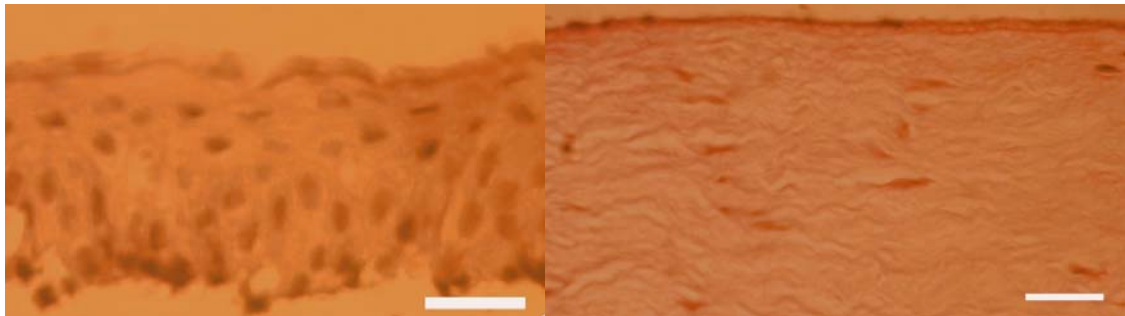


Fig.4_1 Histological sections of Epi-LASIK. **Left,** Cross section of epithelial flap generated with porcine eye in-vitro (the upper side was the surface of cornea); **Right,** Laser-ablated stromal bed in Epi-LASIK. Scale bar: 20 μ m.

Advantages of Epi-LASIK: Avoidance of cellular toxicity by alcohol solution.

Disadvantage: Elimination of Bowman's layer.

1.4 Laser-Assisted in-Situ Keratomileusis (LASIK)

The LASIK procedure introduced 2 year later than PRK, overcoming some of PRK's disadvantages, has now overtaken PRK and become the number one laser eye refractive surgery. Keratomileusis is derived from the Greek words *keratos*, meaning cornea, and *mileusis*, meaning carving. LASIK combines carving of cornea with ablation of stroma by excimer laser without elimination of epithelium and Bowman's layer. It involves using a microkeratome (Fig.5_1) to create a corneal flap (thickness less than 200 μ m), including epithelium, Bowman's layer and anterior part of stroma (Fig.5). This flap, which is left hinged at one side, is then lifted and placed aside with the epithelium side

down. The corneal stroma is thereafter ablated with excimer laser. Finally, the corneal flap is folded back in place again.

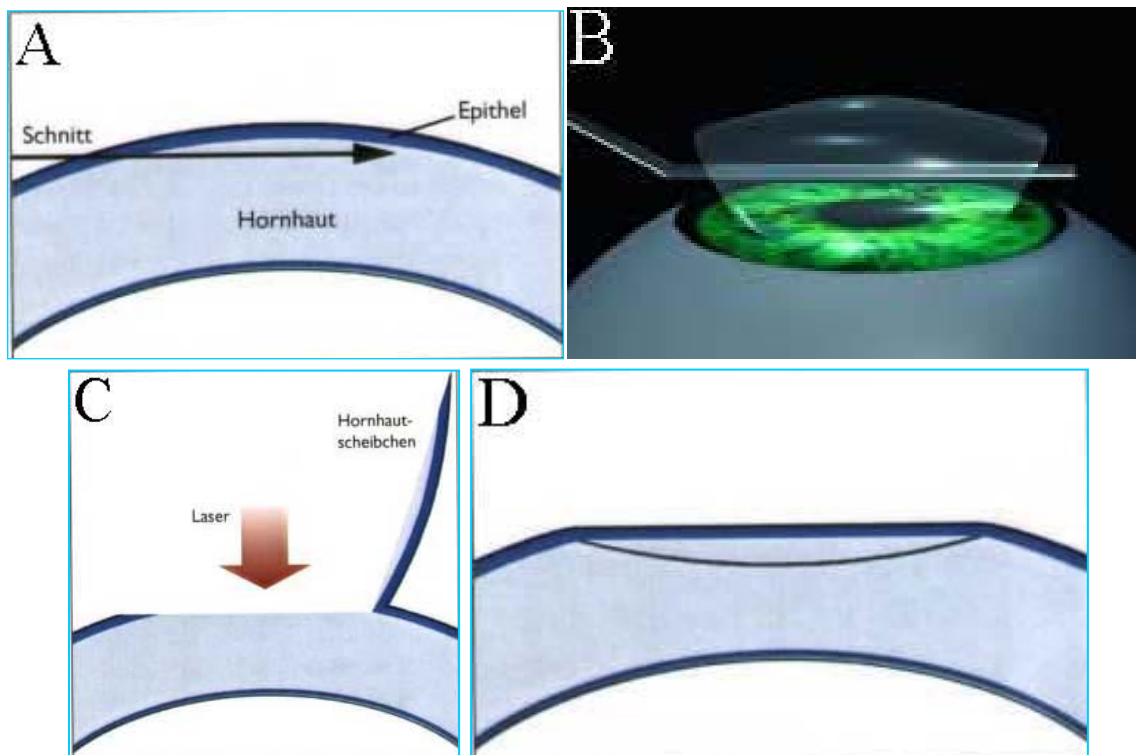


Fig.5 Procedures of LASIK. **A:** Flap generation with mechanical microkeratome; **B:** Flap-lifting; **C:** Laser ablation; **D:** Repositioning of flap (www.allaboutvision.com/visionsurgery).

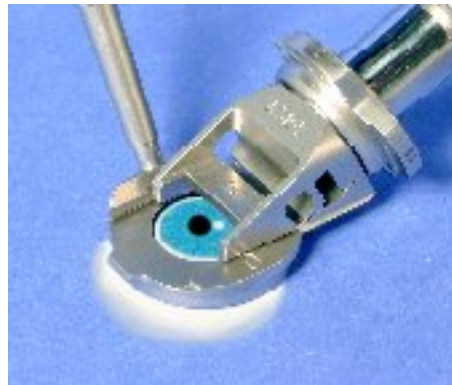


Fig.5_1 Photograph of microkeratome used for mechanical flap generation in LASIK. (www.allaboutvision.com/visionsurgery).

Advantages of LASIK: This procedure circumvents the need to abrade the epithelium and thus prevents the postoperative corneal lesion associated with photorefractive keratectomy (PRK). Hence, vision is recovered quickly with little postoperative pain and a low risk for corneal haze and scarring owing to maintaining Bowman's layer. Results in patients with severe myopia tend to be better with LASIK than with other

previous procedures. Based on the aforementioned advantages, LASIK is now being used not only to treat myopia but also hyperopia.

Disadvantages: Predominant complications are associated with using the mechanical microkeratome. These are rarely serious but may limit vision (Carr *et al.* 1997). For the traditional microkeratome, achieved flap thickness is affected by the used particular head, plate or blade. It might be also influenced by the turbine velocity and translation speed, even the experiences of surgeon and patients factors. Thereby, the flap thickness has relatively large deviations. The complications of flap deviations: (i) Flaps that are too thick increase the potential for a residual bed thickness less than 250 μ m, rising compromise of corneal biomechanical strength, which is relevant with the development of corneal ectasia postoperation (Seiler *et al.* 1998); (ii) Attempts to create thin flaps pose an increased risk of complications such as buttonholes, which cause the feeble vision in the evening. Furthermore, thin flaps may be prone to irregular flap (folds, wrinkles, stria and washing-board, Fig.5_2) that can affect the visual quality (Davidorf *et al.* 1998 and Kezirian *et al.* 2004).

Other complications include diffuse lamellar keratitis, ingrowths of corneal epithelium underneath the flap, microbial keratitis, stromal interface deposits with possible inflammation ("Sands of Sahara" syndrome), and wound margin ulceration.

In addition, photothermal and photochemical damages to the adjacent tissue by UV light were well known. That UV irradiation used for corneal ablation in LASIK can induce cell damage and mutation was reported (Glazer *et al.* 1986, Tyrell *et al.* 1990, and Koenig *et al.* 1996).



Fig.5_2 Flap-related complications: the generated flap with mechanical microkeratome is non-smooth and appears to be like a washing board (www.allaboutvision.com/visionsurgery).

1.5 Femto-LASIK (IntraLase)

In this new procedure, Flap is generated with femtosecond amplified lasers (kHz, microjoule pulse energy, infrared) instead of mechanical microkeratome (Fig.6). The fs-laser pulses focus on a typical depth of 150-200 μ m in cornea to create corneal flap whereas the epithelium and Bowman's membrane keep intact before flap-lifting. The stromal ablation is done thereafter as conventional LASIK with excimer lasers.

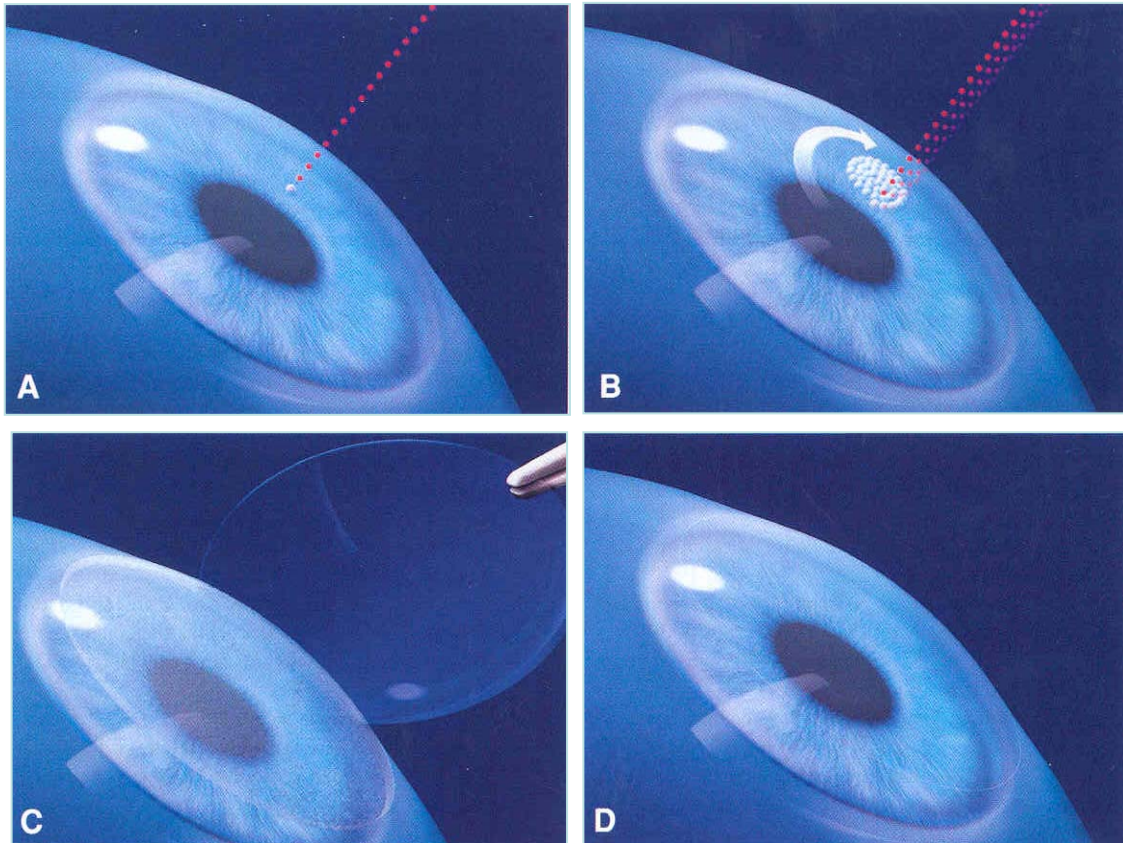


Fig.6 Procedures of Femto-LASIK. **A** and **B**: Flap creation with femtosecond microjoule lasers (kHz, amplified pulse energy, and infrared); **C**: Flap-lifting and stromal ablation with excimer lasers; **D**: Repositioning of flap (www.intralase.com).

More than 200,000 Femto-LASIK operations on patients have been performed since permission of this procedure by FDA in 2001 (Tran *et al.* 2005). This equipment is now produced only by IntraLase, US (www.intralase.com).

Advantages of Femto-LASIK: predictable flap thickness with high precision. The IntraLase laser is over 100 times more accurate than microkeratome for flap generation (Wang M. *et al.* 2003 and Binder *et al.* 2004). In contrast to flap generated with mechanical assistance, the corneal flap is more homogenous (Fig.6_1, have a same thickness from flap centre to periphery). Three to four times more patients achieved

20/16 or better vision by IntraLase in comparison with LASIK with microkeratome (Manger *et al.* 2004 and Durrie *et al.* 2005). In addition, easy-operating and non-contact flap generation were other merits (Kezirian *et al.* 2004). Micrographic comparison of flap thickness-homogeneity from centre to periphery with mechanical microkeratome, femtosecond high pulse energy lasers displayed the more regular, homogenous cornea flap without stria and washing-board (www.femto-lasik-pro.com, Kezirian *et al.* 2004).

Disadvantages: however, this technique is challenged by its intrinsic disadvantages of flap-related complications such as interface microfoldings by flap-repositioning and innervation deficiency in flap (Vesaluoma *et al.* 2000). The number of subbasal and stromal nerve fibre bundles in flap decreases up to 90% immediately after operation. By one year postoperation, the number of nerve fibres still remains less than half of that before operation (Lee *et al.* 2002). The insufficiency of nerve fibres has been confirmed as one of the reasons for the apoptosis of keratocytes (Linna *et al.* 2000). Moreover, decreased corneal sensation can result in stromal ulceration and corneal perforation. UV effects on corneal cells and tissue should not be underestimated in this procedure.

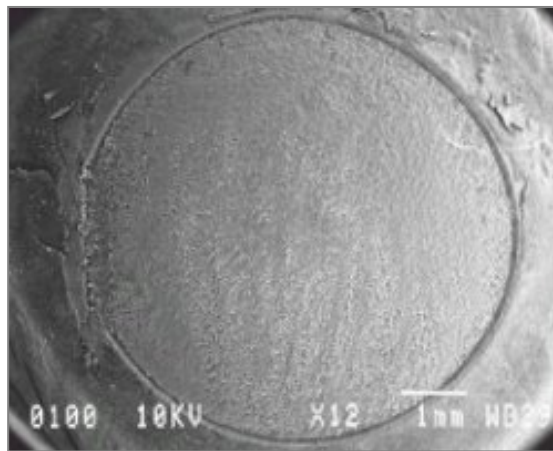


Fig.6_1 Smooth flap bed generated with femtosecond high pulse energy lasers (Kurtz *et al.* 1998).

1.6 New approaches being just under investigations

1.6.1 All-Femto-LASIK: the corneal flap and intrastromal lenticule are generated by one step only with a same femtosecond amplified laser (at an order of microjoule pulse energy) (Fig.7). The in-vitro and in-vivo studies with animals have been performed but there is still no clinic application by now (Kurtz *et al.* 1998, Lubatschowski *et al.* 2000 and Heisterkamp *et al.* 2003).

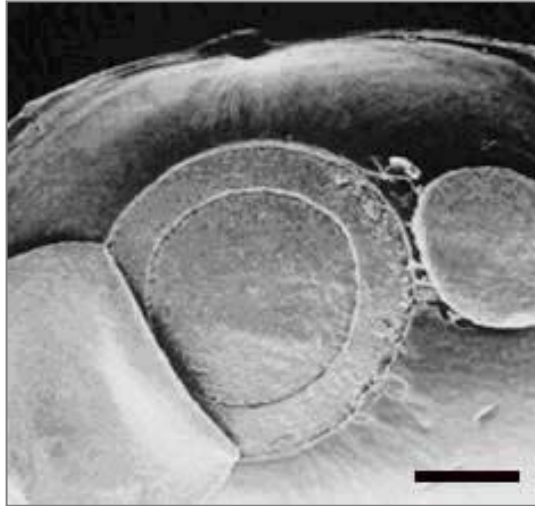


Fig.7 All-Femto-LASIK with infrared, microjoule pulse energy, kHz, ultrashort lasers. The intrastromal lenticule was generated before the flap-lifting. Scale bar: 2.5mm (Kurtz *et al.* 1998, Lubatschowski *et al.* 2000 and Heisterkamp *et al.* 2003).

1.6.2 Flap and stromal lenticule generation by the femtosecond lasers with lower pulse energy at an order of nanojoule (thesis of this work).

1.6.3 Intrastromal ablation with epithelium intact is being tested for laser refractive surgery with animals (thesis of this work).

In addition, intracorneal rings that can be inserted into cornea were also reported to correct myopia (Schanzlin *et al.* 1997). Intraocular lenses are being investigated for patients with extreme myopia or hyperopia.

Exciting advances in refractive surgery have made it a viable option for many patients who want an alternative to eyeglasses or contact lenses. Currently, laser refractive surgery is considered as a very safe and effective procedure to correct vision.

2. Histology of cornea (New Zealand Albino rabbits)

The reasons why the New Zealand Albino rabbits were chosen as experimental animals in this study: **(i)** the previous studies on laser interaction in cornea were performed only with this species, and so that the results in this study can be analysed in comparison with these of other lasers (Kurtz *et al.* 1998, Lubatschowski *et al.* 2000, and Heisterkamp *et al.* 2003); **(ii)** rabbit has big cornea ($11.88 \pm 2.69\text{mm}$, linear distance

from one point on limbus to the other through middle point) so that big flap can be generated; **(iii)** stabile species with high reproducible capability.

2.1 Description of cornea histology

The rabbit cornea comprises epithelium, stroma, Descemet's layer and endothelium (Fig.8_1 and Fig.8_2). Bowman's layer is deficient in this animal (Gipson *et al.* 1987, Wilson *et al.* 2000, and Wang *et al.* 2005).

2.1.1 Epithelium

Three sublayers (Fig.8_2): **(i)** 3-4 layers of superficial, flat squamous cells (epithelial surface cells); **(ii)** 2-3 wing-shaped polygonal cells (wing cells); **(iii)** single layer of columnar basal cells (epithelial basal cells).

Features: **(i)** the surface of the squamous cells is not absolutely smooth but contains myriad projections in the form of finger-like microvilli and ridge-like microplacae that may help stabilize the tear film; **(ii)** two types of intercellular junctions among squamous cells: desmosom (macula adhaerens) and zonula occludens (tight junctions) that encircle the cells. Fluid, electrolytes and metabolites can not pass through the barrier. Oxygen, however, can diffuse across this barrier easily. The tear film is the major source of oxygen for the cornea. This oxygen must diffuse across the epithelium, through the stroma, and then reach the endothelium, even probably also a contribution to the organs in eye chamber located posterior of cornea by way of the aqueous humour; **(iii)** the stem cells located near the limbus are thought to be responsible for regeneration of the epithelial basal cells; **(iv)** the epithelium turns over round once a week in physiological state; **(v)** the ion transport function of epithelium: the active Na^+ transport from tear to stroma with Na^+/K^+ ATPase and active Cl^- transport from stroma to tears with the β -adrenergic receptor/adenylate cyclase complex (Kuwabara *et al.* 1978, Rowsey *et al.* 1981, Edelhause *et al.* 1982, and Waring *et al.* 1982).



Fig.8_1 Imitated diagram of histological cross-section of rabbit cornea stained with HE showing the histological four layers. **a**, epithelium; **b**, basement membrane; **c**, stroma; **d**, Descemet's layer; **e**, endothelium (www.lab.anhb.uwa.edu.au, modified by I.Lemke).

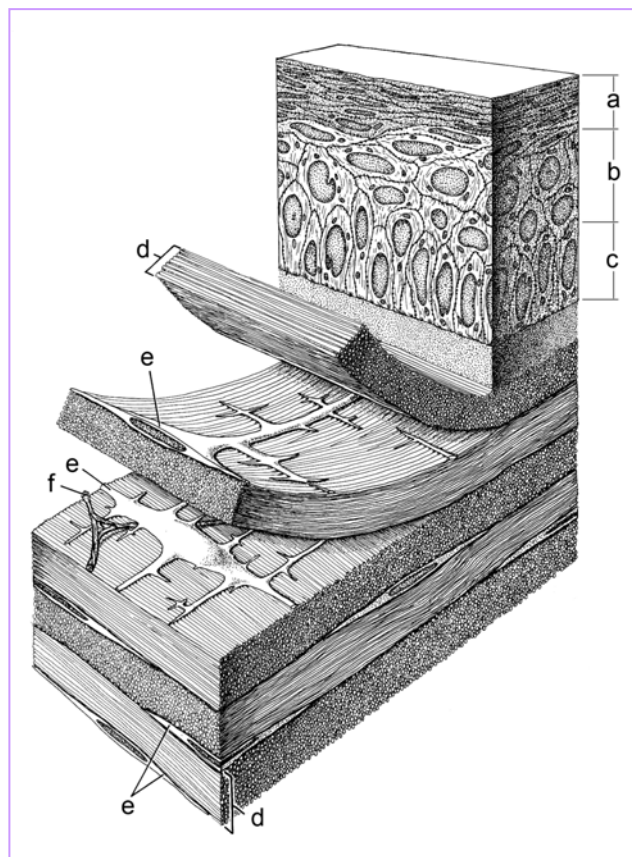


Fig.8_2 Three-dimensional illustration of corneal components. **a**, epithelial squamous cells; **b**, wing cells; **c**, epithelial basal cells; **d**, collagen lamellas; **e**, stromal keratocytes; **f**, nerve fibres (Sandler *et al.* 1974, modified by I.Lemke).

2.1.2 Bowman's layer

The lamina limitans anterior (Bowman's layer) is deficient (Gipson *et al.* 1987, Wilson *et al.* 2000, and Wang *et al.* 2005) in this animal and the basal cells of epithelium connect with the basement membrane which connects to the upperside of the substantia propria (stroma).

2.1.3 Stroma: comprising stromal cells and ECM (collagens and amorphous substance)

(i) Cells in stroma of physiological status:

Keratocyte (Fig.8_2 and Fig.8_3) is the predominant cell responsible for maintaining the integrity and regeneration of corneal components (mean volume measured with multiphoton optical tomography: in the chapter of results), a flat cell sandwiched between the collagen lamellas and extends five to seven cell processes out to adjacent keratocytes for signal communications and exchange of nutritive substance. Corneal keratocytes are connected by gap junctions through cell processes. This cell in physiological state is not phagocytic and thereby cytoplasmic lysosom is normally rare, although intracellular particles of lipid and debris occasionally appear. Under stress such as laser-treatment, the cells can transform into myofibroblasts in the area around the corneal wound, and secret the new ECM that ultimately reconstitutes the components of cornea and factors inducing cascades of wound repair (Moller-Pedersen *et al.* 2000, Watsky *et al.* 2000, Funderburgh *et al.* 2001, and Berryhill *et al.* 2002).

Other cellular components include the phagocytic histiocytes being normally present in the stroma lying flattened between the collagen lamellas like the keratocytes and probably serving as the main phagocytic cell in the non-stimulating cornea. The presence of lysosomes distinguishes them from the keratocytes.

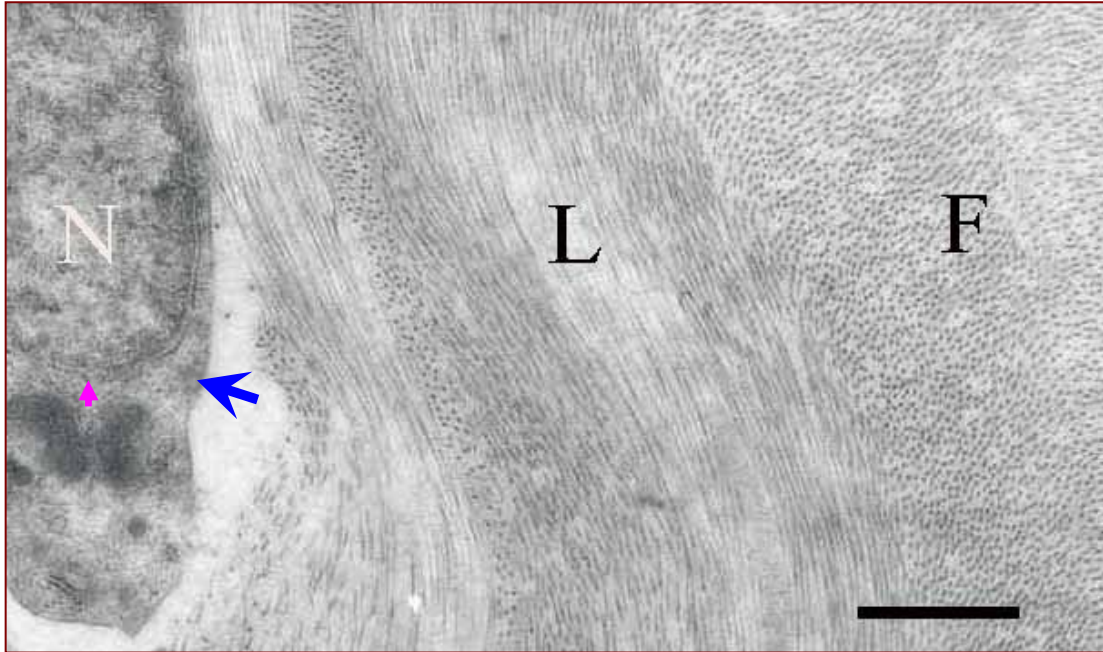


Fig.8_3 TEM of corneal stroma depicting the microscopic topography between keratocyte (blue arrow) and collagen lamellas (L and F). **F**: cross-section of collagen lamellas (F, fibrils) and **L**: long-section.

The microscopic topography between cellular component and ECM in stroma is displayed with ultrahigh resolution by electron microscopic graph (Fig.8_3). In details, the following points can be obtained through this image: **(i)** Keratocytes are tissue fibroblast-like cells sandwiched in corneal stroma; **(ii)** Large irregular nucleus (N), nuclear membrane (red arrow), the cytoplasmatic organelles such as mitochondria, peroxisomes and lipid particles can be identified within this cell; **(iii)** The uniform collagen fibrils varying from 20nm to 32 nm in diameter (F), arranged in order of lamellas. Lamellas have different orientations in the two-dimensional plane. Bar: 500nm.

(ii) Collagen in stroma

The collagen fibrils consist of units of tropocollagen, each containing three protein chains wound together in a helical pattern (Fig.9). The tropocollagen units are assembled into microfibrils and then the microfibrils are cross-linked to form the collagen fibrils. The collagen fibrils can be clearly identified on TEM (Fig.8_3) but the microfibrils can not. With ultrahigh spatial resolution more than 100 000 times, the regular stripe with period length of 65nm on collagen fibril can be observed. The three-

dimensional displaying of tropocollagen is basis for better understanding of mechanism of second harmonic generation (SHG).

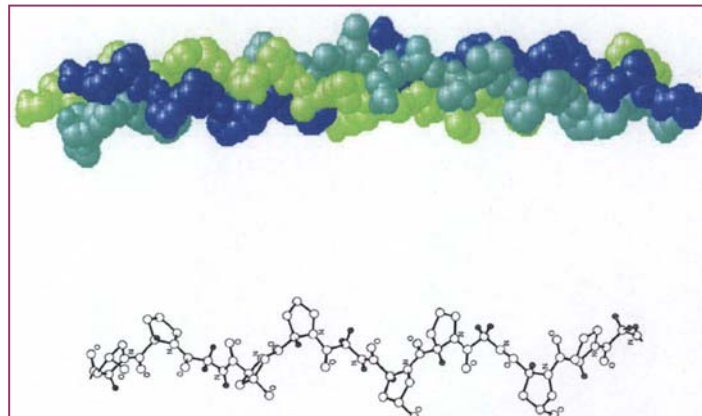


Fig.9 Diagram depicting noncentrosymmetric collagen structure inducing SHG under high light intensity. **Upper:** Tropocollagen and cross-linking of three protein chains; **Lower:** Details of a protein chain (www.indstate.edu/thcme/mwking/extracellularmatrix.html).

The corneal stroma contains different types of collagen, each differentiated from the biochemical composition of the three protein chains. The predominant collagen in normal cornea is type I and VI; type IV is characteristic of basement membranes; type VII constitutes the anchoring fibrils of epithelium, and type III is becoming much more prominent during wound healing. Some other types such collagen XI and XVIII not existing in the physiological state of cornea appear however only during wound reparative phase (Light *et al.* 1979, Tseng *et al.* 1982, Nakayasu *et al.* 1986, Zimmermann *et al.* 1986, and Kato *et al.* 2003).

(iii) Amorphous substance in stroma

Two glycosaminoglycans are present in the normal corneal stroma: keratan sulfate, which involves both galactose and glucosamine, and dermatan sulfate (also called chondroitin sulfate B), which contains both galactosamine and glucuronate. These two proteoglycans are attached to different protein cores. The two glycosaminoglycans make great contributions to maintaining the transparency of cornea (2.3). Glycoprotein is also present in cornea and may aid in communication between cells. The regeneration and repair of amorphous substance takes place in the stromal cells (Meyer *et al.* 1953, Conrad *et al.* 1970, Dawson *et al.* 2005, and Zhang *et al.* 2005).

2.1.4 Descemet's layer

This layer is the normal basement membrane of endothelial cells and forms the scaffolding on which the endothelial cells spread themselves (Fig.8_1). The predominant Descemet's membrane-associated collagen is type IV. Normal adult Descemet's layer has two morphologic components observed by TEM, including an anterior portion of approximately 3 μ m and a posterior homogeneous non-banded layer with thickness of 10-12 μ m thickening with aging. The whole layer was only 3 μ m at birth and becomes thicker when a posterior, homogeneous sublayer is added throughout life (Labermeier *et al.* 1983, Sawada *et al.* 1990, and Danielsen *et al.* 2004).

Function of Descemet's layer: **(i)** scaffolding for endothelium; **(ii)** remarkable tensile strength; **(iii)** keeping the balance of corneal hydration.

2.1.5 Endothelium

The cells are arranged in a continuous monolayer with an average of 4 to 6 μ m thick, 8-11 μ m (human, histological results) in diameter of hexagonal contour and with a uniformity of paving-stone mosaic pattern (Fig.8_1 and Fig.8_2).

The morphologic health of endothelial cells can be approximately judged by the following parameters: **(i)** cell density, normally 2000-3000 cells/mm². Lower density can affect the endothelial function; **(ii)** the percentage of hexagonal cells: the greater the proportion of hexagonal cells is, the better-state the endothelium has. Normal percentages of hexagonal cells are 60-75%. In fact, a cornea can be remained in physiological state only with as few as 300 to 500 endothelial cells/mm² (Laule *et al.* 1978 and Rahi *et al.* 1981).

Function: maintaining stromal hydration and dehydration balance through a passive semi-permeable barrier supported by endothelial integrity and a kind of active ATP-dependent enzyme (Na⁺ /K⁺-ATPase) located in the lateral plasma membrane of endothelial cells that catalyze the movement of ions from stroma to aqueous humour, creating an osmotic gradient that draws water out of the stroma. Hence, endothelial cells are essential for keeping the cornea transparent (Dikstein *et al.* 1972, Van Horn *et al.* 1977, and Waring *et al.* 1982). Thereby, it is necessary to monitor the laser-effect on the endothelial cells during the corneal refractive laser surgery

■ **Speciality:** endothelial cells in rabbits are capable of extensive mitosis. In contrast, by humans and primates, endothelial cells possess minimal or no capacity to replicate by mitosis, therefore the endothelial wound repair largely depends on enlargement and sliding of surrounding cells to cover the wounded site (Van Horn *et al.* 1975, Waring *et al.* 1982, Doughty *et al.* 1990, Moller-Pedersen *et al.* 1997, and Mimura *et al.* 2005).

2.2 Corneal innervations

Innervations are one of the most important factors which are responsible for keeping corneal physiological state and for postoperative corneal wound healing. The deficiencies of nerves result in the apoptosis of keratocytes (Wilson *et al.* 1998). Decreased corneal sensation caused by denervation can have a result of stromal ulceration and perforation. Moreover, normal corneal innervations are important for normal physiology (nutritive regulation, balance of hydration and dehydration) and transparency-maintaining of cornea. Evidence suggests that loss of sensory neuron leads to a severe depletion of acetylcholine (neurotransmitter present in cornea), resulting in a decrease in epithelial cell growth (Linna *et al.* 1998 and Vesaluoma *et al.* 2000).

Generally, cornea has two major nerve stems (Fig.10): **(i)** sensory innervations from trigeminal ganglion, reaching cornea through ophthalmic nerve, dominantly serving for corneal sensitivity; **(ii)** autonomic sympathetic innervations from superior cervical ganglion, entering into eye globes along artery. Toivanen and Mueller suggest that sympathetic nerves are present in adult cornea by histochemical evidences and have specific physiologic roles, especially for nutritive regulation, balancing of hydration and dehydration by exciting state (Toivanen *et al.* 1987). However, in terms of quantity, the number of corneal sensory axons is greater than that of sympathetic axons.

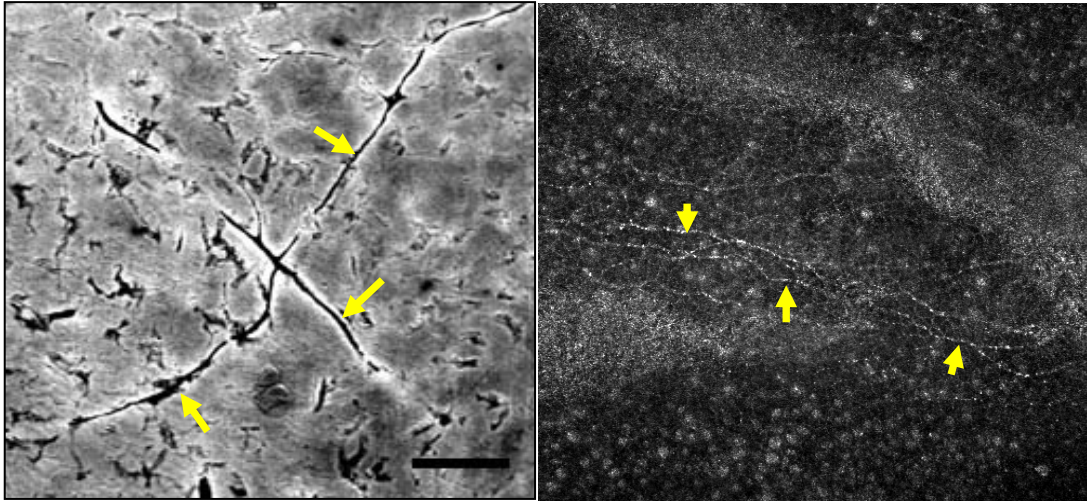


Fig.10 Nerve fibres displayed with conventional gold chloride-staining in corneal stroma (**Left**) and optical imaging in subepithelial layers (**Right**). The keratocytes were also displayed by the non-selective staining of gold chloride on the left image. Arrows show the nerve fibres. Scale bar: 20 μ m.

With the assistance of optical tomography, the nerve distributions can be followed (Fig.10R). Based on Rozsa and Oliverira (Rozsa *et al.* 1982 and Oliverira-Soto *et al.* 2001), the pathway of cornea nerves can be described as following: after penetrating the limbus, the nerve bundles lose their myelin sheaths in the anterior third of the stroma, then dividing dichotomously or trichotomously, finally losing their Schwann's cell sheet. Then, they bend to form the subbasal nerve plexus under the basal membrane and the basal epithelial cells and form the nerve terminal endings between the epithelial cells. The pores in the basal membrane with diameters of 0.5 to 1 μ m may represent the path of the nerves as they enter the epithelium.

2.3 Factors maintaining corneal transparency

2.3.1 Collagen fibrils and lamellas

Uniform of collagen fibrils and regular array of collagen lamellas play an important role in maintaining corneal transparency.

If the distance of two structures is less than half of light wavelength, then the light will pass its way through the structures with minimal scattering. The diameter of corneal collagen microfibrils varies from 20nm to 32nm and the distance is from 30nm to 60nm, which are far less than half of wavelength of visible light; therefore the scattering is minimal during the light penetration in cornea. One can conceptualize this by considering that the light wave has a limit to their resolution, they can not detect variations that are less than half of their wavelengths. This means that light makes their

way through the normal cornea and is unable to detect small variations in the index of refraction that are present between the collagen microfibrils, between collagen fibril and keratocytes, and between the neighbouring layers. Thereby, the regular architecture of collagen fibrils and lamellas play a great role in the corneal transparency. As mentioned in the corneal histology, the EM displays that the collagen fibrils are of uniform diameter and held apart by a fixed distance and are stacked in orderly sheets that form approximately 200 lamellas paralleling to the cornea surface. The factors responsible for maintaining the uniform spacing of collagen fibrils are the proteoglycans, also referred to as acid mucopolysaccharides in the extracellular matrix (ECM). The glycosaminoglycans are negatively charged and lie between the collagen microfibrils. The repulsive forces within the molecules may be responsible for maintaining this regular structure (Maurice *et al.* 1957, and Goldman *et al.* 1967 and 1968).

2.3.2 Stromal hydration

The normal corneal stroma contains approximately 78% water in weight. The stroma imbibes water naturally owing to two forces. **(i)** The glycosaminoglycans exert an osmotic pressure called the swelling pressure (60 mmHg, hypertonicity of stroma) that pulls water into the stroma from aqueous chamber; **(ii)** The intraocular pressure forces aqueous humour into the stroma (Maurice *et al.* 1957 and Goldman *et al.* 1968).

2.3.3 Function of endothelium

Endothelium serves as an indispensable factor in maintaining corneal hydration and dehydration balance. The endothelium counteracts this hydrophilic tendency by two mechanisms named pump-leak model. **(i)** Passive barrier functions: endothelial integrity is crucial in maintaining stromal dehydration state. The establishment of a semi-permeable barrier between endothelial cells keeps most of the aqueous humour out of the cornea. However, some of the aqueous humour is allowed to diffuse into the cornea with its essential nutrients through the leaky intercellular junctions. Mechanical or chemical damages can affect this function. **(ii)** The active removal of water from corneal stroma through a sodium-potassium, adenosine triphosphatase (ATPase)-bicarbonate pump located in the lateral plasma membrane of the endothelial cells. These pumps remove electrolytes that osmotically carry water with them and therefore maintain stromal dehydration at a fixed level. Decreased endothelial cell number, lack of HCO_3^- and decreased temperature can affect this function. Disruption of either the passive

barrier or the active pump function allows excess hydration of the stroma, inducing stromal edema, thickening, and opacification. The swelling displaces the collagen microfibrils and macrofibrils, disturbing their regular alignment so that light is scattered and the stroma appears to be opaque (Van Horn *et al.* 1977 and Waring *et al.* 1982).

2.3.4 Other relevant factors:

(i) Tear film: the pre-ocular tear film became hypertonic to corneal stroma through evaporation. The hypertonicity has a normal function of osmotic drawing some water out of the stroma. This might be the reason why the patient with endothelial dystrophy has more serious stromal edema just after waking in the morning than in the afternoon (Maurice *et al.* 1957).

(ii) Epithelium: (a) Maintenance of a smooth optical surface, decreasing the light scattering. This can be confirmed with light penetrating rate. More than 90% light can penetrate through cornea from epithelial layer while only about 50% from endothelium. This data means that epithelium is more suitable for optical surface with less scattering than endothelium; (b) Mechanical barrier. Epithelial adhesion including tight junction are found to be located among the epithelial cells and hemi-desmosomes along the basal cell membranes, basal laminas and anchoring fibrils; (c) Chloride pump. The superficial squamous epithelial cells are not a mere passive barrier, since they also contain an active chloride pump that plays a role in corneal hydration-dehydration balance (Kuwabara *et al.* 1978, Rowsey *et al.* 1981, Edelhauser *et al.* 1982, and Waring *et al.* 1982).

(iii) Oxygen can also affect the corneal transparency. It is well known that hypoxia induces corneal turbidness (Maurice *et al.* 1957).

3. Mechanism and strategy of nanoprocessing in bulk tissue

Owing to its transparency and accessibility, and the absence of efficient cellular one-photon absorber and the low scattering coefficients, corneal tissue prefers to be applied as a prime experimental tissue for study on the infrared femtosecond laser-based diagnostics and therapeutics.

Nonlinear multiphoton absorption process has revolutionized the field of tissue-nanoprocessing (Koenig *et al.* 1999, Shen *et al.* 2001, Watanabe *et al.* 2004, and Wang *et al.* 2005d). Briefly, this nonlinear absorption process in cornea occurs when the electric field intensities reach at 10^{12} w/cm² and photon flux at 10^{24} photo/cm²s in the focal volume. Nonlinear ionization processes, predominantly multiphoton ionization and cascade ionization, lead to a drastic increase of free electrons density at a order of 10^{18} - 10^{20} cm⁻³ owing to overcoming the binding energy of electron in corneal component such as water and collagen, and then to the formation of luminescent plasma. Subsequently, cavitation bubbles accompanied by shock wave take place. The abrupt expansion of the cavitation bubbles causes a breakdown of the corneal tissue and thereby the cutting effect occurs (Koenig *et al.* 2002a and Arnold *et al.* 2005) (Fig.11).

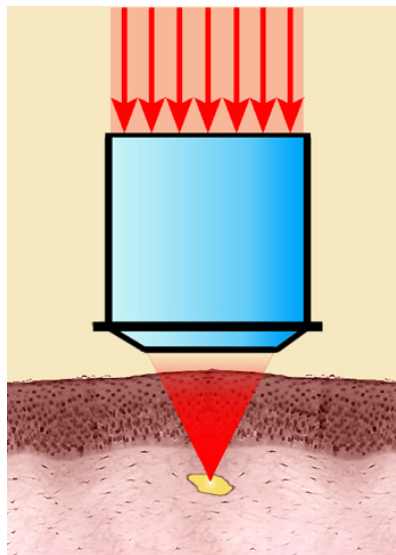


Fig.11 Schematic of intrastromal surgery induced by the nanojoule ultrashort laser pulses (Koenig, 2002).

Here, the process is analysed in details. At low light intensity, electrons of atoms and molecules can be raised to higher energy levels during linear absorption. Ionization occurs if the photon energy exceeds the binding energy E^* of the electron. With increasing light intensity, the simultaneous absorption of two or more photons (multiphoton absorption) becomes possible. If the sum of the energies of the n photons involved in this nonlinear absorption process exceeds E^* , multiphoton ionization occurs with a probability proportional to I^n . The free electrons induced by ionization act as seed electrons. They gain kinetic energy through photon absorption and then free

electron density at a order of of 10^{18} - 10^{20} cm^{-3} can be further created and subsequently the luminescent plasma occurs (Barnes *et al.* 1968, Bloembergen *et al.* 1974, Berns *et al.* 1981, Vogel *et al.* 1999, and Koenig *et al.* 2002a and 2002c).

In the case of water as the major component of most biological materials, energy of 6.5eV is required to provide quasi-free electrons (Grand *et al.* 1979). Using laser wavelength at 750nm to 850nm (about 1.4 eV / photon), the 6.5 eV energy gap can be overcome by a five-photon-process (Koenig *et al.* 2002a). Although water is considered as the major one-photon absorber in non-pigmented cells and tissues, non-resonant two-photon excitation and three photon excitation of biomolecules such as NAD(P)H (one photon absorption maximum at 340nm), flavins (450nm), cytochromes (400-450nm), porphyrins (400nm) and amino acids (260nm) may occur at femtosecond laser intensity of about $500\text{GW}/\text{cm}^2$ (Koenig *et al.* 2000). This was demonstrated by two-photon fluorescence microscopy in the case of fluorescent biomolecules (NADPH, flavins, protoporphyrin IX). Plasma-like luminescence with complex sub-nanosecond decay time and a spectral maximum around 500nm accompanied by destructive effects have been detected within living cells at about 0.9 - $1.6\text{TW}/\text{cm}^2$ laser intensity (80MHz, 130fs). The threshold or optical breakdown in mitochondria (location of two-photon absorber) is lower than in the nuclei (three-photon absorbers). It is inferred that selective ablation of material should be possible when working with power of slightly above the threshold for optical breakdown and plasma formation (Koenig 2002c).

The energy deposition by multiphoton-induced plasma within the bulk of material causes a rapid temperature increase and a rapid rise in the pressure (Gigapascal) of the plasmas followed by an explosive expansion. This leads to the formation of a shock wave and a cavitation bubble as well as jet formation. It is believed that in plasma-mediated ablation of tissue, the shock wave produce effects on a cellular and subcellular level whereas the longer lasting cavitation effects causes a tissue displacement on a macroscopic level (Vogel *et al.* 2001). These optomechanical effects are called photodisruption. They are used in the refractive ocular surgery and other therapeutical applications of ultrashort laser pulses. However, the photodisruptive effects by bubble dynamics are also the major reason of unwanted side effects such as tissue damages in the surroundings and laser cuts of low precision.

The destructive side effects can be avoided if the amount of pulse energy transferred into mechanical energy is reduced. Using the same focussing conditions, the required laser peak power for optical breakdown can be achieved with femtosecond laser pulses with less pulse energy compared to picosecond and nanosecond pulses. It was shown that the threshold value for optical breakdown in water is decreased by a factor of more than 100 when comparing 100fs with 3ns pulses accompanied with less transformation into destructive mechanical energy (Vogel *et al.* 1999). Kurtz reported that femtosecond pulses require only about one tenth energy of picosecond and nanosecond pulses to produce corneal disruption (Kurtz *et al.* 1998). Thereby, a highly precise processing of cells and tissue without collateral damage could be possible with femtosecond lasers of a light intensity near the threshold for optical breakdown and of pulse energy as low as possible. The further details on this point are described in 4.2/corneal surgery/introduction.

In addition, the nonlinear effects of the fs laser pulse during the propagation in the transparent materials are here summarized.

Normally, the propagation of light in the transparent materials is linear. A femtosecond laser pulse with only moderate energy can have an extremely high peak power ($P_{\text{peak}}=P_{\text{av}} \cdot T / \tau$) and peak intensity. When materials are subjected to these high powers and intensities, the interaction become highly nonlinear. For example, the index of refraction of the material becomes intensity dependent and infrared laser energy is absorbed in a normally transparent material, generating free electrons and plasma described above.

Nonlinear propagation of the fs laser pulses in the transparent materials includes: **(i)** Self-focussing: the refractive index is higher at the centre of the beam than at the wings. The spatial dependence on the laser intensity leads to a spatial dependence on the refractive index, forming a lens which focuses the pulse; **(ii)** Self-phase modulation is the temporal analogue of self-focusing. In self-focusing, the spatial intensity profile leads to a spatial refractive index profiles which, in turn, focuses the beams. In self-phase modulation, the temporal dependence of the intensity profile leads to a temporal dependence in the refractive index which, in turn, produce a time-dependent phase shift of the pulse; **(iii)** Self-steeping resulting from the phase velocity dependence on the

intensity variation. The intensity-dependent velocity causes the pulse envelopes; **(iv)** White-light continuum generation. When an ultrashort laser pulse with sufficient power is weakly (loosely) focused into a transparent material, it is transformed into a white-light pulse. The spectrum of the pulse broadens dramatically (from UV-VIS-IR). The mechanism for generating continuum remains largely unknown and misunderstood (Baldwin *et al.* 1974, Shen *et al.* 1984, Butcher *et al.* 1990, Walther *et al.* 1993, Yeh *et al.* 1993, and Bloembergen *et al.* 1996).

The nonlinear effects can be avoided by the tightly focusing of objective with high N.A and the nanojoule femtosecond pulses (Koenig *et al.* 2002a), thereby they are not considered in analysis of the results in this work.

4. Application of femtosecond lasers in biomedical fields

4.1 Diagnostics: Multiphoton microscopy

Multiphoton microscopy based on simultaneous absorption of two or more photons is one of the most exciting recent developments in biomedical imaging (Denk *et al.* 1990, Brakenhoff *et al.* 1996, Cheng *et al.* 1998, Diaspro *et al.* 2002, Zoumi *et al.* 2002, and Halhuber *et al.* 2003). By contrast, the conventional light microscopy utilized in life science includes 2D fluorescence microscopy using discrete incident lights of high pressure mercury lamps and 3D confocal laser scanning fluorescence microscopy with incident radiation of He/Ne lasers, argon/krypton ion lasers, He/Cd lasers and laser diodes (Greulich *et al.* 1992, Halhuber *et al.* 2002, and Krieg *et al.* 2003). Multiphoton microscopy was not commonly known until Goeppert-Meyer who predicted the possibility of simultaneous absorption of two photons in 1931 in her dissertation (Goeppert-Meyer 1931). This technique became popular and met with the interests of biomedical scientists after the introduction of lasers. The first two-photon excitation of electronic states was realized for blue fluorescence of $\text{CaF}_2: \text{Eu}^{2+}$ crystals based on the availability of lasers in 1961 (Kaiser *et al.* 1961). Since Denk's publication in 1990 (Denk *et al.* 1990) and contributions made by Webb's Group from Cornell University in 90's year and the commercialization of this multiphoton technology by Bio-Rad laboratories, the capabilities of the multiphoton imaging technique have been extensively reported (So *et al.* 1995, Masters *et al.* 1998, Koenig *et al.* 2000, and Zipfel

et al. 2003b). To date, tunable mode-locked Ti:sapphire lasers operating at 70-80MHz repetition rate and a pulse duration of less than 100fs are typically used as NIR sources in multiphoton microscopy (Schenke *et al.* 2004 and Koenig *et al.* 2005). The versatile capabilities of femtosecond lasers have advanced their role as integral to not only surgical procedures, but also tissue imaging processes (Masters *et al.* 1997, Koenig *et al.* 2001, and Zoumi *et al.* 2004). Compared with the conventional one-photon laser scanning microscopes, multiphoton imaging induced by high light intensity has distinguished advantages: no out-of-focus photo-bleaching takes place; no cellular and tissue staining or slicing are required; penetration through the biological bulk tissue increases in the NIR spectrum of 700-1200nm (Gu *et al.* 1995 and Huang *et al.* 2002). These advantages, along with 3D demonstrations based on the nonlinear optical tomography, have been employed as invaluable means for in-vivo nonlinear optical sectioning of leaf cells (Tirlapur *et al.* 1999) and human cutaneous cells (Koenig *et al.* 2003).

The corneal multiphoton imaging, including 2PF of corneal cells and SHG of stromal collagen, can only be visualized when the photon intensity reaches MW-GW/cm² as induced by the ultrashort laser pulses in a sub-femtoliter intrastromal focus volume obtained by diffraction-limited objectives (Fine *et al.* 1971, Campagnola *et al.* 2002, and Koenig *et al.* 2002c). The nonlinear optical imagings based on 2PF and SHG have been studied with multiphoton microscopy in this work.

4.1.1 Two-photon autofluorescence (2PF)

The NAD(P)H/NAD(P)⁺ in the cellular mitochondria is the predominant source of endogenous fluophore in corneal cells including epithelial cells, keratocytes and endothelial cells. Only the reduced form of NAD(P)H/NAD(P)⁺ is fluorescent and the NAD(P)H two-photon fluorescence can be easily observed at excitation wavelength of 740-780nm (Koenig 2000, Zipfel *et al.* 2003a and Larson *et al.* 2003). Based on the 2PF, the multiphoton imaging of elastin and elastic fibres can also be acquired. Elastin in rabbit aorta (tunica media) can be excited with maximum at incident wavelength of 800nm and has an emission spectrum maximum at 495nm with 2PF (Zoumi *et al.* 2004). In contrast, the optimal excitation of elastic fibres in native porcine heart leaflet with 2PF is located at 760nm wavelength (Schenke-Layland *et al.* 2004 and Koenig *et al.* 2005). Owing to the deficiency of elastin and elastic fibres in corneal tissue, the 2PF imaging in this work is considered to base on the cellular fluophore.

4.1.2 Second harmonic generation (SHG)

To date, SHG microscopy has become a standard method for non-destructive imaging of bulk specimens with submicron resolution (Zoumi *et al.* 2002, Stoller *et al.* 2002a, Zipfel *et al.* 2003b, and Dombek *et al.* 2003). This technique is an idea imaging method for vital tissue because the specimens are not required to be stained or sliced. Additionally, SHG possesses ability to produce imaging deeply in thick preparation.

SHG is a nonabsorbative scattering process in which two photons are coherently converted into a single photon of twice the energy occurring at a MW-GW/cm² light intensity. It enables direct imaging of anisotropic biological structures possessing large hyperpolarizabilities (Roth *et al.* 1979, Freund *et al.* 1986, and Stoller *et al.* 2002b). Of particular relevance to biological imaging are collagen, microtubules and myosin, all of which are tissue intrinsic and highly noncentrosymmetric molecular assemblies (Campagnola *et al.* 2002 and 2003). The collagen located in corneal ECM can be excited at wavelengths between 800nm and 860nm with the emission lights characterized by half of the incident light during the SHG (Freeman *et al.* 1978, Kim *et al.* 1999, and Moreaux *et al.* 2000).

Second harmonic was firstly observed in isotropic material such as glass (Franken *et al.* 1961), in nonlinear crystal (Kleinman *et al.* 1966 and Bloembergen *et al.* 1968). The study on the orientation of collagen in rat tails using SHG was thereafter extensively reported (Fine *et al.* 1971, Delfino *et al.* 1979, Roth *et al.* 1979, and Freund *et al.* 1986). Biological applications involve either intrinsic SHG from structural proteins such as collagen and cellulose (Brown *et al.* 2003b) or extrinsic SHG from membrane-staining styryl dyes (Campagnola *et al.* 1999, Moreaux *et al.* 2000, and Millard *et al.* 2004). Due to the interfacial specificity, SHG is also as an ideal approach to study on biophysics in model membrane and membrane physiology of living cells (Bouevitch *et al.* 1993, Ben-Oren *et al.* 1996, and Peleg *et al.* 1999). Brown performed SHG imaging of tumorous collagen and proposed this imaging could offer basic knowledge to estimate diffusive hindrance of molecular therapeutics (Brown *et al.* 2003a). Millard observed SHG during the wave of exocytosis after fertilization of eggs (Millard *et al.* 2004). With SHG imaging, the tube-like structure being responsible for the opaqueness and the elasticity of sclera has been as well confirmed (Han *et al.* 2005). Lin found the dependence of

SHG in rat tendon on different temperatures and that SHG signal decreases rapidly starting at 45°C (Lin *et al.* 2005). Owing to the simplicity of the SHG setting and high resolution, the application of SHG microscopy is rapidly increasing.

4.2 Corneal surgery

4.2.1 Intrastromal ablation with epithelial intact

With the rapidly growing popularity of laser refractive surgery such as LASIK and IntraLase, more than hundred thousands visual disorders such as myopia and astigmatism are currently being corrected every year (Statistics, www.allaboutvision.com). However, this technique is challenged by its intrinsic disadvantages of flap-related complications such as interface microfoldings and innervation deficiency in flap (Latvala *et al.* 1996 and Vesaluoma *et al.* 2000). In addition, the compromising viability of cells and biological tissue induced by UV irradiation used for corneal ablation in laser refractive surgery is well-known (Tyrell *et al.* 1990). Photo-thermal and photochemical damages to the cellular components by UV light were also reported (Koenig *et al.* 1996). Based on this background, we are exploring a novel approach to change the corneal refractive index without flap generation or UV Excimer lasers in this work.

Femtosecond laser pulses provide high peak intensities that reduce the energy threshold for tissue removal and enable laser surgery to be carried out with a low-energy source (Vogel *et al.* 2003). Previous studies confirmed that the amplified (at an order of μJ) fs lasers can induce surgical effects (Loesel *et al.* 1996, Kurtz *et al.* 1998, and Lubatschowski *et al.* 2000). Plasma generation of fs lasers has been shown to be effective (Fujimoto *et al.* 1985, Stern *et al.* 1989 and Vogel *et al.* 1999) and to induce ultra-precise knock-out of subcellular organelles (Stuart *et al.* 1996, Watanabe *et al.* 2004, and Shen *et al.* 2005). Nonamplified (at an order of nJ pulse energy) fs lasers characterized by high cut precision with maximum 5 μm -diameter intratissue bubbles (Koenig *et al.* 2002a) may offer novel methods in the field of refractive surgery. The finest cuts in human chromosomes with a FWHM of less than 70nm using the nanojoule ultrashort lasers were also reported before that (Koenig *et al.* 2001). The efficient non-resonant multiphoton absorption by nJ lasers might therefore provide the best opportunity to ablate bulk transparent materials such as corneal tissue.

Recently, perforations in cell membrane to transfer the foreign gene into cells and an ultra-precise ablation of cell wall with cut size less than 400nm by the nJ lasers were also demonstrated in our group (Tirlapur *et al.* 2002a and b). These results suggested that the plasma-mediated tissue ablation of nJ fs laser could be employed as a precise and effective surgical tool for instantaneous ablation of tissue and cellular components.

4.2.2 Multiphoton-mediated generation of corneal flap and intrastromal lenticule

It has been recently proved that the ultrashort lasers are the most convenient tools for high-precision cellular and tissue-processing in biomedical fields (Koenig *et al.* 1999, Berns *et al.* 2000, Shen *et al.* 2001, Watanabe *et al.* 2004, and Yanik *et al.* 2004) and microstructuring of solid targets (Krueger *et al.* 1996, Lenzner *et al.* 1998, Nolte *et al.* 1999, Schaffer *et al.* 2001 and 2003). In ophthalmology, laser refractive surgery to correct myopia, hyperopia and astigmatism is becoming the most commonly performed laser procedure. Since 2003, the non-mechanical LASIK (fs-LASIK, IntraLase) is as a new method in clinic to correct ametropia of human eye using near-infrared amplified (microjoule pulse energy) femtosecond lasers. The clinical studies on corneal flap generation using femtosecond microjoule laser pulses in fs-LASIK showed attractive surgical performance with minimal collateral effects in comparison with other laser eye surgery such as PRK, LASIK, LASEK (Kurtz *et al.* 1998, Juhasz *et al.* 1999, and Sugar *et al.* 2002). However, in fs-LASIK, the collateral effects of intratissue streaks due to using low N.A. and the microjoule femtosecond pulses extend up to 100 μ m far away from the surgical site in both directions towards the epithelium and endothelium. Moreover, the in-vivo study showed that the stromal streaks could be permanent, since they were still observable at 14th day after laser treatment and even without any wound-healing reaction noticeable (Heisterkamp *et al.* 2003).

Eye surgeons are always aiming at higher precision with laser refractive surgery. It was evidenced that optical breakdown could be acquired with a significant reduction in pulse energy when wave width decreased by using femtosecond laser pulses and therefore had a result of smaller shock waves and cavitation bubbles (Stern *et al.* 1989, Kurtz *et al.* 1997, and Vogel *et al.* 1999). Thereby, the nanojoule femtosecond lasers applied to perform surgery could have higher precision and less collateral effects than microjoule lasers. As aforementioned, a FWHM of less than 70nm cut in human chromosomes, perforations in cell membrane to transfer the foreign gene into cells and

an ultra-precise ablation of cell wall with cut size less than 400nm by the nanojoule lasers are recently just demonstrated in our Lasermicroscopy Research Group. Micromaching in bulk glass with high precision by use of nanojoule femtosecond lasers was also reported (Schaffer *et al.* 2001, Taylor *et al.* 2003, and Campbell *et al.* 2005). These results suggested that the multiphoton-mediated tissue-processing of nanojoule femtosecond lasers could be employed as a more precise and more effective surgical tool for flap generation. At these low pulse energies, we would also expect mechanical collateral effects to be significantly reduced due to decreased plasma expansion and shock waves.

Acknowledgments

I have had great fortune in my career and in my life to be advised by two great professors and to work with many colleagues who helped me with my dissertation in the Centre for Lasermicroscopy, Division of Institute of Anatomy/Anatomy II, Friedrich-Schiller University Jena, Germany.

Firstly, I would like to acknowledge Professor Dr. Karl-Jürgen Halbhuber for the opportunity to do my doctoral work in the Friedrich-Schiller University Jena and for his excellent mentoring during my work including research and teaching course. Prof. Halbhuber provided me a convenient work environment and has always been receptive to and supportive of my research ideas. I am very grateful to him for each step for publishing including careful viewing and editing manuscripts. The help with leasing of the slip lamp being indispensable equipment for the animal experiments was unforgettable. I would like to thank him for the critical discussions and suggestions on the preparation for thesis defence. In addition, he offered me an opportunity to teach the first and second year of medical students in the subject of histology and macroscopic anatomy.

I would like to thank Professor Dr. Karsten König for offering me the interesting doctoral thesis and for supplying the multiphoton microscopic experimental setup. He helped me with organisation of the animal investigations. He has always consulted me how the experiments should go further and help me with conquering difficulties occurring in the animal nanosurgical laser experiments. We have worked together to find out how to relocalize the intrastromal surgery postoperation. The Christmas Eve of year 2003 with the König's family in Jena was impressive.

I thank all of the members in the Centre for Lasermicroscopy, Institute of Anatomy II who gave me the feeling that I was one of them. I worked closely with some colleagues. Dr. Iris Riemann introduced me the laser microscope 310 and 410 at begin of this study. Her patient explanation provided me with a firm understanding from which all subsequent works developed. I felt very lucky to have collaborated with a great scientist Dr. Uday Tirlapur in spite of his unforgettable joke. I wish to thank Ursula Eschler, Helmut Hoerig, Michael Szabo, Sabine Hitschke, and Ursula Möller for their outstanding technical assistance and Dr. Richter and Ingemarie Herrmann for electron microscopy. The improvement of experimental images by Isa Lemke was very helpful. I will never forget her preparation of figures for the SPIE proceeding Bios during the two weeks before Christmas Eve 2004.

I thank Dr. Harald Schubert for the three-day animal experiment course in his Institute of Animal Experiment which was indispensable to the further *in-vivo* laser refractive surgery study. The support of his for the relocalization of intrastromal surgery was also very impressive. My thanks should also

give Sigrun Kirste, Petra Dobermann, and Dr. Thomas Müller for the generous supply of eye specimens and the outstanding cooperation in the animal experiments.

I knew Dr. Christof Donitzky and Christian Wüllner from WaveLight Company during the three-month internship of *in-vitro* and *in-vivo* corneal refractive surgery with amplified femtosecond lasers in JenLab Company. The work of Rainer Bückler's was very impressive. I thank Dr. Jens Kobow, Dr. Peter Fischer, and Pittasch for their friendly support for my research-stay in JenLab.

I thank DFG (Germany Research Foundation) for the support of the animal experiment (DFG, KO1361/10-3) and the meeting grants for Bios 2006 in the United States (WA 2158/2-1).

The experimental equipment slit lamp and Zeiss 510 was supplied by Zeiss Jena Company. I thank Dr. Joerg Lindenau for the introduction of microscopic operation and Dr. S. Fröber for the intermediation of slit lamp.

I thank Dr. Schweitzer and Dr. Hammer from Eye Clinic of University Jena for the outstanding support in the retina examination with Fundus Camera and OCT.

I thank Dr. M. Gliesing for his recommendation of Fig.8_2 in this work, Dr. R. Krieg and Dr. H. Oehring for their perfect support and helpful discussion during this work and Dr. A. Eitner for the complimentary experiments in Zeiss Company with porcine eyes.

I want to thank my previous colleagues, especially Professor Hai-Qian Su, from Institute of Anatomy, Capital University of Medical Sciences (Shunyi campus, Peking), China, for their lasting encouragement.

I had a study on the laser refractive surgery in Eye Clinic University of Regensburg. I thank Professor Dr. Chris P. Lohmann and Professor Dr. Veit-Peter Gabel for the permission and the illustrating discussion on part of this work. Andrea Huber was an outstanding assistant for my study in the laser eye processing.

Last but not least, I would like to thank my wife Shuping and my parents for their loving support and encouragement throughout my stay in Germany, and I hope I can count on more of the same in the future.

Appendix

1. Strategy of intratissue optical nanosurgery including flap-free non-invasive intrastromal ablation and multiphoton-mediated flap generation.

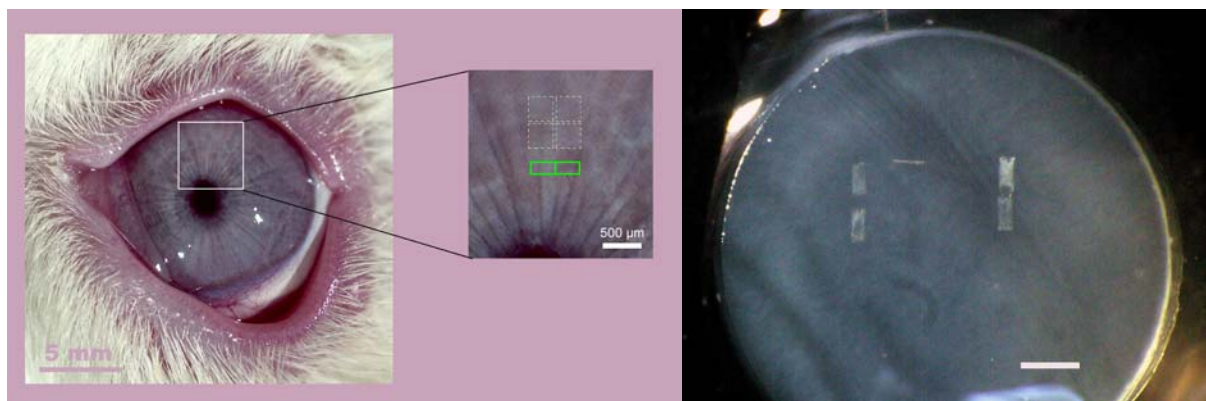


Fig.1 Schematic illustrating the flap-free non-invasive intrastromal ablation. **Left:** The two green quadrilaterals imply the laser-epithelial marking and the upper 4 squares indicate the intrastromal ablation located in the cornea depth of 120 μ m; **Right:** Showing the 4 laser-mediated marks on the epithelial surface serving as relocalization of intrastromal surgery. The intrastromal ablation in the deep cornea located between the two rows could not be defined in visibility. Bar: 500 μ m.

2. Memory of the corneal lesions for the long-termed follow-up observations of the wound-healing process.

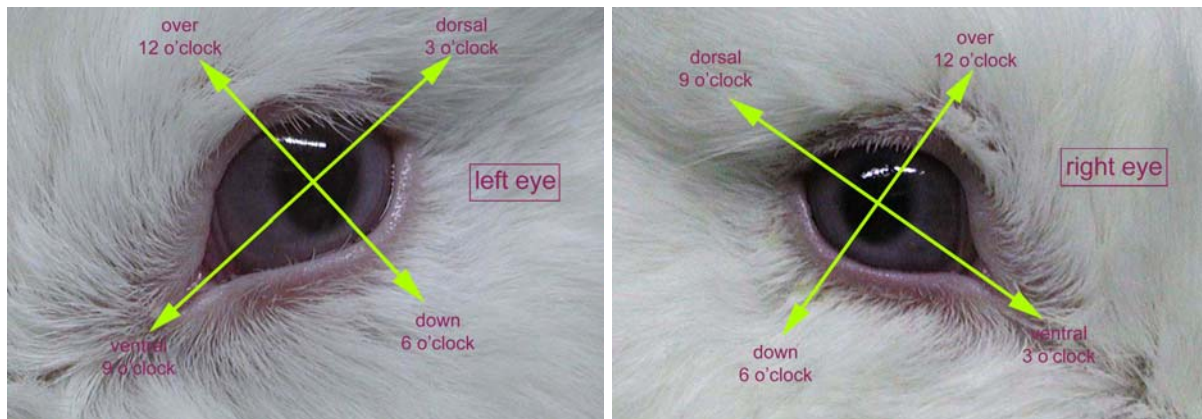


Fig.2 Memorial skill called *Clock-Memory* for relocalization of intrastromal nanosurgery and ablation for the long-termed follow-up observations.

The stromal lesion and epithelial marks can not be identified any more some days post-operation due to the wound healing. The limbus between cornea and sclera remains constant; therefore it is the most ideal orientation to relocalize the treated spot. *Clock-Memory* was designed to relocalize the treated spot in the cornea for intrastromal ablation and follow-up studies on the corneal flap.

List of Figures and Diagrams

Fig.1 Diagrams illustrating radial keratotomy (RK).....	P6
Fig.2 Diagrams illustrating PRK.....	P6
Fig.3 Procedures of LASEK.....	P8
Fig.4 Procedures of Epi-LASIK.....	P9
Fig.4_1 Histological sections of Epi-LASIK.....	P9
Fig.5 Procedures of LASIK.....	P10
Fig.5_1 Photograph of microkeratome.....	P10
Fig.5_2 Flap-related complications.....	P11
Fig.6 Procedures of Femto-LASIK.....	P12
Fig.6_1 Smooth flap bed generated with femtosecond high pulse energy lasers.....	P13
Fig.7 All-Femto-LASIK.....	P14
Fig.8_1 Imitated diagram of histological cross-section of rabbit cornea.....	P16
Fig.8_2 Three-dimensional illustration of corneal components.....	P16
Fig.8_3 TEM of corneal stroma.....	P18
Fig.9 Diagram depicting noncentrosymmetric collagen structure.....	P19
Fig.10 Nerve fibres in cornea displayed by gold chloride and optical imaging.....	P22
Fig.11 Schematic of intrastromal surgery induced by nanojoule ultrashort laser pulses.....	P25
Fig.12 Photographic illustration of animal laser eye surgery.....	P35
Fig.12_1 Modified photograph of laser operations on rabbit.....	P37
Fig.12_2 Schematic of experimental setup for multiphoton microscopy and intrastromal surgery.....	P38
Fig.12_3 Schematic illustrating intrastromal ablation.....	P38
Fig.13 Threshold power for intratissue surgery and optimized power for multiphoton imaging.....	P39
Fig.14 An indispensable instrument in this work: Zeiss slit lamp 120.....	P42
Fig.14_1 Epithelial marks taken by slit lamp.....	P42
Fig.15 Comparison of average central cornea thickness of rabbits, human and porcine.....	P44
Fig.16_1 Nonlinear optical images of epithelial squamous cells and basal cells.....	P45
Fig.16_2 Nonlinear optical images of keratocytes and endothelial cells.....	P45
Fig.17_1 Optical nonlinear tomography of epithelium.....	P46
Fig.17_2 Optical nonlinear tomography of stromal keratocytes.....	P47
Fig.17_3 In-vivo collagen lamellar nonlinear optical sectioning.....	P48
Fig.18 Nonlinear optical imaging of stromal tissue with different wavelengths.....	P49
Fig.19 Real-time nonlinear optical observations of intrastromal femtosecond laser nanosurgery.....	P50
Fig.20 SHG image and λ -scanning of emission wavelength.....	P51
Fig.20_1 SHG observations on intrastromal nanosurgery 24 hours postoperation.....	P51
Fig.20_2 Reflexion imaging of intrastromal nanosurgery 24 hours postoperation.....	P52
Fig.21_1 On-line optical observations on intrastromal ablation.....	P53
Fig.21_2 Histological cross-sections displaying the immediate ablation outcomes.....	P54

Fig.21_3 Histological observations on wound repair of intrastromal ablation at 4 th and 7 th days.....	P55
Fig.21_4 Optical detecting on emergence of myofibroblasts.....	P56
Fig.22_1 Optical images during flap generation.....	P57
Fig.22_2 Photographs of corneal flaps taken immediately after the laser operation.....	P58
Fig.23 SEM of the lifted corneal flap.....	P58
Fig.24 Observations on wound repair at 1 st day.....	P59
Fig.24_1 Histological observations on the migrating inflammatory cells at 1 st day.....	P59
Fig.25_1 Histological observations of a flap at 7 th day postoperation.....	P60
Fig.25_2 Flap at 16 th day.....	P61
Fig.25_3 Flap at 28 th day.....	P62
Fig.25_4 Flap at 66 th day.....	P63
Fig.25_5 Flap at 90 th day.....	P64
Fig.26 Photograph showing simultaneous generation of corneal flap and intrastromal lenticule.....	P65
Fig.27 In-vivo cellular nonlinear optical tomography of myofibroblasts based on 2PF.....	P66
Fig.27_1 In-vivo optical imaging of the treated region 24 hours postoperation.....	P67
Fig.28 Histological observations on inflammatory cells and discrimination of eosinophils.....	P68

Explanation of independence in writing this work

Selbständigkeitserklärung

hiermit erkläre ich, dass mir die Promotionsordnung der Medizinischen Fakultät der Friedrich-Schiller-Universität bekannt ist,

ich die Dissertation selbst angefertigt habe und alle von mir benutzten Hilfsmittel, persönlichen Mitteilungen und Quellen in meiner Arbeit angegeben sind,

mich folgende Personen bei der Auswahl und Auswertung des Materials sowie bei der Herstellung des Manuskripts unterstützt haben: Professor Dr. med. habil. **Karl-Jürgen Halbhuber** und Professor Dr. rer. nat. habil. **Karsten König**,

die Hilfe eines Promotionsberaters nicht in Anspruch genommen wurde und dass Dritte weder unmittelbar noch mittelbar geldwerte Leistungen von mir für Arbeiten erhalten haben, die im Zusammenhang mit dem Inhalt der vorgelegten Dissertation stehen,

dass ich die Dissertation noch nicht als Prüfungsarbeit für eine staatliche oder andere wissenschaftliche Prüfung eingereicht habe und

dass ich die gleiche, eine in wesentlichen Teilen ähnliche oder eine andere Abhandlung nicht bei einer anderen Hochschule als Dissertation eingereicht habe.

Jena, Juli 2006

Bao-Gui Wang

Abbreviations and definitions

CLSM	-confocal laser scanning microscope
DLEK	-deep lamellar endothelial Keratoplasty
ECM	-extracellular matrix
EGF	-epidermal growth factor
FGF	-fibroblast growth factor
FRET	-fluorescence resonance energy transfer
Fs	-femtosecond (10^{-15} s)
Fs-LASIK	-femtosecond laser in situ Keratomileusis
FWHM	-full width at half maximum
HGF	-hepatocyte growth factor
LASIK	-laser-assisted in-situ Keratomileusis
KGF	-keratocyte growth factor
MMP	-matrix metalloproteinase
MNA	-multiphoton nonlinear absorption
MW-GW	-megawatt (10^6 W)-gigawatt (10^9 W)
NJ	-nanojoule (10^{-9} J)
NAD ⁺	- β -nicotinamide adenine dinucleotide
NADP ⁺	- β -nicotinamide adenine dinucleotide Phosphate
NADH	-reduced NAD
NADPH	-reduced NADP
N. A.	-numerous aperture
NIR	-near-infrared
PDGF	-platelet-derived growth factor
PMT	-photomultiplier tube
SHI (G)	-second harmonic imaging (generation)
TAI (2PF)	-two-photon autofluorescence imaging
TGF- β 1	-transforming growth factor- β 1
THG	-third harmonic generation
TPTC	-two-photon tissue cytometry
Ti: sapphire lasers	-titanium sapphire laser ($\text{Al}_2\text{O}_3:\text{Ti}^{3+}$)
3D	-three-dimensional

Table of contents

Summary.....	1
1. Introduction.....	5
1. History and advances in laser refractive surgery.....	5
1.1 Radial keratotomy (RK).....	5
1.2 Excimer laser-assisted photorefractive keratectomy (PRK).....	6
1.3 Laser epithelial keratomileusis (LASEK) and Epi-LASIK.....	7
1.4 Laser-assisted in-situ keratomileusis (LASIK).....	9
1.5 Femto-LASIK (IntraLase).....	12
1.6 New approaches being just under investigations.....	13
2. Histology of cornea (New Zealand Albino rabbits).....	14
2.1 Description of cornea histology.....	15
2.1.1 Epithelium.....	15
2.1.2 Bowman’s layer.....	16
2.1.3 Stroma.....	17
2.1.4 Descemet’s layer.....	19
2.1.5 Endothelium.....	20
2.2 Corneal innervations.....	21
2.3 Factors maintaining corneal transparency.....	22
2.3.1 Collagen fibrils and lamellas.....	22
2.3.2 Stromal hydration.....	23
2.3.3 Function of endothelium.....	23
2.3.4 Other relevant factors.....	24
3. Mechanism and strategy of nanoprocessing in bulk tissue.....	24
4. Application of femtosecond lasers in biomedical fields.....	28
4.1 Diagnostics: Multiphoton microscopy.....	28
4.1.1 Two-photon autofluorescence (2PF).....	29
4.1.2 Second harmonic generation (SHG).....	30
4.2 Corneal Surgery.....	31
4.2.1 Intrastromal ablation with epithelial intact.....	31
4.2.2 Multiphoton-mediated generation of corneal flap and intrastromal lenticule.....	32
2. Purposes of this work.....	34
3. Materials and Methods.....	35
1. Multiphoton microscope.....	35
2. Laser systems.....	36
2.1 Chameleon.....	36
2.2 Mai Tai.....	37
2.3 Coherent Vitesse.....	38
3. Threshold value for intrastromal nanosurgery and optimized parameters for multiphoton microscopy.....	39
4. Animals, narcosis, and disinfection.....	40
5. Tissue-processing postoperation: specimen preparation, harvest and analysis.....	41
4. Results.....	44

1. In-vivo corneal optical nonlinear imaging based on multiphoton microscopy.....	44
1.1 Optical tomography of corneal tissue based on 2PF.....	44
1.1.1 Three-dimensional imaging of epithelial cells (three sublayers).....	46
1.1.2 Three-dimensional imaging of stromal keratocytes.....	47
1.2 Optical tomography of stromal collagen lamellas based on SHG.....	47
1.3 Comparison of optical nonlinear images based on 2PF and SHG.....	48
2. In-vivo application of multiphoton imaging in viewing intrastromal surgery.....	49
2.1 Evaluating intrastromal nanosurgery.....	50
2.2 Advantages of SHG in visualizing intrastromal surgery.....	50
2.2.1 Physiological architecture of collagen lamellas imaged with SHG.....	50
2.2.2 Observations of intrastromal surgery 24 hours postoperation.....	51
3. In-vivo intrastromal ablation with epithelium intact.....	53
3.1 Optical imaging during laser intrastromal ablation.....	53
3.2 Histological observations on intrastromal ablation (immediate results).....	54
3.3 Follow-up on wound repair of intrastromal ablation	55
3.4 Cell activations in the treated cornea during wound healing process.....	56
4. In-vivo multiphoton-mediated generation of corneal flap.....	57
4.1 Optical observations during performing of corneal flaps.....	57
4.2 Immediate outcomes of corneal flaps.....	57
4.3 Follow-up on wound repair of the unlifted corneal flaps.....	58
5. Simultaneous generation of corneal flap and stromal lenticule.....	64
6. Observations on cells activation and migration in cornea during wound repair.....	66
6.1 Optical tomography of activated keratocytes (myofibroblasts).....	66
6.2 Histological observations: migrating inflammatory cells and discrimination of eosinophils.....	67
5. Discussion, conclusions and outlook.....	70
1. Multiphoton tomography and nanoprocessing.....	70
1.1 Application of multiphoton microscopy in visualizing intrastromal surgery.....	70
1.2 Intrastromal ablation with epithelium intact.....	74
1.3 Multiphoton-mediated corneal flap generation.....	75
2. Wound repair after nanojoule ultrashort laser surgery in cornea.....	77
6. References.....	79
7. Appendix.....	91
8. List of figures and diagrams.....	93
9. Explanation (Selbständigkeitserklärung).....	95
10. Curriculum Vitae.....	96
11. Published and submitted works, Awards and advanced courses.....	97
12. Acknowledgments.....	100

Discussion, conclusions and outlook

1. Multiphoton tomography and nanoprocessing

1.1 Application of multiphoton microscopy in visualizing intrastromal surgery

This study confirmed that multiphoton microscopy including 2PF and SHG is an efficient and convenient imaging technique for in-vivo revealing corneal micro-architectures and in-vivo evaluating intrastromal surgery. Based on this study, we can immediately infer the advantages of this nonlinear optical imaging including **(i)** reduced specimen photo-perturbation to the areas outside the laser focus because the high light intensity is spatially confined to the subfemtoliter focal volume of objectives; **(ii)** reproducible imaging technique. Implementing the optimized laser parameters (Fig.13, Wang *et al.* 2005), cornea can be scanned for imaging numerous times without photobleaching; **(iii)** enhanced penetration depth with infrared laser. With a 20x (N.A. 0.95, water) objective, the whole layers of cornea can be visualized (Wang *et al.* 2005b); **(iv)** increased signal-noise ratio; **(v)** subcellular resolution was acquired without pinholes; **(vi)** in particular, the four layers of rabbit cornea have been perfectly differentiated in-vivo without any labelling or slicing, thereby avoiding artefacts induced by the additional sample preparations and slicing procedures.

Cell structures and collagen lamellas of cornea have been selectively demonstrated only with two different laser wavelengths, which induced two absolutely distinguishable figures for one region (Fig.18). By contrast, conventional histology explains the corneal layer structures and electron microscopy depicted the ultra-structure of collagen and keratocytes. However, the in-vivo three-dimensional collagen architectures in stroma and the topography between collagen and keratocytes have not been interpreted up to now. Multiphoton microscopy offers a convenient and reliable approach to selectively study cell structures and stromal ECM in-vivo and can reveal its mystery without slicing or staining.

The signal canals for reflective SHG and intrinsic fluorescence were not separated in this study. We have demonstrated with our experimental setup that the cell structures can be

selectively displayed (Fig.16_2, 17_2, 18, 21_4) at wavelength of 760nm (owing to absence of elastic fibres in cornea) and the in-vivo stromal collagen lamellas can also be selectively demonstrated at 830nm (Fig.17_3, 18, 20). Conversely, we can therefore conclude that the NAD(P)H in corneal cells had a higher fluorescence at 760nm and the collagen had a higher SHG excitation at 830nm in-vivo.

Multiphoton microscopy enables in-vivo non-destructive study of biological specimens in three-dimensions with submicron resolution. Above all, this imaging technique is essential for evaluation of intratissue and intracellular nanosurgery in real time because the conventional histological methods are not suitable to display the cuts with submicron size due to merging of the two cut edges after absorption of the tiny hydrolysis bubbles (Fig.19). Additionally, the required histological treatment including fixation, embedding, and slicing procedures could induce considerable artefacts. Thereby, histology could not on-line monitor the surgical outcomes. Electron microscopy can surely demonstrate the nanosurgical results but the procedure is very complicated and time-consuming. In particular, the optical tomography of cornea was perfectly suited for determining the targeted region preoperation and for visualizing the surgical outcomes of laser intrastromal nanosurgery and ablation. The layers of cornea were visualized with this imaging technique before the surgical procedure. Hence, the corneal layers and depth confirmed by this optical tomography assure the precision of nanojoule femtosecond laser surgery. Therefore, the integration of the two techniques in one system used in this study is currently the most convenient setting for investigations on the intratissue surgery with nanojoule femtosecond lasers. This non-invasive, high-resolution, on-line-optical imaging method was highly rewarded in evaluating nanojoule femtosecond laser intratissue surgery performance. Moreover, the nanosurgery of microtubules (Botvinick *et al.* 2004) has been recently reported. An interesting potential application of the multiphoton imaging would be its use in intracellular organelle nanosurgery.

The nanojoule ultrashort lasers were employed not only as diagnostic means but also as a surgical tool. Thick, dense and unfixed corneal tissue can be easily probed and imaged with strong contrast thanks to the endogenous fluorophore and collagen. The surgical performance can be simultaneously visualized and evaluated in real time, which makes the multiphoton-mediated imaging an essential component of the laser intrastromal surgery. In conclusion, large sensing depth and high resolution make the multiphoton imaging an outstanding tool for displaying the corneal architectures and monitoring the intrastromal laser surgical

performance. This nonlinear optical imaging technique continues to find an increasing number of applications in biology and medicine.

1.1.1 Based on 2PF

We have successfully performed the corneal optical tomography based on intrinsic 2PF and were able to display the intrastromal surgical results on-line with the assistance of this nonlinear imaging in animal studies. In particular, the deep endothelial layer of cornea was as well visualized with a suitable objective (20x 0.9 N.A.). The postoperative follow-up to examine the activated keratocytes was also successfully performed in-vivo using this imaging technique. To the best of our knowledge, this is the first report on the successful implementation of these methods in intrastromal surgery and follow-up study with animals.

As shown in Fig.16_1 and Fig.18, the cytoplasmatic organelles, such as mitochondria located round the nuclei, were granular-fluorescent based on the autofluorescence of NAD(P)H at wavelength of 760nm, which might be a valid basis for the nanosurgical study on the subcellular organelles.

The volume of endothelial cells has been measured with the nonlinear optical tomography in this work. However, the values of measurement here (Fig.16_2R, thickness of $8.42 \pm 2.12 \mu\text{m}$ and diameter of $7.38 \pm 1.25 \mu\text{m}$) are not in agreement with the conventional histological results (thickness of $4\text{-}6 \mu\text{m}$ and diameter of $8\text{-}11 \mu\text{m}$). The reasons for the discrepancy might involve (i) different value between in-vivo (nonlinear optical tomography) and in-vitro (histological); (ii) different species between human and rabbit (in this work).

To date, DLEK is an innovative approach to treat Fuchs' cornea dystrophy and other endothelial disorders (Terry *et al.* 2005). Until now, in-vivo follow-up on the condition of the transplanted endothelial cells has not reported. With the assistance of multiphoton-mediated imaging (with reference to Fig.16_2R), the in-vivo evaluation and monitoring of the implanted endothelium is now possible.

In addition, this nonlinear cellular optical tomography also provides a new approach to studying the dried eye and corneal dysplasia in-vivo. Application of intrinsic 2PF to distinguish dysplastic and neoplastic tissue from normal tissue has been reported, for instance in identifying tumorous tissue (Guo *et al.* 1999 and Brown *et al.* 2003a) or the decrepit brain tissues associated with Alzheimer's disease (Hensley *et al.* 1998, Christie *et al.* 2001, and

Dombeck *et al.* 2003). Owing to emerging technologies such as fluorescence resonance energy transfer (FRET), fluorescence correlation spectroscopy, two-photon fluorescence endoscopy and two-photon tissue cytometry (TPTC), 2PF is now being widely applied to image living cells, probing single molecules and investigations of other biomedical procedures (Xu *et al.* 1996, Combs *et al.* 2001, and Campagnola *et al.* 2002).

1.1.2 Based on SHG

We have used SHG imaging to monitor and to evaluate the intrastromal collagen surgery *in-vivo*. It is shown that the outcomes of the intrastromal collagen nanodissection can be better visualized with second harmonic imaging than with other imaging method such as reflection imaging (Fig.20_2) and 2PF imaging due to fulfilling of the migrating cells in the cut spaces.

Interestingly, the difference between the nonlinear imaging of collagen in forward directions and in backward directions was demonstrated (Han *et al.* 2005 and Williams *et al.* 2005). Fig.17_3 and Fig.18 show the collagen SHG only in backward direction. Compared with the forward SHG displaying the regular arrangement of the collagen fibrils (Han *et al.* 2005), the backward SHG in this study revealed the three-dimensional arrangement of collagen lamellas. Since the forward SHG is not practical (not realizable) for thick-tissue and *in-vivo* study, the corneal collagen fibrils in transmissive SHG were not imaged in this study. However, the reasons leading to different images with two directions need to be further studied.

Third harmonic generation (THG) can take place in the nonlinear multiphoton process by the tightly focused ultrashort lasers (Guo *et al.* 1997 and Mueller *et al.* 1998). The detection of THG was avoided using the specialized filter systems (chapter 2, materials and methods) in this work.

Compared with the corneal images of other animals such as porcine, the lamina limitans anterior, normally located between the epithelial basal cells and stroma, was not detected with SHG in rabbit specimens used in this study. Here, the very thin collagen membrane (<1 μm , optically verified by z-adjusting of the multiphoton microscope, Fig.25R) acts as the basement membrane for epithelial basal cells. This optical result of absence of this layer in rabbit cornea was in agreement with the histological results (Gipson *et al.* 1987). However, other reports suggest this layer is present and has a thickness of only 2-3 μm (Prince *et al.* 1960). Wilson reported that the Bowman's layer has no critical function in corneal physiology (Wilson *et al.* 2000).

The ultraprecision of intrastromal surgery by nanojoule femtosecond lasers can be studied with SHG imaging characterized by high-spatial resolution and high contrast. SHG imaging in cornea allowed visualization of collagen lamellas in physiological state and monitoring of the intrastromal laser surgery on-line and postoperation. In conclusion, SHG possesses capability to perform three-dimensional visualization of collagen lamellas; this may lead to simple non-invasive three-dimensional evaluation of postoperative intrastromal laser surgery and to investigate the regeneration of collagen during the wound repair. These properties of SHG thus can provide a novel imaging methodology that complements existing linear and nonlinear optical schemes.

1.2 Intrastromal ablation with epithelium intact

A flap-free intrastromal ablation based on multiphoton nonlinear absorption process induced by the nJ fs lasers with animals has been successfully demonstrated in this work. These studies depict the outcomes of an intratissue fissure with perpendicular distance of 5-7 μ m on histological sections, which of this specimen was laser-ablated in-vivo from 110 μ m to 120 μ m. The epithelium and subepithelial layer were kept intact. Since no opening of the cornea and no mechanical processing is involved, corneal damage and postoperative complications are largely reduced. Short- and middle-termed follow-up observations on wound repair were performed in this study.

Our study immediately suggests several distinct advantages of nonamplified (nanojoule pulse energy) fs lasers in comparison with amplified (microjoule) fs lasers. **(i)** The absence of big intratissue bubbles makes it feasible to ablate the tissue more precisely. The sharp boundary between the treated and untreated area on the optical images (Fig.21_1) also indicates the ultra-precision of surgical results. By contrast, the big intratissue bubbles characterized by a diameter of more than 50 μ m induced by the μ J fs lasers (10kHz, 2.5 μ J, 400fs, unpublished results) can not be completely absorbed, leading to intratissue cavity being formed in the absence of tissue removal. Intracorneal tissue removal can not therefore be performed by this μ J laser; **(ii)** The collateral effects of tissue streaks (Lubatschowski *et al.* 2002) induced by the amplified fs lasers in intracorneal surgery were not observed in this study with nJ pulses.

With reference to Fig.21_2A, the histological outcomes show the surgical result (5-7 μ m) is a little narrower than that of planned (10 μ m). Possible explanations include the collapse of the

generated fissure and the tissue elasticity of cornea. The artefacts due to embedding and fixation might have also contributed.

Since this study is the first in-vivo systematic investigation using nJ fs laser techniques, some issues worthy of further research have been raised. **(i)** The occurrence of impaired surrounding tissue is difficult to explain. Theoretically, only the central spot provides sufficient photon density to induce highly-localized two-photon-induced ionization and optical breakdown. The collateral effects out of focus should therefore have been absent; **(ii)** The operation time could be shorter when the parameters including laser power, wavelength and wave duration have been optimized for the intrastromal surgery (in this study, approximately 100s were required based on 320 μ m x 320 μ m, full frame, 10 μ m with interval of 2 μ m, and a frame scan time of 16s); **(iii)** The increased intrastromal pressure during the treatment owing to the occurrence of plasma and gas must be resolved.

With nJ fs lasers, the multiphoton nonlinear absorption-initiated tissue ablation supplies more predictable and reproductive surgical outcomes while excluding the severe thermal damages and mechanical effects. Also the nonlinear side effects such as self-focussing can be avoided due to using the high numerical aperture of the objectives used in this study (Koenig *et al.* 2002a). This animal study has demonstrated that the nJ fs lasers possess the capability to perform flap-free intrastromal ablation, which removes the corneal collagens and consequently, can induce flattening the central corneal curvature, thereby resulting in changing of the refractive index. This method suggests an encouraging advance to treat the visual disorders without flap-related complications or UV-induced tissue and cellular damages. This non-invasive intrastromal ablation strategy by nJ fs lasers could be especially valuable for correcting early-stage vision aberrations and relapses post-LASIK. Further potential applications of this advanced technique include ultra-precise ablation of the intratissue and intracellular neoplasia, endothelial flap generation for DLEK, and knock-out of subcellular organelle, inactivation of certain DNA region and embryo surgery.

1.3 Multiphoton-mediated corneal flap generation

Here, the in-vivo generation of corneal flaps with nonamplified femtosecond infrared lasers has been demonstrated successfully. Short and middle-termed observations on wound repairs in respective schedules were also made. Our results, demonstrating higher-precision flap generation (Fig.22_1 and 23) meanwhile preservation of corneal transparency, suggest that

more predicable and safer refractive corrections are possible with this technique in comparison with microjoule femtosecond lasers (Kurtz *et al.* 1998, Lubatschowski *et al.* 2000, Nordan *et al.* 2003, and Heisterkamp *et al.* 2003). The long-term studies on would repair of the unlifted and lifted corneal flap with this type of laser are subject to a next work.

By contrast to microjoule femtosecond lasers, several distinct advantages of this nJ lasers can be immediately inferred through our results: **(i)** Without tissue streaks not only on optical images but also on histological sections; and **(ii)** Precise cut verified by the sharp boulder between the treated and untreated area on the optical images (Fig.21_1 and Fig.22_1) and no disturbing out of focus on the histological cross-section. However, since this study is the first in-vivo systematic investigations on flap generation using nanojoule femtosecond lasers, further research on the optimizing of laser operation parameters is required.

As shown on Fig.22_1, near-continuous cutting without significant collateral effects could be acquired by scanning the laser focus at a high repetition rate. Due to the parallel arrangement of collagen lamellas to corneal surface, it was easier to perform the generation of flap bed than vertical walls. The powers used for generation of flap walls and bed were different, for instance, the power for bed was 188mW and for walls 210mW at a depth of 120 μ m.

Previous studies using a picosecond laser (which used laser pulse energy 10000 times greater than those in this study) did not induce endothelial damage when intrastromal surgery was performed in the anterior third of the stroma (Habib *et al.* 1995). Mardelli made a long-term follow-up on PRK (up to 55 months) and concluded that PRK does not cause endothelial damage (Mardelli *et al.* 1995). By contrast, PRK with excimer laser caused no detectable changes in central corneal endothelial cell, but it caused a modest loss of peripheral corneal endothelial cells by 1 year (Hanna *et al.* 1990 and Stulting *et al.* 1996). By analogy, further study is also required to investigate on the state of endothelial cells during the flap generation and postoperation due to the high penetration of infrared pulses used in this study.

Currently, DLEK is performed in clinic for treating Fuchs' dystrophy and other endothelial disorders with mechanical generation of endothelial flap. We are now attempting to perform the endothelial flap with the more precise and less deleterious nJ ultrashort lasers.

We evaluated the potential use of the nanojoule femtosecond lasers for performing minimally invasive and highly localized corneal surgical procedure of flap generation. The surgical results and follow-up studies show that this fs laser at nJ pulse energy possesses the capacity for highly precise generation of corneal flaps without visible collateral damage to the surrounding tissue and overlying epithelium. The availability of practical femtosecond laser surgical tools may lead to significantly improved ophthalmic surgical procedures and techniques. Femtosecond laser technology has the potential to become the preferred corneal laser scalpel in this century by improving existing procedures and application of this entirely new technology.

2. Wound repair after nanojoule ultrashort laser surgery in cornea: concentration on cells activation and migrating in this work.

Interestingly, the migrating eosinophils and the myofibroblasts induced by this nanojoule ultrashort laser pulses were detected in this study. **(i)** Eosinophils participate primarily in the allergic inflammations and become active by tetrapeptide released from mast cells. The cells prefer to take up antigen-antibody complex and to restrain allergic inflammation (Garcia *et al.* 1996). In our study, the debris of the ablated tissue and plasma substance might be the antigen source, of which the antigen-antibody complex induced the amoeboid crawling of eosinophils stemming from the limbal blood vessels. However, further study on the reasons is still required. **(ii)** The in-vivo recorded myofibroblasts with the assistance of 2PF imaging were identified by their special cellular morphology in this study (Fig.27). The existence of myofibroblasts transformed from stromal keratocytes was evidenced in-vitro by a smooth muscle actin-staining method (Masur *et al.* 1996). Myofibroblasts transformation may take up to a month to become apparent (Moller-Pedersen *et al.* 2000). Wounds that have completely healed contain few myofibroblasts, presumably because they revert to the fibroblast phenotype or undergo apoptosis during wound healing. This may take a year or more (Jester *et al.* 1996). These cells transformed from keratocytes appeared as satellite cells, were highly reflective and characterized by high cytoplasmic fluorescence. After the intrastromal surgery, the first cellular reaction in cornea might be the immediate activation of keratocytes, which synthesized chemokines and chemotaxis, leading to characteristic inflammatory cascade reactions. The contribution of the myofibroblasts involving wound contraction and phagocytosis in the healing process has been also discussed elsewhere (Funderburgh *et al.* 2001, Berryhill *et al.* 2002, and Chakravarti *et al.* 2004). The in-vivo long-term follow-up on myofibroblasts and characteristics of migrating inflammatory cells in

cornea induced by the laser lesions are subject to a next study with multiphoton autofluorescence imaging in our group. The histiocytes can also be activated around incisions to help cleaning up and remodelling the wound. Polymorphonuclear leukocytes (PMN), plasma cells, and lymphocytes can also appear during the early phases of wound healing. The systematic investigations on characteristics of these migrating inflammatory cells in respective healing phases with MAI are an ongoing thesis.

The severed epithelium within this study became integral again within 24 hours postoperation. Concomitant with the epithelial wound healing, the process of stromal wound repair commences but often lasts for a longer time period and underwent keratocytes apoptosis (Fini *et al.* 1999), proliferation (Harris *et al.* 1981), stromal remodelling involving production of collagen and ECM (Zieske *et al.* 2001), and epithelial and stromal maturation. The proliferation of keratocytes within 24 hours postoperation was described above. The activated keratocytes existed in aggregate form and suggested initiating the subsequent cascade reaction of wound-healing. The inflammatory cells migrating into cut spaces during the healing process have been also detected in this study, which occurred later than the activated keratocytes. Although exact details still remain to be studied, it is well known that the inflammatory cells played important roles throughout the healing process.

Cytokines are involved in wound healing. Transforming growth factor- β 1 (TGF- β 1) stimulates myofibroblasts differentiation; Fibroblast growth factor-2 (FGF-2) and platelet-derived growth factor (PDGF) inhibit such transformation. The temporal and spatial correlation between matrix metalloproteinase 13 (MMP-13) and corneal re-epithelization suggests that MMP-13 plays a role in reepithelization after corneal wounding. Epithelial proliferation and migration are mediated by epidermal growth factor (EGF), TGF- α , FGF, keratocyte growth factor (KGF), and hepatocyte growth factor (HGF) (Rocha *et al.* 1996, Ye *et al.* 2000, Maltseva *et al.* 2001, and Baldwin *et al.* 2002). As shown on Fig.25_3 and Fig.25_4, epithelial ingrowth took place at the site of the vertical incision and might result from hyperplastic epithelial plugs. Type IV collagen has been localized at this region suggesting that basement membrane components may participate at wound healing (Kato *et al.* 1999).

Materials and Methods

The employed femtosecond laser scanning system enables highly-precise plasma-mediated ablation of material as well as three-dimensional fluorescence and SHG diagnostics with submicron spatial resolution. The system consists of two divisions: multiphoton microscope and femtosecond laser system (Fig.12).



Fig.12 Photographic illustration of laser eye surgery with rabbit based on a modified Zeiss inverted laser scanning microscope integrated with a compact non-amplified 80 MHz Ti: sapphire femtosecond laser. **a:** Multiphoton-microscope; **b:** Draeger dialogue 2000; **c:** Imaging monitor.

1. Multiphoton microscope

The multiphoton microscope used in this work was a modified inverted laser scanning microscope Zeiss Axiovert LSM 410. This Zeiss LSM 410 was characterized by **(i)** bright-field, phase or differential interference contrast (DIC) imaging; **(ii)** high-resolution optics for fluorescence microscopy; **(iii)** focus motor with 0.1 μ m resolution and modified to possess the capability to fulfil multiphoton microscopy in such a way that **(i)** scanning module with specialized beam deflection mirrors which realize a high transmittance of 75% at wavelength of 800nm; **(ii)** motorized beam attenuator; **(iii)**

motorized beam shutter; **(iv)** laser power detection module; **(v)** fast x,y galvo scanner (different operation modes) and motorized z-turning system with an accuracy of 40nm; **(vi)** an interface before the entrance into microscope to introduce femtosecond laser beams; **(vii)** a special baseport unit with a CCD camera system was built up; and **(viii)** equipped with the diffraction-limited 40x objective (1.3 N.A. with oil, Zeiss Plan Neofluar) with a work distance up to 200 μ m and 20x objective (0.95 N.A. with water) with more than 1000 μ m work distance in bulk tissue were essential to induce the multiphoton process. The modifications made it suitable to couple with the Ti: sapphire femtosecond laser beams for multiphoton microscopy and corneal surgery. The microscope and alignment were commanded by control modules with power supply and image-processing hardware as well as object-viewing-based software which includes the features: **(i)** to operate the laser, the attenuator, the shutter, the scanner, the z-alignment, detectors; **(ii)** to realize fast image calculation and image processing; **(iii)** to control the laser power on-line; **(iv)** to realize mono-directional and bi-directional scanning up to 1024 x 1024 pixels, line scan and single-point-illumination (Koenig *et al.* 2002b and 2002c, Wang *et al.* 2005).

Another microscope named Zeiss Axiovert 200 microscope 510 Meta (Zeiss Jena, Germany) was used to measure the emission wavelength of collagen SHG with λ -scanning in this work.

2. Laser system

Three laser systems were employed to fulfil different purposes. Laser powers at the object plane were routinely measured using a field master FM power meter (Coherent Inc., US). The pulse duration was measured with an autocorrelator (APE, Germany).

2.1 Chameleon

The compact solid-state mode-locked 90MHz Ti: Sapphire laser Chameleon (Coherent Inc., USA) with a wide wavelength range of 715nm to 930nm, a maximum mean laser power output of 940mW and 140fs pulse duration was employed in multiphoton optical imaging (Fig.12_1).

The laser powers were set between 20 and 35mW (with respect to different depths in cornea) for multiphoton imaging (2PF at wavelength of 760nm and SHI at 830nm) in this study.

A filter set consisting of beam-splitters (BS 720nm) and short-pass filters (SP 720nm) set in the channel of backward direction was essential to separate the emitted light from the reflected incident light. In addition, beam-pass filters (BG 39, 320-650nm) were set up just before the external PMT. By means of this filter setup, the emitted lights, including 2PF and SHG, were deflected backward in the direction towards the PMT and the signal-processor to record nonlinear optical images. Owing to the high numerical aperture objectives used here, the emission light was high efficiently collected in the backward directions.



Fig.12_1 Modified photograph of operations on rabbit depicting the integrated system involving the laser head Chameleon and the modified Zeiss multiphoton microscope. The optical mirrors deflecting the laser beam are here illustrated with a simple way. **a:** Compact tunable non-amplified 90MHz Ti:sapphire Chameleon; **b:** Multiphoton microscope based on inverted Zeiss LSM 410; **c:** The animal on animal bed in operation; **d:** Wavelength tuner; **e:** Imaging-monitor.

2.2 Mai Tai

The compact turn-key solid-state mode-locked 80MHz Ti: sapphire laser Mai Tai (Spectra Physics, USA) with a wavelength range of 750nm to 850nm, a maximum mean laser output of 940mW and 80fs pulse duration at the exit of laser head (170fs in specimen) was used for intrastromal nanosurgery and ablation(Fig.12_2). The surgical procedures in this study were performed only with a wavelength of 800nm.

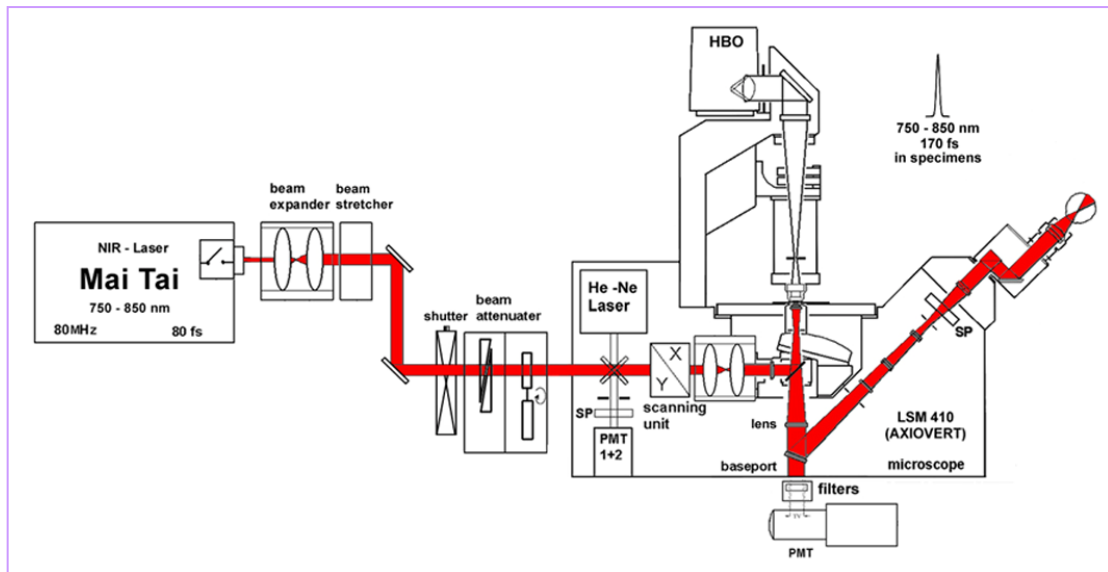


Fig.12_2 Schematic of experimental setup for multiphoton imaging and multiphoton-mediated intrastromal ablation involving the laser head Mai Tai and the modified Zeiss multiphoton microscope.

Procedure of intrastromal ablation (Fig.12_3): The ultrashort nJ pulses were packed on the region of interest with a focus volume of 0.1 femtoliter so that the ultrahigh light intensity at an order of TW/cm^2 was achieved at wavelength of 800nm. Based on multiphoton nonlinear absorption, intrastromal ablation was obtained with frame scan. The iterative processes were performed with z-interval of $2\mu\text{m}$. The powers used for in-vivo intrastromal ablation were described in 3/threshold threshold.

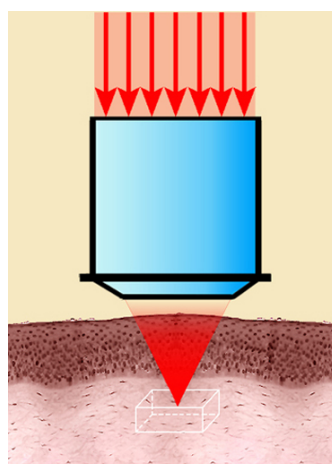


Fig.12_3 Schematic illustrating intrastromal ablation. The ultrashort ultrafast lasers with nanojoule pulse energy are focused in corneal stroma by a diffraction-limited high N.A. objective and the stromal cube delimited will be ablated.

2.3 Coherent Vitesse

The compact turn-key solid-state mode-locked 80MHz Coherent Vitesse (Coherent Inc., USA) with a fixed-wavelength operating at 800nm, a maximum mean laser output of 1000 mW and 100fs pulse width was used for flap generation. The laser head has characteristics of active pointing control for long-term alignment stability, light-loop stabilization for long-term power stability, and verdi DPSS pump laser for proven reliability and ease of maintenance. Laser powers at the object plane could be acquired with a maximum power of 230mW.

The parameters for generation of corneal flap with respect to corneal depth:

(i): flap bed was performed with frame scan by following parameters:

At a depth of 60 μ m: 118mW, 16s, zoom=1; At 120 μ m: 188mW, 16s, zoom=1.

(ii): perpendicular cuts for generation of cube walls of flap were performed with cut line and following parameters:

From 60 μ m to surface: 130mW-66mW, z-interval=2 μ m, 1s; from 120 μ m to surface: 210mW-66mW, z-interval=2 μ m, 1s.

Laser powers for tissue processing were correlated with corneal depth.

3. Threshold value for intrastromal nanosurgery and optimized parameters for multiphoton microscopy

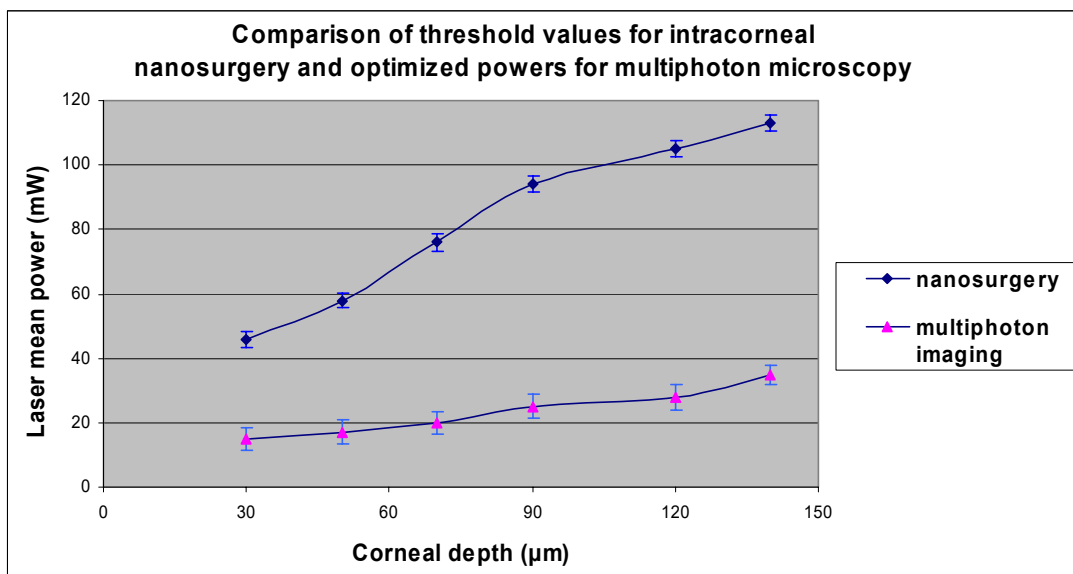


Fig.13 Threshold power for intrastromal nanosurgery and optimized parameters for multiphoton imaging with correlation of cornea depth in-vivo.

The upper diagram (Fig.13) depicts the threshold power value for corneal nanosurgery (zoom=1, t=1s, line scan, 40x 1.3 oil) at 800nm and the optimized laser power employed for multiphoton imaging meaning that the imaging was taken without photobreakdown effects at 760nm. Actually, the mean power for intrastromal ablation used for intrastromal ablation varied from 190mW (at depth of 110 μ m) to 210mW (at depth of 120 μ m) in order to remove the collagenous tissue with better performance. With pulse duration of 170fs in the specimen, the mean power of 200mW corresponds to 16kW peak power and 2.5nJ pulse energy.

4. Animals, narcosis, and disinfection

4.1 Animals

Animal care and procedures in this study were in accordance with the guidelines of “the German Law on the Protection of Animals” and “principles of laboratory animal care”. All animals in this study were permitted by Thuringia Research Ministry (permission licence Nr.: 02-17/03 Thuringia).

New Zealand Albino rabbits (Charles River Wiga, Germany) with average age of 6 \pm 1.5 months and mean weight of 4.1 \pm 1.1Kg were used. One eye was laser-treated while the other served as control. The animals were anesthetized using the narcotics ketamine (Atarost, Germany) and xylazine (Bayer Vital, Germany) and then positioned on an animal bed (Fig.12) linking up with the multiphoton microscope. The eye globes were laid on a 170 μ m-thick glass coverslips lying in a specimen chamber specialized for the in-vivo animal experiment.

4.2 Narcosis procedures

In the introduction phase, the animal was firstly given 3ml anaesthesia mixture at slow tempo and then 2ml was added. The 5ml anaesthesia mixture was composed of 40mg ketamine (Atarost, Germany) and 10mg xylazine (Bayer Vital, Germany) dissolved in 5ml NaCl solution. This means that we have used altogether 40mg ketamine + 10mg xylazine in the introduction phase. For preserve this state, more 1ml mixture every 30 minutes should be added.

The animal pulse was measured and controlled on the back extremity with a device named Draeger dialogue 2000 (Draegerwerke, Germany). The animals had a pulse

frequency of approximately 170-180/min for introduction then reduced to values of between 80-100/min in narcosis state (normal HR 130-325/min). The saturation of blood oxygen was round 92% constantly.

4.3 Disinfection

The saccus conjunctivalis of treated eye was rinsed only with PBS pre-and post-treatment for corneal imaging, intrastromal nanosurgery, and intrastromal ablation. In contrast, for flap generation, the saccus conjunctivalis was rinsed with PBS and Betaisodona (Mundipharma, Germany) for disinfection preoperation. Antibiotic Floxal AT (Dr. Winzer Pharma, Germany) was employed for 3 days (two times every day) postoperation.

5. Tissue-processing postoperation: Specimen preparation, harvest and analysis

The treated corneas were intensively observed 3 days postoperation. In details, every 6 hours on 1st day, every 12 hours on 2nd day and once on 3rd day.

At the end of each observation, the treated corneas were further processed in histological laboratory to observe and evaluate the surgical performance and state of wound repair as well as the cell activations. In details, the cornea specimens were extracted from globes using a biopsy punch with a diameter of 5mm and then immediately fixed in 3% cacodylate-buffered glutaraldehyde with pH 7.4 for 72 hours. After certain additional fixations with alcohol and acetonitril, the corneal samples were embedded in epon, and polymerized at 65⁰C for 4-6 days. After that, the corneas were glued on a block which was afterwards cutted into semi-thin sections (1µm-2.5µm) using an ultramikrotome (Leica Reichert Ultracut, Austria). After air-drying, the sections were stained with methylene blue, azan and HE.

For electron microscopy (TEM), the corneal sample were fixed with osmiumtetroxid 1% for 1 hour before embedding and then treated with 2% uranylacetat in aqua bidest for additional contrast. The electron microscopic graphs of ultrathin-sections were taken with Zeiss EM 900 (spatial resolution of 0.6 nm, Fig.8_3).

The lifted corneal flap and bed were imaged with a LEO-1450 VP scanning electron microscope (SEM, spatial resolution of 0.4 nm, Fig.23).

6. An indispensable instrument to carry out follow-up on wound repair: Zeiss slit lamp with digital camera.

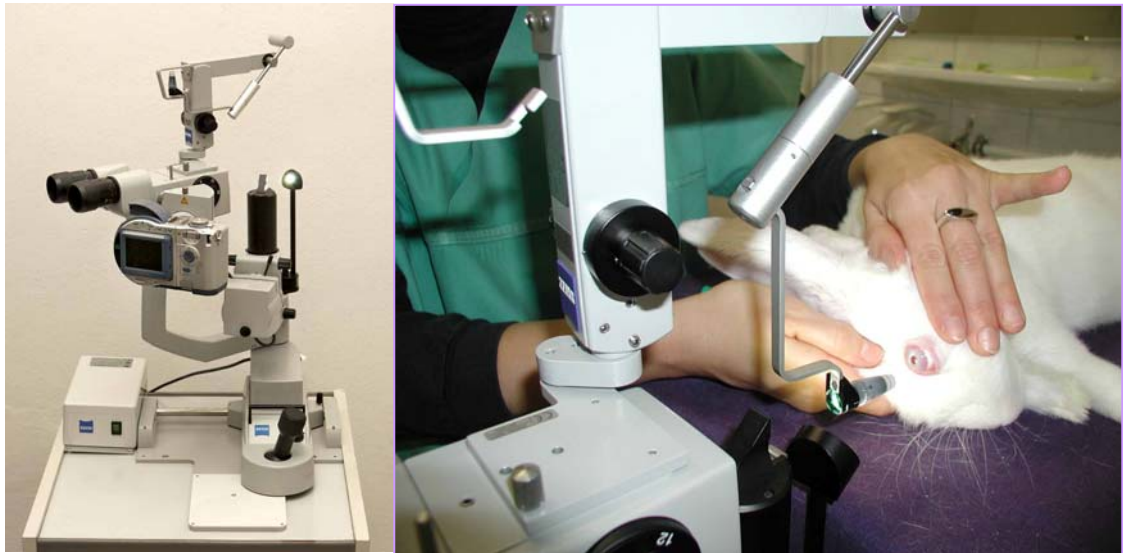


Fig.14 Left: The powerful and convenient all-rounder Zeiss slit lamp 120 supplied by Carl Zeiss Jena GmbH which was one of the most important instruments in the intrastromal laser surgery serving for examination of cornea preoperation and observation, relocalization, and evaluation of intrastromal wound repair. **Right:** In-live photograph of examination of cornea preoperation and measurement of intraocular pressure.

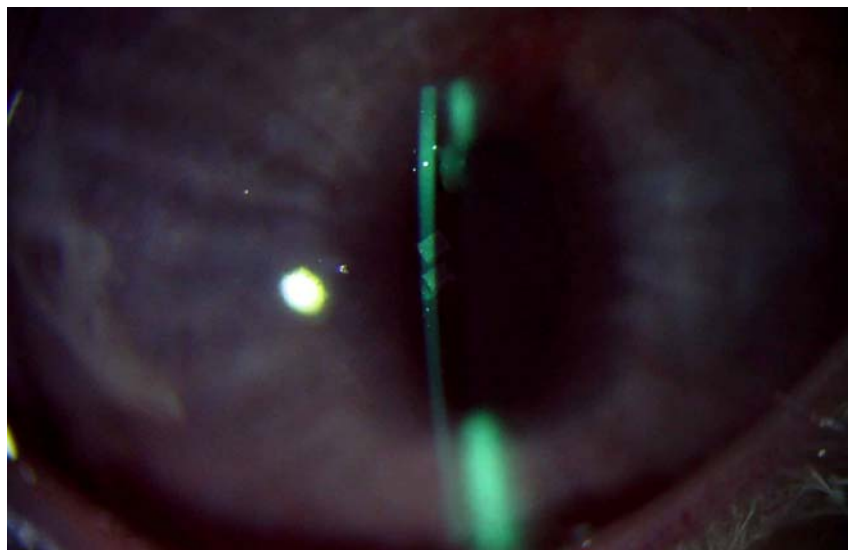


Fig.14_1 Photograph taken by the above-mentioned slit lamp just after laser-treatment showing the epithelial marks serving for relocalization of intrastromal nanosurgery and ablation.

The intraocular pressure was not measured regularly postoperation in this work because **(i)** the laser-treated corneas became much sensitive and **(ii)** the contact to cornea could bring in infection. Thereby, we are trying to use another more convenient non-contact pressure device in the ongoing study.

Purposes of this work

- (i) In-vivo study on cornea with three-dimensional nonlinear optical imaging based on multiphoton microscopy including 2PF and SHG with biomedical aspects; Comparison of corneal optical images based on 2PF and SHG; Study on in-vivo applications of multiphoton microscopy in intrastromal surgery.
- (ii) In-vivo intrastromal ablation by means of the nonamplified infrared femtosecond lasers and investigating on a novel approach to perform the laser refractive surgery called flap-free, non-invasive intrastromal ablation; Observations on wound repair.
- (iii) In-vivo corneal flap generation with high precision by near-infrared nanojoule femtosecond lasers; Observations on wound repair.

References

- Arnold CL, Heisterkamp A, Ertmer W, and Lubatschowski H.** “Streak formation as side effect of optical breakdown during processing the bulk of transparent Kerr media with ultra-short laser pulses.” *Applied Physics B*, 80-2, p.247-53 (2005).
- Baldwin GC .** “An Introduction to Nonlinear Optics.” 2nd ed. New York: Plenum (1974).
- Baldwin HC and Marshall J.** “Growth factors in corneal wound healing following refractive surgery: a review.” *Acta Ophthalmol Scand.* 80(3), 238-47 (2002).
- Barnes PA and Rieckoff KE.** “Laser induced underwater sparks.” *Appl. Phys. Lett.* 13, 282-284 (1968).
- Ben-Oren I, Peleg G, Lewis A, Minke B, and Loew L.** “Infrared nonlinear optical measurements of membrane potential in photoreceptor cells.” *Biophysical J.* Vol 71, 1616-20 (1996).
- Berns MW, Aist J, Edwards J, Strahs K, Girton J, McNeil P, Rattner JB, Kitzes M, Hammer-Wilson M, Liaw LH, Siemens A, Koonce M, Peterson S, Brenner S, Burt J, Walter R, Bryant PJ, Van Dyk D, Couclombe J, Cahill T, and Berns GS.** “Laser microsurgery in cell and developmental biology.” *Science* 213, 505-513 (1981).
- Berns MW, Wang Z, Dunn A, Wallace V, and Venugopalan V.** “Gene inactivation by multiphoton-targeted photochemistry.” *PNAS*, vol. 97. No. 17 9504-07 (2000).
- Berretty PJ and cormane RH.** “The aniline blue fluorescence staining of eosinophilic granulocytes.” *Br J Dermatol.* 99(4):377-82 (1978).
- Berryhill BL, Kader R, Kane B, Birk DE, Feng J, and Hassell JR.** “Partial restoration of the keratocyte phenotype to bovine keratocytes made fibroblastic by serum.” *Invest Ophthalmol Vis Sci.* 43:3416–3421 (2002).
- Binder PS.** “Flap dimensions created with the IntraLase laser.” *J Cataract Refract Surg.* 30(1):26-32 (2004).
- Bloembergen N, Chang RK, Jha SS, and Lee CH.** “Optical Second-Harmonic Generation in Reflection from Media with Inversion Symmetry.” *Phys. Rev.* 174, 813–22 (1968).
- Bloembergen N.** “Laser-induced electric breakdown in solids.” *IEEE J. Quantum Electron.* QE-10, 375-386 (1974).
- Bloembergen N.** “Nonlinear Optics.” 4th ed. River Edge, NJ: World Scientific (1996).
- Botvinick EL, Venugopalan V, Shah JV, Liaw LH, and Berns MW.** “Controlled Ablation of Microtubules Using a Picosecond Laser.” *Biophys J.* 87:4203-12 (2004).
- Bouevitch O, Lewis A, Pinevsky I, Wuskell JP, and Loew LM.** “Probing membrane potential with nonlinear optics.” *Biophysical J.*, Vol 65, 672-79 (1993).
- Bowman CB, Beebe WE, Gelender H, et al.** “Photorefractive keratectomy for myopia: current status.” *Ophthalmol Clin North Am* 10(4):517-31 (1997).

- Brakenhoff GJ, Squier J, Norris T, Bliton AC, Wade WH, and Athey B.** "Real-time two-photon confocal microscopy using a femtosecond, amplified Ti:sapphire system," *J. Microsc.* 181, 253-259 (1996).
- Brown E, McKee T, Ditomaso E, Pluen A, Seed B, Boucher Y, and Jain RK.** "Dynamic imaging of collagen and its modulation in tumors in vivo using second-harmonic generation." *Nat. Med.* 9:796–800 (2003a).
- Brown RM Jr, Millard AC, and Campagnola PJ.** "Macromolecular structure of cellulose studied by second-harmonic generation imaging microscopy." *Opt Lett.* 28(22):2207-9 (2003b).
- Butcher PN and Cotter D.** "The Elements of Nonlinear Optics." Cambridge, England: Cambridge University Press (1990).
- Campagnola PJ, Wei MD, Lewis A, and Loew LM.** "High-resolution nonlinear optical imaging of live cells by second harmonic generation." *Biophys J.* 77(6):3341-9 (1999).
- Campagnola PJ, Millard AC, Terasaki M, Hoppe PE, Malone CJ, and Mohler WA.** "Three-dimensional high-resolution second-harmonic generation imaging of endogenous structural proteins in biological tissues." *Biophys J.* 82. 493-508 (2002).
- Campagnola PJ and Loew LM.** "Second-harmonic imaging microscopy for visualizing biomolecular arrays in cells, tissues and organisms." *Nat. Biotech.* 21, 1356-60 (2003).
- Campbell S, Dear FC, Hand DP, and Reid DT.** "Single-pulse femtosecond laser machining of glass." *J. Opt. A.* 7 162-8 (2005).
- Carr JD, Stulting RD, Thompson KP, et al.** "Laser in-situ keratomileusis." *Ophthalmol Clin North Am* 10(4):533-42 (1997).
- Chakravarti S, Wu F, Vij N, Roberts L, and Joyce S.** "Microarray Studies Reveal Macrophage-like Function of Stromal Keratocytes in the Cornea." *Invest Ophthalmol Vis Sci.* 45:3475-3484 (2004).
- Cheng PC, Pan SJ, Shih A, Kim KS, Liou WS, and Park MS.** "Highly efficient upconverters for multiphoton fluorescence microscopy." *J. Microsc.* 189:199-212 (1998).
- Christie RH, Bacskai BJ, Zipfel WR, Williams RM, Kajdasz ST, Webb WW, and Hyman BT.** "Growth arrest of individual senile plaques in a model of Alzheimer's disease observed by *in vivo* multiphoton microscopy." *J. Neurosci* 21(3), 858-864 (2001).
- Combs CA and Balaban RS.** "Direct Imaging of Dehydrogenase Activity within Living Cells Using Enzyme-Dependent Fluorescence Recovery after Photobleaching (ED-FRAP)." *Biophys J*, 2018-28, Vol. 80, No. 4 (2001).
- Conrad GW.** "Collagen and mucopolysaccharide biosynthesis in the developing chick cornea." *Dev Biol.* 21:292–317(1970).
- Danielsen CC.** "Tensile mechanical and creep properties of Descemet's membrane and lens capsule." *Exp Eye Res.* 79(3):343-50 (2004).
- Dawson DG, Kramer TR, Grossniklaus HE, Waring GO III, Edelhauser HF.** "Histologic, ultrastructural, and immunofluorescent evaluation of human laser-assisted in situ keratomileusis corneal wounds." *Arch Ophthalmol.* 123(6):741-56. Erratum in: *Arch Ophthalmol.* 123(8):1087(2005).

Davidorf JM and Zaldivar R. “Results and complications of laser in situ keratomileusis by experienced surgeons.” *J Refract Surg* 14(2):114-22 (1998).

Delfino M. “A comprehensive optical second harmonic generation study of the non-centrosymmetric character of biological structures.” *J. Biol. Phys.* 6:105-17 (1979).

Denk W, Strickler JH, and Webb WW. “Two-photon laser scanning fluorescence microscopy.” *Science* 248, 73-76 (1990).

Diaspro A and Sheppard C. “Two-Photon Microscopy: Basic Principles and Architectures.” Diaspro A (Editor), *Wiley-Liss Inc*, 0-471-40920-0 (2002).

Dikstein S, and Maurice DM. “The metabolic basis to the fluid pump in the cornea.” *J Physiol.* 221:29–41(1972).

Dombeck DA, Kasischke KA, Vishwasrao HD, Ingelsson M, Hyman BT, and Webb WW. “Second Harmonic Generation Microscopy of Uniformly Oriented Microtubules in Native Brain Tissue.” *PNAS* 100(12), 7081-86 (2003).

Doughty MJ. “The ambiguous coefficient of variation: polymethism of the corneal endothelium and central corneal thickness.” *Int Contact Lens Clin* 17,240-247 (1990).

Durrie DS and Kezirian GM. “Femtosecond laser versus mechanical keratome flaps in wavefront-guided laser in situ keratomileusis Prospective contralateral eye study.” *J Cataract Refract Surg.* 31(1):120-6 (2005).

Edelhaue HF, Van Horn DL, and Records RE. “Cornea and sclera.” In Duane TD and Jaeger EA:Biomedical Foundations of Ophthalmology. Vol. 2, Hagerstown, Md. Harpe & Row, Chapter 4 (1982).

El-Agha MS, Johnston EW, Bowman RW, et al. Excimer laser treatment of spherical hyperopia: PRK or LASIK? *Trans Am Ophthalmol Soc* 2000;98:59–60.

Fine S and Hansen WP. “Optical second harmonic generation in biological systems.” *Appl. Opt.* 10:2350-53 (1971).

Fini ME. “Keratocyte and fibroblast phenotypes in the repairing cornea.” *Prog Retin Eye Res.* 18(4):529-51(1999).

Franken PA, Hill AE, Peters CW, and Weinreich G. “Generation of Optical Harmonics.” *Phys. Rev. Lett.*7, 118-19 (1961).

Freeman IL. “Collagen polymorphism in mature rabbit cornea.” *Invest Ophthalmol Vis Sci.* 17(2):171-7 (1978).

Freund I and Deutsch M. “Connective tissue polarity. Optical second-harmonic microscopy, crossed-beam summation, and small-angle scattering in Rat-tail tendon.” *Biophys. J.* 50, 693–712 (1986).

Fujimoto JG, Lin WZ, Ippen EP, Puliafito CA, and Steinert RF. “Time-resolved studies of Nd:YAG laser-induced breakdown: Plasma formation, acoustic wave generation, and cavitation.” *Invest Ophthalmol Vis Sci.* 26(12):1771-7 (1985).

Funderburgh JL, Funderburgh ML, Mann MM, Corpuz L, and Roth MR. “Proteoglycan expression during transforming growth factor beta-induced keratocyte-myofibroblast transdifferentiation.” *J.Biol.Chem.*276:44173–44178 (2001).

Garcia ZE, Rothenberg ME, Ownbey RT, Celestin J, Leder P, and Luster AD. “Human eotaxin is a specific chemoattractant for eosinophil cells and provides a new mechanism to explain tissue eosinophilia.” *Nat. Med.* 2:449–456 (1996).

Gipson IK, Spurr-Michaud SJ, and Tisdale AS. “Anchoring fibrils form a complex network in human and rabbit cornea.” *Invest Ophthalmol Vis Sci.* 28(2):212-220 (1987).

Glazer PM, Saumyen N. Sarkar, and William C. Summers, “Detection and Analysis of UV-Induced Mutations in Mammalian Cell DNA Using a λ Phage Shuttle Vector.” *PNAS* vol. 83-4 1041-44 (1986).

Goepfert-Meyer M. “über elementarakte mit zwei quantansprüngen.“ Goettinger Dissertation. *Ann.Phys.* 9. 273-294 (1931).

Goldman JN and Benedek GB. “The relationship between morphology and transparency in the nonswelling corneal stroma.” *Invest. Ophthalmol. Vis. Sci* 6, 574-600 (1967).

Goldman JN, Benedek GB, Dohlman CH, and Kravitt B. “Structural alterations affecting transparency in swollen human corneas.” *Invest. Ophthalmol. Vis. Sci* 7, 501-519 (1968).

Grand D, Bernas A, and Amouyal E. “Photonionisation of aqueous indole, conducting band edge and energy gap in liquid water.” *Chem. Phys.* 44, p73-79 (1979).

Greulich KO and Weber G. “The light microscope on its way from an analytical to a preparative tool.” *J. Microsc.* 167, 127-151 (1992).

Grimmett MR and Holland EJ. “Complications of small clear-zone radial keratotomy.” *Ophthalmology* 103(9):1348-56 (1996).

Gu M and Sheppard CJR. “Comparison of three-dimensional imaging properties between two-photon and single-photon fluorescence microscopy.” *J. Microsc.* 177:128-137 (1995).

Guo Y, Ho PP, Savage H, Harris D, Sacks P, Schantz S, Liu F, Zhadin N, and Alfano RR. “Second-harmonic tomography of tissue.” *Opt. Lett.* 22:1323-25 (1997).

Guo Y, Savage HE, Liu F, Schantz SP, Ho PP, and Alfano RR. “Subsurface tumor progression investigated by noninvasive optical second harmonic tomography.” *PNAS* 14, 96(19): 10854-56 (1999).

Habib MS, Speaker MG, Kaiser R, and Juhasz T. “Myopic intrastromal photorefractive keratectomy with the neodymium-yttrium lithium fluoride picosecond laser in the cat cornea.” *Arch Ophthalmol.*113:499-505 (1995).

Halbhuber KJ, Koenig K, “Modern Laser Scanning Microscopy in Biology, Biotechnology and Medicine.” *Ann. Anat.* 185, 1-20 (2003).

Halbhuber KJ, Krieg R, Fischer P, Koenig K, Nasse H, Dietz W, “Jenfluor-ap - A novel fluorogenic substrate for in situ detection of alkaline phosphatase activity.” *Cell. Mol. Biol.*10.1170/42 (2002)

Han M, Giese G, and Bille JF. “Second harmonic generation imaging of collagen fibrils in cornea and sclera.” *Opt. Express* 13, 5791-97 (2005).

Hanna KD, Pouliquen YM, Savoldelli M, Fantes F, Thompson KP, Waring GO 3rd, and Samson J. “Corneal wound healing in monkeys 18 months after excimer laser photorefractive keratectomy.” *Refract. Corneal Surg.* 6(5):340-5 (1990).

Harris AK, Stopak D, and Wild P. “Fibroblast traction as a mechanism for collagen morphogenesis.” *Nature* 290: 249-51 (1981).

Hensley K, Maidt ML, Yu Z, Sang H, Markesbery WR, and Floyd RA. “Electrochemical analysis of protein nitrotyrosine and dityrosine in the Alzheimer brain indicates region-specific accumulation.” *J. Neurosci.* 18, 8126-32 (1998).

Heisterkamp A, Mamom T, Kermani O, Drommer W, Welling H, Ertmer W, and Lubatschowski H. “Intrastromal refractive surgery with ultrashort laser pulses: in vivo study on the rabbit eye.” *Graefes Arch Clin Exp Ophthalmol.* 241(6):pp511-7 (2003).

Huang S, Heikal AA, and Webb WW. “Two-Photon Fluorescence Spectroscopy and Microscopy of NAD(P)H and Flavoprotein.” *Biophys. J.* 82(5), 2811-25 (2002).

Jester JV, Barry-Lane PA, Cavanagh HD, and Petroll WM. “Induction of alpha-smooth muscle actin expression and myofibroblast transformation in cultured corneal keratocytes.” *Cornea*, 15(5):505-16 (1996).

Juhasz T, Loesel FH, Horvath C, Kurtz RM, and Mourou G. “Corneal Refractive Surgery with Femtosecond Lasers.” *IEEE J. Sel. Top. Quantum Electron.* 5, 902-10 (1999).

Kato T, Nakayasu K, Hosoda Y, Watanabe Y, and Kanai A. “Corneal wound healing following laser in situ keratomileusis (LASIK): a histopathological study in rabbits.” *Br J Ophthalmol* 83:1302-05 (1999).

Kato T, Chang JH, and Azar DT. “Expression of type XVIII collagen during healing of corneal incisions and keratectomy wounds.” *Invest Ophthalmol Vis Sci.* 44(1):78-85 (2003).

Kaiser W and Garrett CGB. “Two-Photon Excitation in CaF₂: Eu²⁺.” *Phys. Rev. Lett.* 7, 229–231 (1961).

Kezirian GM and Stonecipher KG. “Comparison of the IntraLase femtosecond laser and mechanical keratomes for laser in situ keratomileusis.” *J Cataract Refract Surg.* 30:804-811(2004).

Kim BM, Eichler J, and Da Silva LB. “Frequency doubling of ultrashort laser pulses in biological tissues.” *Appl. Optics.* 38:7145-50(1999).

Kleinman DA, Ashkin A, and Boyd GD. “Second-Harmonic Generation of Light by Focused Laser Beams.” *Phys. Rev.* 145, 338–79 (1966).

Koenig K, Krasieva T, Bauer E, Fiedler U, Berns MW, Tromberg BJ, and Greulich KO. “Cell Damage by UVA Radiation of a Mercury Microscopy Lamp Probed by Autofluorescence Modifications, Cloning Assay, and Comet Assay.” *J. Biomedical Optics*, 1(2) 217-222 (1996).

Koenig K, Riemann I, Fischer P, and Halbhuber KJ. “Intracellular nanosurgery with near infrared femtosecond laser pulses.” *Cell Mol Biol* 45(2):195-201 (1999).

Koenig K. “Multiphoton Microscopy in Life Sciences.” *J. Microscopy* 200, 83-104 (2000).

Koenig K, Riemann I, and Fritzsche W. “Nanodissection of human chromosomes with near-infrared femtosecond laser pulses”. *Optics Letters*, Vol.26, pp819-821 (2001).

- Koenig K, Krauss O, and Riemann I.** “Intratissue surgery with 80 MHz nanojoule femtosecond laser pulses in the near infrared.” *Opt. Express* 10, 171-176 (2002a).
- Koenig K, Wollina U, Riemann I, Peuckert C, Halbhuber KJ, Fünfstück V, Fischer TW, and Elsner P.** “Optical tomography of human skin with subcellular spatial and picosecond time resolution.” *SPIE-Proceed.* 4620191-201 (2002b).
- Koenig K, Riemann I, Krauss O, Fritzsche W.** “Nanodissection of human chromosomes and ultraprecise eye surgery with nanojoule near-infrared femtosecond laser pulses.” *Proc. SPIE* Vol. 4633, p. 11-22 (2002c).
- Koenig K and Riemann I.** “High-resolution multiphoton tomography of human skin with subcellular spatial resolution and picosecond time resolution.” *J Biomed Opt.* 8(3):432-9 (2003).
- Koenig K, Schenke-Layland K, Riemann I, Stock UA.** “Multiphoton autofluorescence imaging of intratissue elastic fibers.” *Biomaterials.* 26(5):495-500 (2005).
- Krieg R and Halbhuber KJ.** “Recent advances in catalytic peroxidase histochemistry.” *Cell. and Mol. Biol.* 49, 547-563 (2003).
- Krueger J and Kautek W.** “Femtosecond-pulse visible laser processing of transparent materials.” *Appl. Surf. Sci.* 430–38 (1996).
- Kurtz RM, Liu X, Elnor VM, Squier JA, Du D, and Mourou GA.** “Photodisruption in the human cornea as a function of laser pulse width.” *J Refract Surg.* 13 (7):pp653-8 (1997).
- Kurtz RM, Horvath C, Liu HH, Krueger RR, and Juhasz T.** “Lamellar refractive surgery with scanned intrastromal picosecond and femtosecond laser pulses in animal eyes.” *J Refract Surg.* 14(5):pp541-8 (1998).
- Kuwabara T.** “Current concepts in anatomy and histology of the cornea.” *Cont Introc Lens Med J.* 4:101 (1978).
- Labermeier U, Demlow TA, and Kenney MC.** “Identification of collagens isolated from bovine Descemet's membrane.” *Exp Eye Res.* 37(3):225-37(1983).
- Larson DT, Zipfel WR, Williams RM, Clark S, Bruchez M, Wise F, and Webb WW.** “Water-Soluble Quantum Dots with Large Two-Photon Cross-sections for Multiphoton Fluorescence Imaging *in vivo*.” *Science* 300 (5624), 1434-36 (2003).
- Latvala T, Barraquer–Coll C, Tervo K, and Tervo T.** “Corneal wound healing and nerve morphology after excimer laser in situ keratomileusis (LASIK) in human eyes.” *J Refract Surg* 12,677-683 (1996).
- Laule A, Cable MK, Hoffman CE, and Hanna C.** “Endothelial cell population changes of human cornea during life.” *Arch Ophthalmol.* 96:2031–2025(1978).
- Lee BH, McLaren JW, Erie JC, Hodge DO, and Bourne WM.** “Reinnervation in the Cornea after LASIK.” *Invest. Ophthalmol. Vis. Sci.* 43(12): 3660 – 3664 (2002).
- Lenzner M, Krüger J, Sartania S, Cheng Z, Spielmann Ch, Mourou G, Kautek W, and Krausz F.** “Femtosecond optical breakdown in dielectrics.” *Phys. Rev. Lett.* 80, 4086 (1998).
- Light ND.** “Bovine type I collagen: A study of cross-linking in various mature tissues.” *Biochim Biophys Acta.* 581(1):96-105 (1979).

Lin SJ, Hsiao CY, Sun Y, Lo W, Lin WC, Jan GJ, Jee SH, and Dong CY. “Monitoring the thermally induced structural transitions of collagen by use of second-harmonic generation microscopy.” *Opt. Lett.* 30(6), 622-4 (2005).

Linna TU, Pérez-Santonja JJ, Tervo K, Sakla, HF, Alió JL, and Tervo TMT. “Recovery of corneal nerve morphology following laser in situ keratomileusis.” *Exp Eye Res* 66,755-763 (1998).

Linna TU, Vesaluoma MH, Pérez-Santonja JJ, Petroll WM, Alió JL, and Tervo TMT. “Effect of Myopic LASIK on Corneal Sensitivity and Morphology of Subbasal Nerves.” *Invest Ophthalmol Vis Scie* 41:393-397 (2000).

Loesel FH, Niemz MH, Bille JF, and Juhasz T. “Laser-Induced Optical Breakdown on Hard and Soft Tissues and Its Dependence on the Pulse Duration: Experiment and Model.” *IEEE J. Quantum Electron* 32, 1717- 1722 (1996).

Lubatschowski H, Maatz G, Heisterkamp A, Hetzel U, Drommer W, Welling H, and Ertmer W. “Application of ultrashort laser pulses for intrastromal refractive surgery.” *Graefe’s Arch. Clin. Exp. Ophthalmol.* 238, 33-39 (2000).

Lubatschowski H, Heisterkamp A, Will F, Singh A, Serbin J, Ostendorf A, Kermani O, Heermann R, Welling H, and Ertmer W. “Medical applications for ultrafast laser pulses”. *Focused on Laser Precision Microfab* (2002).

Manger CC. “The IntraLase Advantage.” *Ophthalmology Management* (2004).

Maltseva O, Folger P, Zekaria D, Petridou S, and Masur SK. “Fibroblast Growth Factor Reversal of the Corneal Myofibroblast Phenotype.” *Invest Ophthalmol Vis Sci.* 42:2490-95 (2001).

Mardelli P, Piebenga L, Matta C, Hyde L, and Gira J. “Corneal Endothelial Status 12 to 55 Months after Excimer Laser Photorefractive Keratectomy.” *Ophthalmology* 102:544-9 (1995).

Masters BR, So PT, and Gratton E. “Multiphoton excitation fluorescence microscopy and spectroscopy of in vivo human skin.” *Biophysical J.* Vol 72, 2405-12 (1997).

Masters, B.R., So, P. and Gratton, E., "Optical Biopsy of In Vivo Human Skin: Multi-photon Excitation Microscopy," *Lasers in Medical Science*, 13, 197-204 (1998).

Masur SK, Dewal HS, Dinh TT, Erenburg I, and Peteridou S. “Myofibroblasts differentiate from fibroblasts when plated at low density.” *PNAS*, 93: 4219-23 (1996).

Maurice DM. “The structure and transparency of the cornea.” *J. Physiol* 136, 263-286 (1957).

McCrone EL, Lucey DR, and Weller PF. “Fluorescent staining for leukocyte chemotaxis. Eosinophil-specific fluorescence with aniline blue.” *J Immunol Methods* 114:79-88 (1988).

Meyer K, Linker A, Davidson EA, and Weissmann B. “The mucopolysaccharides of bovine cornea.” *J Biol Chem.* 205:611–616 (1953).

Millard AC, Jin L, Wie MD, Wuskell JP, Lewis A, and Loew LM. “Sensitivity of Second Harmonic Generation from Styryl Dyes to Transmembrane Potential.” *Biophysical J.* 86:1169-76 (2004).

Mimura T, Yamagami S, Yokoo S, Yanagi Y, Usui T, Ono K, Araie M, and Amano S. “Sphere therapy for corneal endothelium deficiency in a rabbit model.” *Invest Ophthalmol Vis Sci.* 46(9):3128-35 (2005).

- Moller-Pedersen T.** “A comparative study of human corneal keratocyte and endothelial cell density during aging.” *Cornea* 16,333-338 (1997).
- Moller-Pedersen T, Cavanagh HD, Petroll WM, and Jester JV.** “Stromal wound healing explains refractive instability and haze development after photorefractive keratectomy: a 1-year confocal microscopic study.” *Ophthalmology*. 107(7):1235-45 (2000).
- Moreaux L, Sandre O, Blanchard-Desce M, and Mertz J.** “Membrane imaging by second-harmonic generation microscopy.” *Optics Lett*. 25, 320-22 (2000).
- Mueller M, Sqier J, Wilson KR, and Brakenhoff GJ.** “3D-microscopy of transparent objects using third-harmonic generation.” *J. Microsc* 191, 266-74 (1998).
- Munnerlyn CR, Koons SJ, Marshall J:** Photorefractive keratectomy: a technique for laser refractive surgery. *J Cataract Refract Surg* 1988 Jan; 14(1): 46-52.
- Nakayasu K, Tanaka M, Konomi H, and Hayashi T.** “Distribution of types I, II, III, IV and V collagen in normal and keratoconus corneas.” *Ophthalmic Res*. 18(1):1-10 (1986).
- Nolte S, Chichkov BN, Welling H, Shani Y, Lieberman K, and Terkel H.** “Nanostructuring with spatially localized femtosecond laser pulses.” *Opt. Lett*. 24, 914 (1999).
- Nordan LT, Slade SG, Baker RN, Suarez C, Juhasz T, and Kurtz R.** “Femtosecond laser flap creation for laser in situ keratomileusis: six-month follow-up of initial U.S. clinical series”. *J Refract Surg*. 19(1):8-14 (2003).
- Oliveira-Soto L and Efron N.** “Morphology of corneal nerves using confocal microscopy.” *Cornea*. 20(4):374-84(2001).
- Pallikaris IG, Siganos DS:** Excimer laser in situ keratomileusis and photorefractive keratectomy for correction of high myopia. *J Refract Corneal Surg* 1994 Sep-Oct; 10(5): 498-510.
- Patel SV, McLaren JW, Hodge DO, and Bourne WM.** “Normal human keratocyte density and corneal thickness measurement by using confocal microscopy in vivo.” *Invest Ophthalmol Vis Sci* 42,333-339 (2001).
- Peleg G, Lewis A, Linial M, and Loew LM.** “Nonlinear optical measurement of membrane potential around single molecules at selected cellular sites.” *PNAS*, Vol. 96, Issue 12, 6700-04 (1999).
- Prince JH, Diesem CD, Eglitis I, and Ruskell GL.** “Anatomy and Histology of the Eye and Orbit in Domestic Animals.” Charles C. Thomas, *Springfield* (1960).
- Rahi AH and Robins E.** “Human corneal endothelial cell repair in health and disease.” *Trans Ophthalmol Soc UK*. 101:30–34 (1981).
- Rocha G and Schultz GS.** “Corneal wound healing in laser in situ keratomileusis.” *Int Ophthalmol Clin*. 36(4):9-20 (1996).
- Roth S and Freund I.** “Second harmonic-generation in collagen.” *J. Chem. Phys*. 70:1637-43 (1979).
- Rowsey JJ, Reynolds AE, and Brown R.** “Corneal topography.” *Arch Ophthalmol* 99, 1093 (1981).

- Rozsa AJ and Beuerman RW.** "Density and organization of free nerve endings in the corneal epithelium of the rabbit." *Pain*.14(2):105-20(1982).
- Sandler SS.** "Direct three-dimensional reconstruction of a corneal stromal lamella from electron micrographs." *J Theor Biol.* 48, 207-13 (1974).
- Sawada H, Konomi H, and Hirosawa K.** "Characterization of the collagen in the hexagonal lattice of Descemet's membrane: its relation to type VIII collagen." *J Cell Biol.* 110(1):219-27(1990).
- Schaffer CB, Brodeur A, Garcia JF, and Mazur E.** "Micromachining bulk glass by use of femtosecond laser pulses with nanojoule energy." *Optics Letters*, Vol.26 pp 93-5 (2001).
- Schaffer CB, Garcia JF, and Mazur E.** "Bulk heating of transparent materials using a high-repetition-rate femtosecond laser." *Appl. Phys. A* 76, 351-354 (2003).
- Schanzlin DJ, Asbell PA, Burris TE, and Durrie DS.** "The intrastromal corneal ring segments: phase II results for the correction of myopia." *Ophthalmology* 104(7):1067-78 (1997).
- Schenke-Layland K, Riemann I, Opitz F, Koenig K, Halbhuber KJ, Stock UA.** "Comparative study of cellular and extracellular matrix composition of native and tissue engineered heart valves." *Matrix Biol.* 23(2):113-25 (2004).
- Seiler T, Koufala K, and Richter G.** "Iatrogenic keratectasia after laser in situ keratomileusis." *J.Refract Surg* 14:312-317 (1998).
- Shen N, Schaffer CB, Datta D, and Mazur E.** "Photodisruption in biological tissues and single cells using femtosecond laser pulses." Conference on *Lasers and Electro-Optics*, pp. 403-04 (2001).
- Shen N, Datta D, Schaffer CB, LeDuc P, Ingber DE, and Mazur E.** "Ablation of cytoskeletal filaments and mitochondria in live cells using a femtosecond laser nanoscissor." *Tech Science Press MCB*, vol.2, no.1, pp.17-25 (2005).
- Shen YR.** "The Principles of Nonlinear Optics." New York: Wiley (1984).
- So, P.T.C., French, T., Yu, W., Berland, K.M., Dong, C.Y., and Gratton E.,** "Time-resolved Fluorescence Microscopy Using Two-photon Excitation," *Bioimaging*, 3, 49-63 (1995).
- Stern D, Schoenlein RW, Puliafito CA, Dobi ET, Birngruber R, and Fujimoto JG.** "Corneal Ablation by Nanosecond, Picosecond, and Femtosecond Lasers at 532 nm and 625 nm." *Arch. Ophthalmol.* 107, 587-592 (1989).
- Stoller PC., Celliers PM., Reiser KM, and Rubenchik AM.** "Imaging collagen orientation using polarization-modulated second harmonic generation." *Proc. SPIE* Vol. 4620, p. 157-165 (2002a).
- Stoller PC, Reiser KM, Celliers PM, and Rubenchik AM.** "Polarization-modulated second harmonic generation in collagen." *Biophys. J.* 82:3330-42 (2002b).
- Stuart BC, Feit MD, Herman S, Rubenchik AM, Shore BW, and Perry MD.** "Optical ablation by high-power short-pulse lasers." *J. Opt. Soc. Am. B* 13, 459-468 (1996).
- Stulting RD, Thompson KP, Waring GO 3rd, and Lynn M.** "The effect of photorefractive keratectomy on the corneal endothelium." *Ophthalmology.* 103(9):1357-65 (1996).

Sugar A, Rapuano CJ, Culbertson WW, Huang D, Varley GA, Agapitos PJ, de Luise VP, and Koch DD. “Laser In Situ Keratomileusis for Myopia and Astigmatism: Safety and Efficacy.” *Ophthalmology* 109:175-87 (2002).

Talley AR, Hardten DR, Sher NA, et al: Results one year after using the 193-nm excimer laser for photorefractive keratectomy in mild to moderate myopia. *Am J Ophthalmol* 1994 Sep 15; 118(3): 304-11.

Taylor RS, Hnatovsky C, Simova E, Rayner DM, Bhardwaj VR, and Corkum PB. “Femtosecond laser fabrication of nanostructures in silica glass.” *Opt. Lett.* 28, 1043–45 (2003).

Terry MA, Ousley PJ, and Will B. “Practical Femtosecond Laser Procedure for DLEK Endothelial Transplantation: Cadaver Eye Histology and Topography.” *Cornea.* 24 (4):453-59 (2005).

Tirlapur UK and Koenig K. “Near-infrared femtosecond laser pulses as a novel non-invasive means for dye-permeation and 3D imaging of localised dye-coupling in the *Arabidopsis* root meristem.” *Plant J.* 20:363–70 (1999).

Tirlapur UK and Koenig K. “Targeted transfection by femtosecond laser.” *Nature* 418, pp290-291(2002a).

Tirlapur UK and Koenig K. “Femtosecond near-infrared laser pulses as a versatile non-invasive tool for intra-tissue nanoprocessing in plants without compromising viability.” *Plant J.* 31(3):365-74. (2002b).

Toivanen M, Tervo T, Partanen M, Vannas A, and Hervonen A. “Histochemical demonstration of adrenergic nerves in the stroma of human cornea.” *Invest Ophthalmol Vis Sci.* 28(2):398-400 (1987).

Tseng SC, Smuckler D, and Stern R. “Comparison of collagen types in adult and fetal bovine corneas.” *J Biol Chem.* 257(5):2627-33 (1982).

Tran DB, Sarayba MA, Bor Z, Garufis C, Duh YJ, Soltes CR, Juhasz T, and Kurtz RM. “Randomized prospective clinical study comparing induced aberrations with IntraLase and Hansatome flap creation in felloweyes: potential impact on wavefront-guided laser in situ keratomileusis.” *J Cataract Refract Surg.* 31(1):97-105 (2005).

Tyrrell RM and Keyse SM. “The interaction of UVA radiation with cultured cells.” *J Photochem Photobiol B.*4(4):349-61 (1990).

Van Horn DL and Hyndiuk RA. “Endothelial wound repair in primate cornea.” *Exp Eye Res.* 21:113 (1975).

Van Horn DL, Sendele DD, Seideman S, and Bucu PJ. “Regenerative capacity of the corneal endothelium in rabbit and cat.” *Invest Ophthalmol Vis Sci.*16:597–613(1977).

Vesaluoma M, Pérez-Santonja J, Petroll W, Linna T, Alió J, and Tervo T. “Corneal Stromal Changes Induced by Myopic LASIK.” *Invest Ophthalmol Vis Scie.*41:369-376 (2000).

Vogel A, Noack J, Nahen K, Theisen D, Busch S, Parlitz U, Hammer D, Noojin G, Rockwell B, and Birngruber R. “Energy balance of optical breakdown in water at nanosecond to femtosecond time scales.” *Appl. Phys. B* 68, 271–280 (1999).

Vogel A. “Optical breakdown in water and ocular media, and its use for intraocular photodisruption.” *Shaker Verlag, Aachen* (2001).

Vogel A and Venugopalan V. “Mechanisms of Pulsed Laser Ablation of Biological Tissues.” *Chem. Rev.* 103, 2, 577-644 (2003).

Walther H. et al. (Eds.). “Frontiers in Nonlinear Optics.” (1993).

Wang M. “Femtosecond technology: Is now the time to buy?” *Refractive Eye care for Ophthalmologists* (2003).

Waring GO III, Bourne WM, Edelhauser HF, and Kenyon KR. “The corneal endothelium. Normal and pathologic structure and function.” *Ophthalmology* 89:531-590 (1982).

Waring GO: History of radial keratotomy. In: Sanders DR, Hofmann RF, Salz JJ, eds. *Refractive Corneal Surgery*. Thorofare, NJ; 1985: 3-14.

Waring GO III, Casebeer JC, and Dru RM. “One year results of prospective multicenter study of the Casebeer system of refractive keratotomy.” *Ophthalmology* 103(9):1337-47 (1996).

Watanabe W, Arakawa N, Matsunaga S, Higashi T, Fukui K, Isobe K, and Itoh K. “Femtosecond laser disruption of subcellular organelles in a living cell.” *Opt. Express* 12, 4203-4213 (2004).

Watsky MA, Griffith M, Wang DA, and Tigyi GJ. “Phospholipid Growth Factors and Corneal Wound Healing.” *Annals of the New York Academy of Sciences* 905:142-158 (2000).

Wilson SE and Kim WJ. “Keratocyte apoptosis: implications on corneal wound healing, tissue organization, and disease.” *Invest Ophthalmol Vis Sci* 39,220-226 (1998).

Wilson SE and Hong JW. “Bowman's layer structure and function: critical or dispensable to corneal function? A hypothesis.” *Cornea*;19(4):417-20 (2000).

Williams RM, Zipfel WR, and Webb WW. “Multiphoton microscopy in biological research.” *Curr Opin Chem Biol* 5(5): 603-8 (2001).

Williams RM, Zipfel WR, and Webb WW. “Interpreting Second-Harmonic Generation Images of Collagen I Fibrils.” *Biophys. J.* 88, 1377-86 (2005).

www.femto-lasik-pro.com/femto-lasik/ablauf.html

www.pacificseyecare.com/eyecare

www.allaboutvision.com/resources/statistics-laser-eye-surgery.htm

Xu C, Williams RM, Zipfel WR, and Webb WW. “Multiphoton Excitation Cross-Sections of Molecular Fluorophores.” *Bioimaging* 4(3), 198-207 (1996).

Yanik MF, Cinar H, Cinar HN, Chisholm AD, Jin Y, and Ben-Yakar A. “Neurosurgery: Functional regeneration after laser axotomy.” *Nature* 432, 822 (2004).

Ye HQ, Maeda M, Yu FSX, and Azar DT. “Differential expression of MT1-MMP (MMP14) and collagenase III (MMP13) genes in normal and wounded rat corneas.” *Invest. Ophth. Vis. Sci.* 41: 2894–9 (2000).

Yeh P. “Introduction to Photorefractive Nonlinear Optics.” New York: Wiley (1993).

Zhang Y, Conrad AH, Tasheva ES, An K, Corpuz LM, Kariya Y, Suzuki K, and Conrad GW. “Detection and quantification of sulfated disaccharides from keratan sulfate and chondroitin/dermatan sulfate during chick corneal development by ESI-MS/MS.” *Invest Ophthalmol Vis Sci.* 46(5):1604-14 (2005).

Zieske JD. “Extracellular matrix and wound healing.” *Curr. Opin. Ophthalmol.* 12(4):237-41 (2001).

Zimmermann DR, Trueb B, Winterhalter KH, Witmer R, and Fischer RW. “Type VI collagen is a major component of the human cornea.” *FEBS Lett.* 3;197(1-2):55-8 (1986).

Zipfel WR, Williams RM, and Webb WW. “Nonlinear Magic: Multiphoton Microscopy in the Biosciences.” *Nat. Biotechnol.* 21(11), 1369-77 (2003a).

Zipfel WR, Williams RM, Christie R, Nikitin AY, Hyman BT, and Webb WW. “Live tissue intrinsic emission microscopy using multiphoton-excited native fluorescence and second harmonic generation.” *PNAS*, 100(12), 7075-80 (2003b).

Zoumi A, Yeh A, and Tromberg BJ. “Imaging cells and extracellular matrix in vivo by using second-harmonic generation and two-photon excited fluorescence.” *PNAS.* 99(17):11014-19 (2002).

Zoumi A, Lu X, Kassab GS, and Tromberg BJ. “Imaging Coronary Artery Microstructure Using Second-Harmonic and Two-Photon Fluorescence Microscopy.” *Biophysical J.* 87:2778-2786 (2004).

Results

Before the multiphoton imaging, the cornea thickness of rabbits was measured with a Pachometer (Corneo-Gagetm plus 2, Sonogage, U.S.) and made a comparison with cornea of porcine and human being.

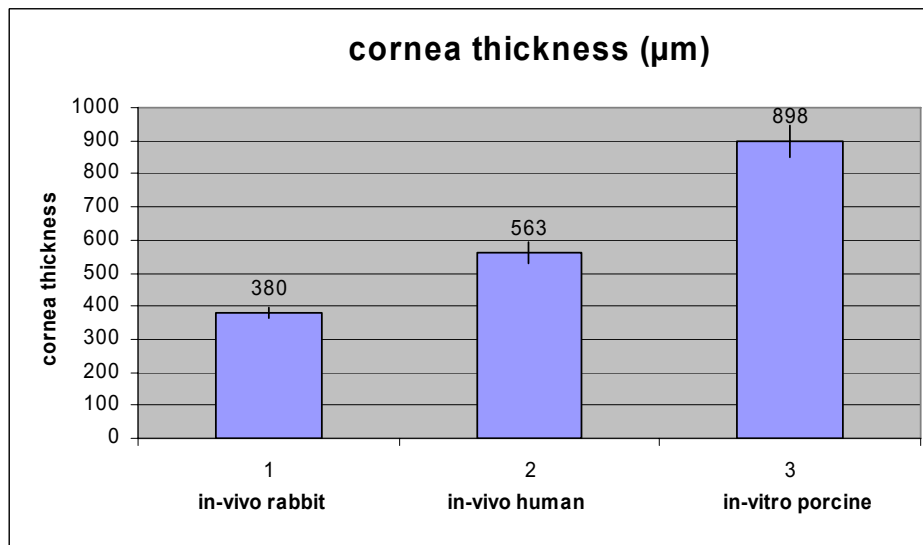


Fig.15 Comparison of average central cornea thickness of rabbits, human and porcine. **1:** In-vivo rabbits: $380\mu\text{m}\pm 18\mu\text{m}$ measured with Pachometer (measurement of this work); **2:** In-vivo human: $563.0\pm 31.1\mu\text{m}$ (Patel *et al.* 2001); **3:** In-vitro porcine: $898\mu\text{m}\pm 48\mu\text{m}$, measurement with Pachometer ($n=50$, measurement of this work).

1. In-vivo corneal optical nonlinear imaging based on multiphoton microscopy

1.1 Optical tomography of corneal tissue based on 2PF: Optical overview of cornea

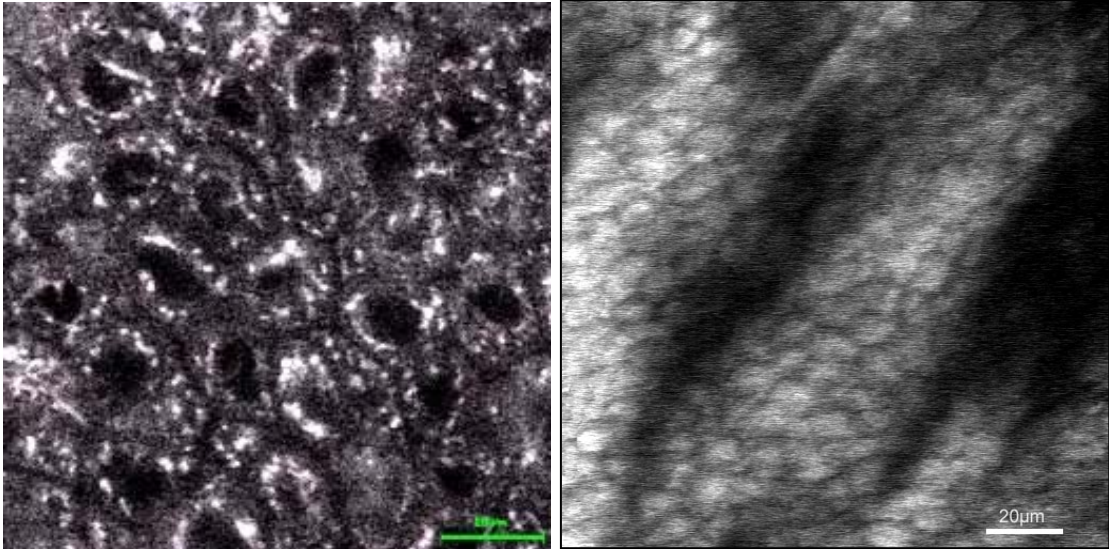


Fig.16_1 Nonlinear optical images of epithelial squamous cells and basal cells. **Left:** Corneal epithelium (squamous cells) at a depth of 10 μ m. Scale bar: 10 μ m; **Right:** Image of fluorescent epithelial basal cells and non-fluorescent collagen in basement membrane with 760nm at a depth of 36 μ m. Scale bar: 20 μ m.

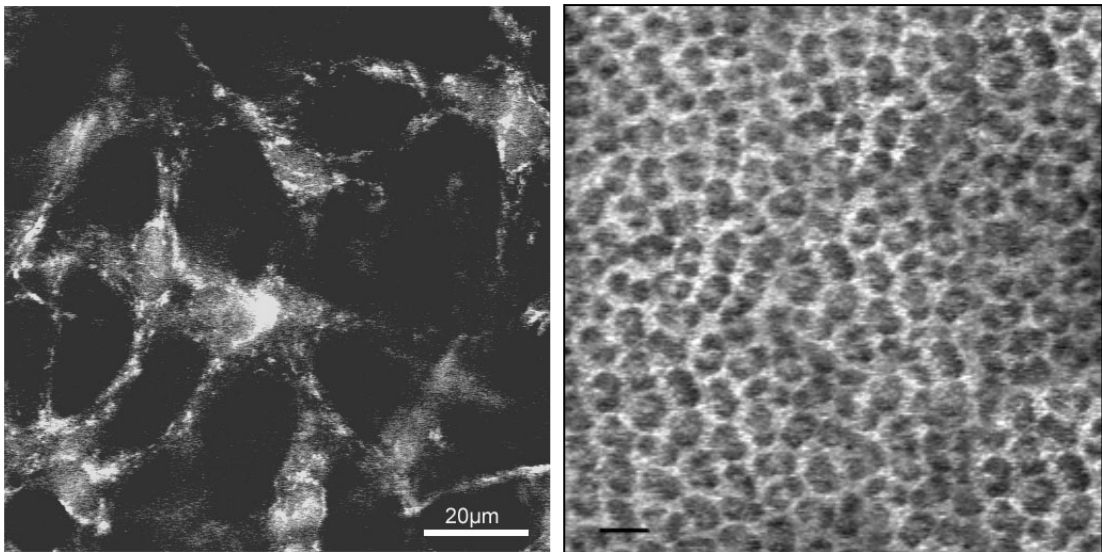


Fig.16_2 Nonlinear optical images of keratocytes and endothelial cells. **Left:** Stromal keratocytes at a depth of 80 μ m. Scale bar: 20 μ m; **Right:** Endothelial cells at a depth of 375 μ m. Scale bar: 10 μ m.

In general, the cells imaged at 760nm displayed (i) the fluorescent cytoplasmatic granules of mitochondria; (ii) non-fluorescent nuclei displayed darkly on the optical section surrounded by the fluorescent mitochondria; (iii) and the clear cellular boundary.

With respect to Fig.16_1R, the fluorescent basal cells and the non-excited collagen at the wavelength of 760nm are displayed. With 1 μ m-depth further scanning, the

keratocytes in stroma would be detected. Presumably, the non-fluorescent black portion on this optical image was the basement membrane of the basal cells belonging to epithelium.

The pave-stone mosaic pattern of the hexagonal endothelial cells (Fig.16_2R) shows only slight variation in size and shape. With this optical tomography, the thickness of the continuous monolayer endothelial cells was determined to be $8.42 \pm 2.12 \mu\text{m}$. The homogenous cells have an average volume of $7.38 \pm 1.25 \mu\text{m}$ in diameter.

1.1.1 Three-dimensional imaging of epithelial cells (three sublayers) with subcellular resolution and high contrast based on 2PF imaging at wavelength of 760nm.

According to conventional histology, the epithelium of cornea is distinguished into 3 sub-layers (squamous cells, wing cells and basal cells) based on the different cell morphology. With the assistance of TAI at wavelength of 760nm, the three epithelial layers can be also optically visualized in-vivo.

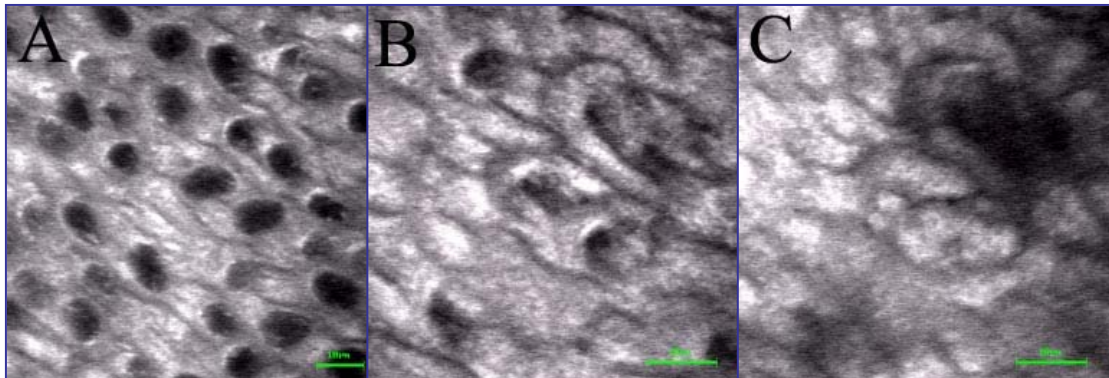


Fig.17_1 Optical nonlinear tomography of epithelium. **A**, epithelial squamous cells at a depth of $10 \mu\text{m}$; **B**, epithelial wing cells at a depth of $20 \mu\text{m}$; **C**, epithelial basal cells at a depth of $30 \mu\text{m}$. Scale bar: $10 \mu\text{m}$.

The in-vivo thickness of epithelium of New Zealand rabbit was determined to be approximately $38.6 \pm 5.8 \mu\text{m}$ under multiphoton microscope.

As shown in Fig.17_1, squamous cells are characterized by flat cell bodies and oval to round non-fluorescent nuclei surround by the cytoplasmic fluorescent granules (NAD(P)H in mitochondria) and located in the surfacial epithelial layer. Wing cells have 2-3 wing-shaped polygonal cellular contours and are in the middle epithelial layer. The single columnar basal cells contact with the basal membrane which lays over the stroma.

1.1.2 Three-dimensional imaging of stromal keratocytes based on 2PF at wavelength of 760nm.

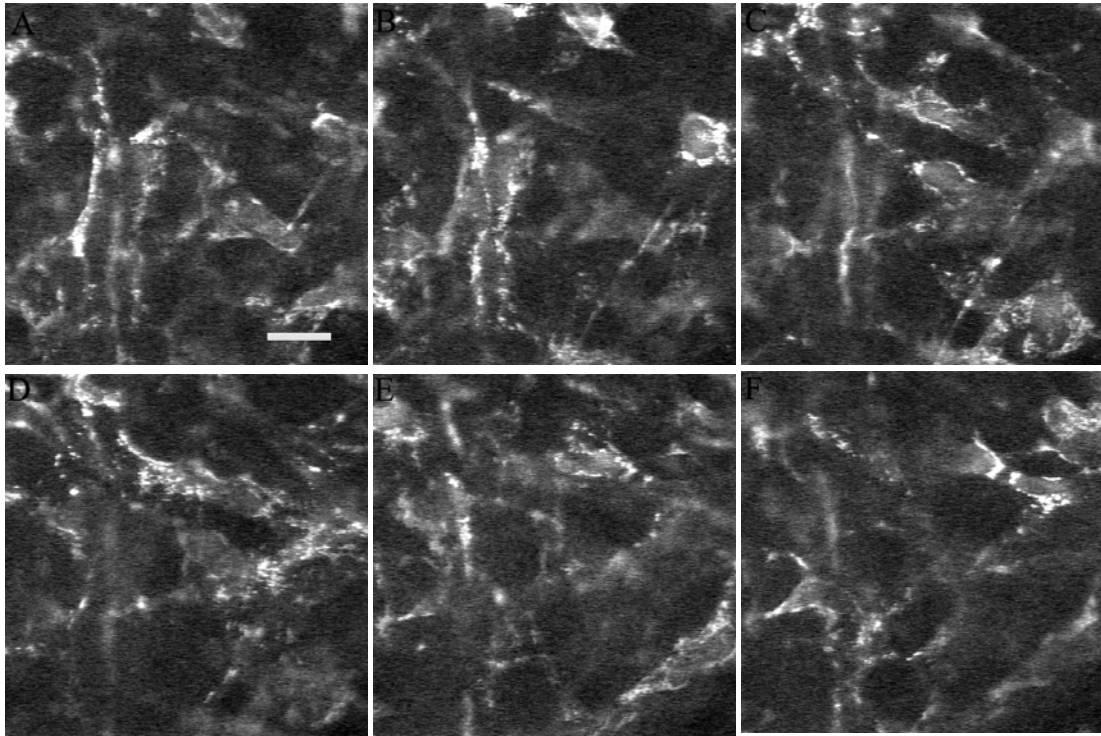


Fig.17_2 Optical nonlinear tomography of stromal keratocytes with z-interval of 5 μ m based on multiphoton autofluorescence imaging at wavelength of 760nm. **A:** at a depth of 80 μ m. Scale bar: 15 μ m.

Based on the intrinsic fluorescence, the stroma cells can be three-dimensionally visualized. As showed in Fig.17_2, the keratocytes can be defined by the non-fluorescent nuclei and fluorescent cytoplasm filled with mitochondria. The cell processes connecting cells with each other responsible for communications of signal and nutritive substance can be also observed. Owing to the high spatial resolution, each cell can be morphologically studied (Fig.18).

1.2 Nonlinear optical tomography of stromal collagen lamellas based on SHG

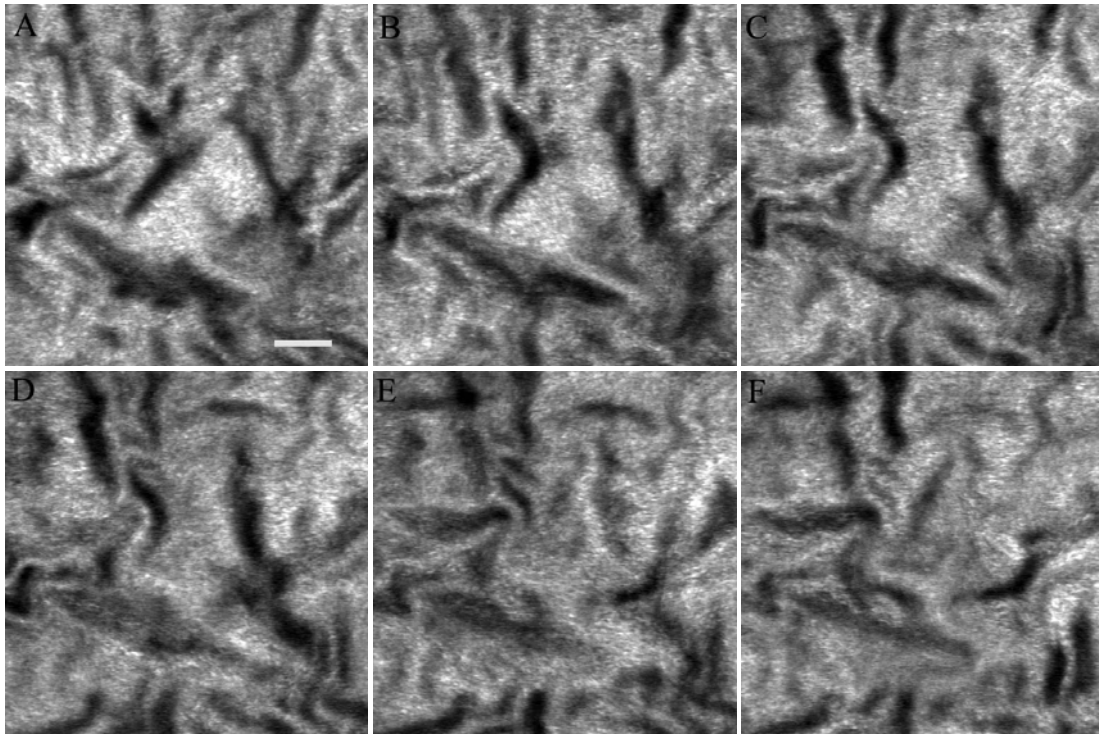


Fig.17_3 In-vivo collagen lamellar nonlinear optical sectioning with z-interval of 5 μ m based on second harmonic imaging at wavelength of 830nm in backward direction. **A:** at a depth of 90 μ m. Scale bar: 10 μ m.

With the assistance of SHG, the in-vivo nonlinear optical tomography of collagen lamellas in cornea with high resolution becomes realizable for the first time. The collagen can be selectively demonstrated owing to autofluorescence deficiency of keratocytes at wavelength of 830nm. As illustrated in Fig.17_3, distribution and orientation of the collagen lamella is clearly revealed by the optical imaging. In correlation with the z-position, the three-dimension of collagen architectures can be studied. They are densely packed with characteristic fluctuation and run parallel to the corneal surface. However, in the x-y dimension, the lamellas have different orientations, especially on the surface of keratocytes.

1.3 Comparison of optical nonlinear images based on 2PF and SHG at a same plane of cornea stroma, only with two different wavelengths (760nm and 830nm respectively).

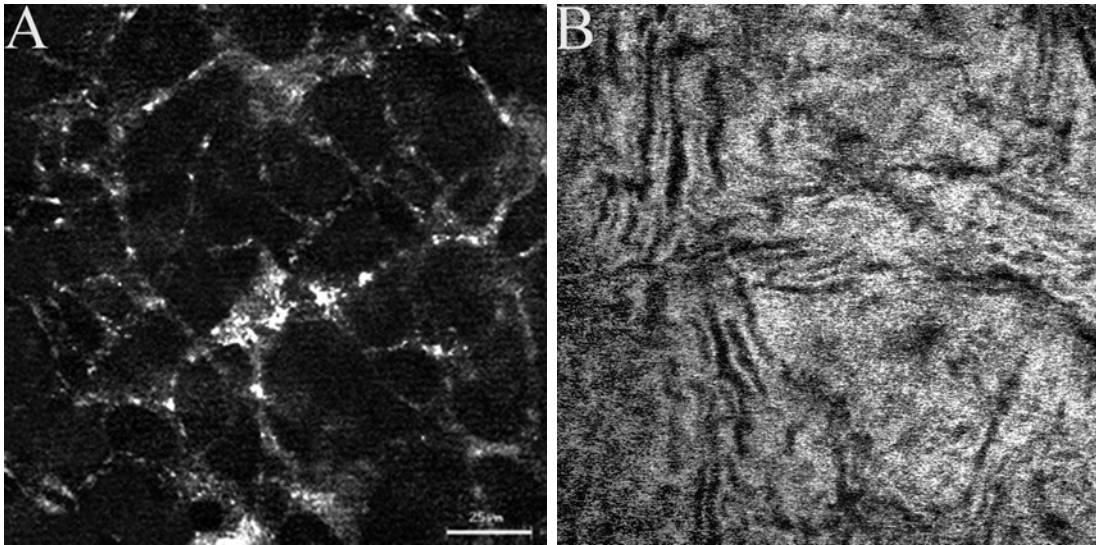


Fig.18 Nonlinear optical imaging of stromal tissue at a depth of 100µm. **A:** Image of keratocytes at wavelength of 760nm; **B:** Collagen lamellas based on SHG at wavelength of 830nm in backward direction. Scale bar: 25µm for both.

Interestingly, keratocytes and ECM such as collagen lamellas can be selectively displayed only with two different laser wavelengths, which yield two distinct images for a same region in stroma.

The keratocytes can be identified through the fluorescent cytoplasm and dark non-fluorescent nuclei on Fig.18A with wavelength of 760nm. Cellular boundary can be identified since the collagen in ECM at 760nm can only be excited very weakly (Zoumi *et al.* 2004). Using this high-resolution optical imaging, the cell morphology could be studied in-vivo. Here, based on measurement of more than 100 cells, the mean volume value of three-dimensional keratocytes was calculated. ($18.48 \pm 3.46 \mu\text{m} \times 13.53 \pm 2.87 \mu\text{m} \times 9.78 \pm 1.88 \mu\text{m}$; measurement based only on the cell body without processes, up to 140 µm depth of stroma).

As illustrated in Fig.18B, distribution and orientation of the collagen lamellas is clearly revealed by this optical imaging. The in-vivo optical imaging of stromal collagens provides reliable evidence to the characteristics of cornea which accords perfectly with the conventional histological architectures of the cornea described previously (Freeman *et al.* 1978).

2. In-vivo application of multiphoton imaging in viewing intrastromal surgery

2.1 Evaluating intrastromal nanosurgery performed by near-infrared nanojoule femtosecond lasers at a depth of 100 μm .

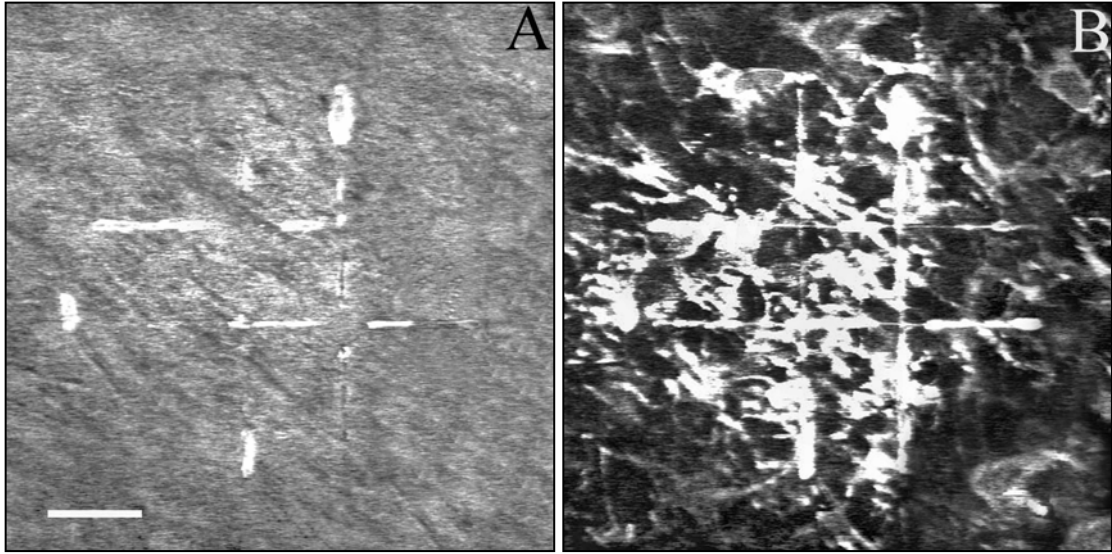


Fig.19 Real-time nonlinear optical observations of intrastromal femtosecond laser nanosurgery with submicron size (0.4-0.6 μm) at a depth of 100 μm . **A**: Imaging at wavelength of 830nm in backward directions; **B**: Imaging at wavelength of 760nm. Scale bar: 45 μm .

With assistance of the nonlinear optical imaging, the targeted region for intrastromal surgery could be determined pre-operation. After the visualization of cornea by this imaging, the laser was directed in the region of interest for surgical procedures. After intrastromal nanosurgery performed with a laser power of 130mW at wavelength of 800nm with line scan (zoom=1.3, t=1s, at a depth of 100 μm), the optical imaging (autofluorescence at 760nm Fig.19B and SHG at 830nm Fig.19A) were taken with lower laser power of 20mW immediately (within 10s).

As seen on the optical sections, 4 laser cuts were acquired with submicron size (0.4-0.6 μm). Some transient subtle bubbles with a diameter of 2-3 μm , lifetimes of within 2 seconds along the lines were detected. The cut edges became more luminescent. With this imaging technique, the surgical performance can be visualized and evaluated on-line and in real time. Additionally, the intact keratocytes were displayed very nicely on the image at 760nm and the collagen lamella was showed on the figure at 830nm, which are comparable with Fig.18. The intactness of surrounding tissue indicates the ultrahigh precision of intrastromal nanosurgery.

2.2 Advantages of SHG in visualizing intrastromal surgery

2.2.1 Physiological architecture of collagen lamellas imaged with SHG

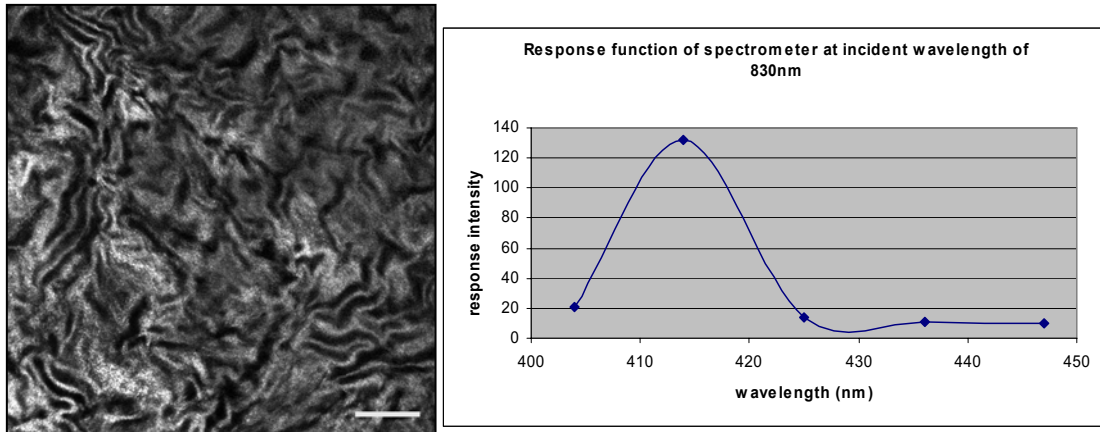


Fig.20 SHG image and λ -scanning of emission wavelength. **Left:** SHG imaging with emission spectrum from 405nm to 425nm (415/10) in backward direction of intact corneal stroma at incident wavelength of 830nm (40x 1.3 oil, 16s, zoom=1.5). Scale bar: 10 μ m. **Right:** The response function of used spectrometer at incident wavelength of 830nm was measured by λ -scanning (Zeiss Axiovert 200 microscope, 510-Meta) with spectrum from 404nm to 447nm. This diagram showed that the highest intensity of collagen SHG was located at 415nm with the excitation wavelength of 830nm.

Cells could not be observed on the SHG image due to deficiency of suitable intrinsic cellular noncentrosymmetric structures. Presumably, the unluminescent site on Fig.20L surrounded by the confused collagen lamellae could correspond to the cell bodies in position.

2.2.2 Observations of intrastromal surgery 24 hours postoperation

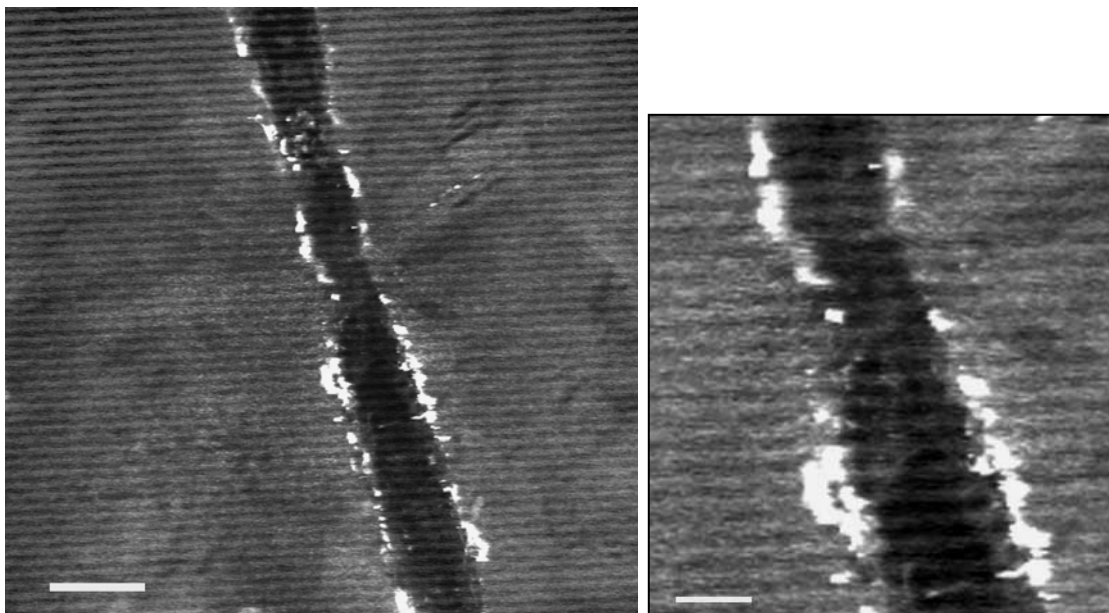


Fig.20_1 SHG observations on intrastromal nanosurgery 24 hours postoperation. **Left:** SHG imaging of nanosecond-laser corneal laser surgery in stroma imaged 24 hours postoperation (depth of 115 μ m, 40x 1.3 oil, 16s, zoom=1.3 for imaging). **Right:** The magnification of portion of left figure. Scale bar: Left, 15 μ m; Right, 5 μ m.

The space of intrastromal collagen dissection with z-step of 2 μm from 110 μm up to 120 μm can be clearly observed even 24 hour after the intrastromal surgery (Fig.20_1). The surgery was performed with mean power of 160mw (at depth of 110 μm) to 178mW (at depth of 120 μm) only in perpendicular direction at wavelength of 800nm (Fig.20_2). The figure shows the collagen lamellas were 100% dissected. The luminescence at the edges of the cut becomes much weaker but can be still seen. The cell infiltration in the surrounding tissue has been also recorded in-vivo (Wang *et al.* 2005). The Fig.20_1R with high resolution shows the ultrahigh precision of surgical outcomes without destructive effects in the surrounding edges and tissue, which is the most overwhelming advantages comparing with μJ femtosecond lasers which induce the intratissue huge bubbles and tissue streaks in the surrounding region.

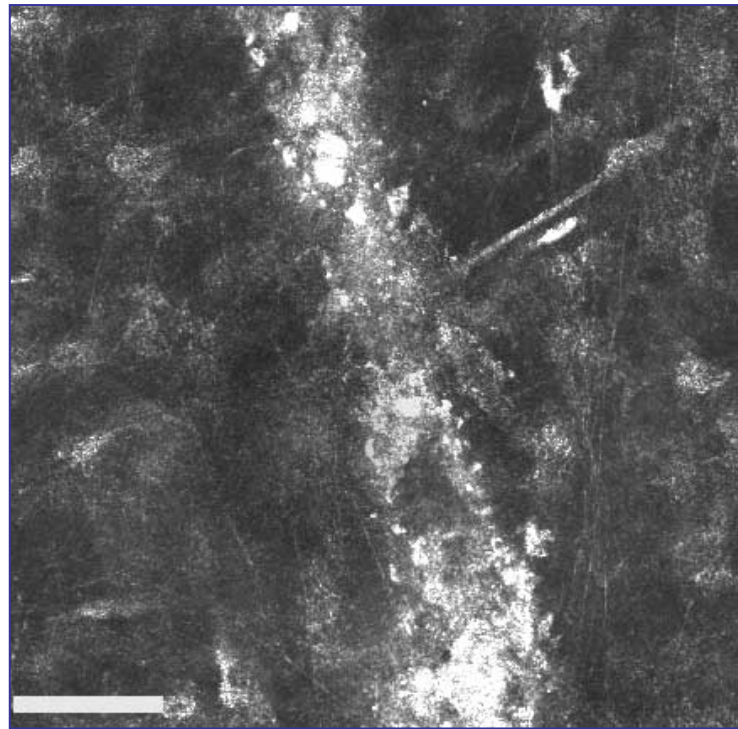


Fig.20_2 Optical imaging of intrastromal nanosurgery 24 hours postoperation. In order to demonstrate the advantages of SHG in displaying the intrastromal cut postoperation, the reflexion imaging at the same plane was also taken with the same wavelength and other imaging parameters. Scale bar: 15 μm .

The interface of the intrastromal cut could no more be evaluated with this reflecting imaging (Fig.20_2) method because migrating cells such as myofibroblasts, eosinophils filling this space (the differentiation of migrating cells on histological sections was described previously, Fig.21_4). Furthermore, the cells in the interface space can be excited at wavelength of 760nm due to the intrinsic fluophore NAD(P)H, thereby it can

be inferred that the surgical performance could also not be demonstrated with the 2PF imaging at 760nm. In this case, the second harmonic imaging showed its significant advantage in comparison with reflecting and autofluorescence imaging.

3. In-vivo intrastromal ablation with epithelium intact

3.1 Optical imaging during laser intrastromal ablation

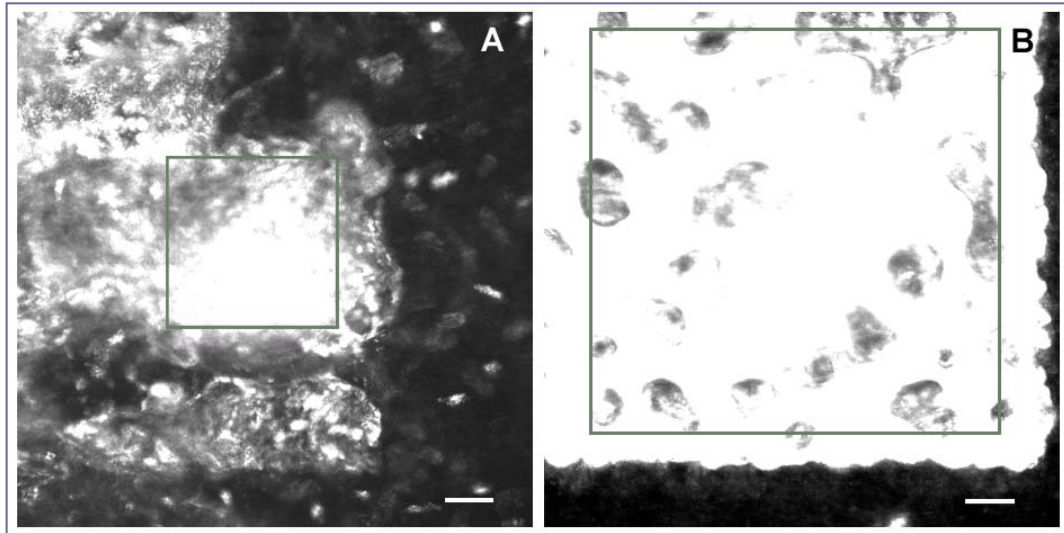


Fig.21_1 On-line optical observations on intrastromal ablation. **A:** Optical imaging during intrastromal ablation at a depth of 113 μm (scan parameters: 16s, 195mW, 800nm, 512 x 512 pixels covering full frame 320 μm x 320 μm , 40x 1.3 oil). **B:** Magnification of portion of ablated area in A. The boundary line between the ablated and unablated region is clearly sharp. Scale bar: A, 15 μm ; B, 10 μm .

With the assistance of nonlinear optical tomography, the laser beam was directed on an intrastromal targeted region between 110 μm and 120 μm . The mean laser power was then enhanced to 190-210mW (mean power, corresponding to 2.4-2.6nJ pulse energy and 15.2-16.8kW peak power) to obtain a high focus light intensity of an order of TW/cm^2 , which induced the intrastromal surgical process. Since the formation of plasma is spatially confined to the 0.1 femtoliter focal volume of the 40x objective with high numerical aperture, there is virtually no perturbation in the surrounding components.

During and immediately following the laser treatment, the localization and lifetime of the plasma-induced ablation was monitored on-line with a CCD camera. The clear boundary between the treated and untreated area implicates the high precision of the nanojoule laser pulses. The treated tissue became more luminous than the untreated tissue under the reflexion images. Collateral effects including tissue streaks, thermal and

mechanical effects out of the focus to the surrounding tissue could not be observed even with the high-spatial resolution (Fig.21_1B).

3.2 Histological observations on intrastromal ablation (immediate results)

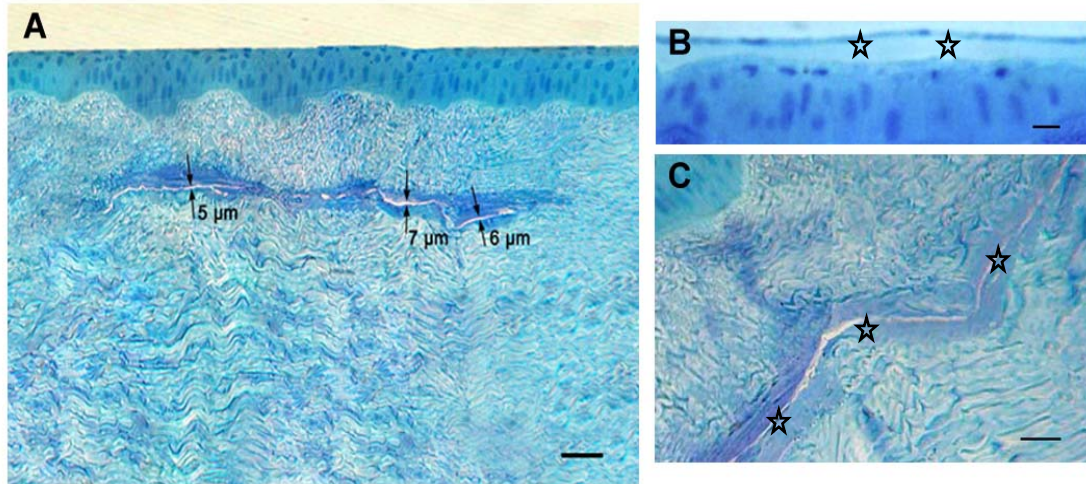


Fig.21_2 Histological cross-sections stained with methylene blue displaying the immediate ablation outcomes. **A:** Intrastromal ablation. The distance of the intrastromal fissure amounts to 5-7 μ m. **B:** The ultra-precise intraepithelial ablation meanwhile leaving the 1-2 layers of squamous cells intact. **C:** The magnifications of portion of the ablated area on Fig. A. The stars mark the intratissue fissure. Scale bar: A, 30 μ m; B, 10 μ m; C, 15 μ m.

The removal of the stromal tissue such as collagen was verified by histological outcomes (Fig.21_2). The intrastromal ablation with fissure formation was generated by parking the laser into a depth of 120 μ m with full frame of 320 x 320 μ m, at 16s scan time per frame and 210mW mean laser power. Subsequently, five further focal planes were processed in the same way using z-step of 2 μ m up to 110 μ m tissue depth with less power (for example, 190mW at depth of 110 μ m). The optical imaging after the 10 μ m stack-tissue ablation was similar to that shown in Fig.21_1 and displayed obviously more luminescence than the untreated surrounding region. No each distinguished bubble was detected during the laser process at suitable power (190-210mW) at depth (110-120 μ m).

The cornea was clear after the treatment. The laser-exposed eyes underwent histological examination. This was the hardest part of this study due to the difficulty in relocalizing the treated intrastromal site, especially in the follow-up studies in which the intrastromal lesions have healed. With the special methods developed in our group, we have been able to definitely relocalize the treated region although the wounds have healed.

As showed in Fig.21_2, the ablated intrastromal tissue varied from 5 to 7 μ m on the histological section. The epithelial layer and part of stroma ventral to the ablated area remained nicely intact. The tissue of the surrounding region seemed to be changed due to the strengthening of the stained colour. The streak effect in adjacent tissue was not observed on the histological sections. With the high-resolution of magnified illustration (Fig.21_2C), the intratissue ablation can be more precisely studied. With the similar procedure (much lower laser power), we have tried the intratissue ablation in epithelium and attained as well the intraepithelial fissure (Fig.21_2B).

3.3 Follow-up on wound repair of intrastromal ablation (at days of 4th, 7th, 15th and 28th postoperation)

Using a slip lamp and a stereomicroscope as well the aforementioned self-developed techniques, the treated region has been conclusively relocated. However, the treated cornea at each of the respective schedule was as clear as the control eye.

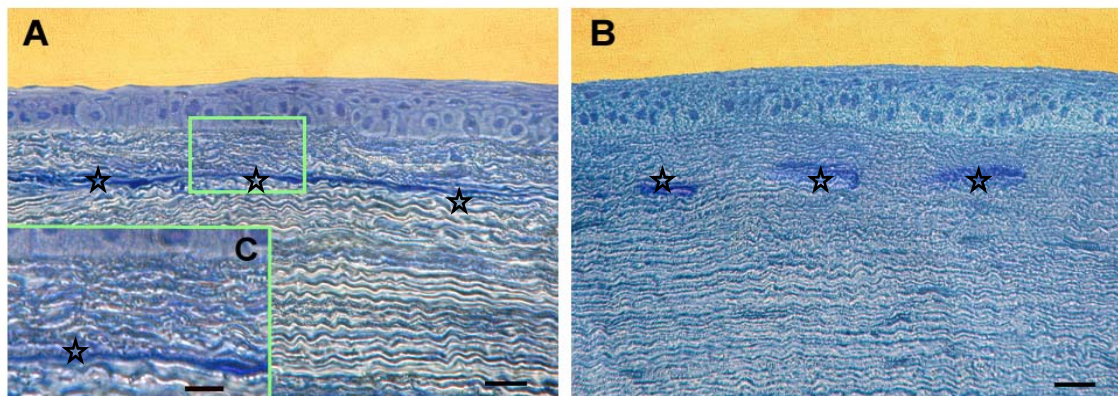


Fig.21_3 Histological observations on wound repair of intrastromal ablation at 4th and 7th days. **A:** Showing that the fissure disappeared and the two cut edges merged again at 4th day postoperation. **B:** The surgical fissure in stroma became more unclear and unctiguous at 7th day. **C:** Magnification of portion of figure A. The stars mark the interfaces. Scale bar: A and B, 20 μ m; C, 5 μ m.

As showed on Fig.21_3, the space of the fissure can no longer be observed due to merging of the two cut edges. The interface was still continuous at 4th day (Fig.21_3A). By contrast, only portion of the interface could be perceived at 7th day (Fig.21_3B). In addition, the epithelium kept nicely intact. At 15th and 28th day, the traces of the intrastromal ablation could no longer be identified on histological sections by visual inspection due to wound healing and tissue reconstruction.

3.4 Cells activations in the treated cornea during wound healing process:

In-vivo 2PF imaging of activated stromal keratocytes (myofibroblasts).

The intensified granular autofluorescence imaging based on two-photon excitation of NAD(P)H in mitochondria enabled the activated cells to be selectively demonstrated at 760nm. The mean powers used here were 25mW at a depth of 115 μ m and the scan time was 8s (frame scan).

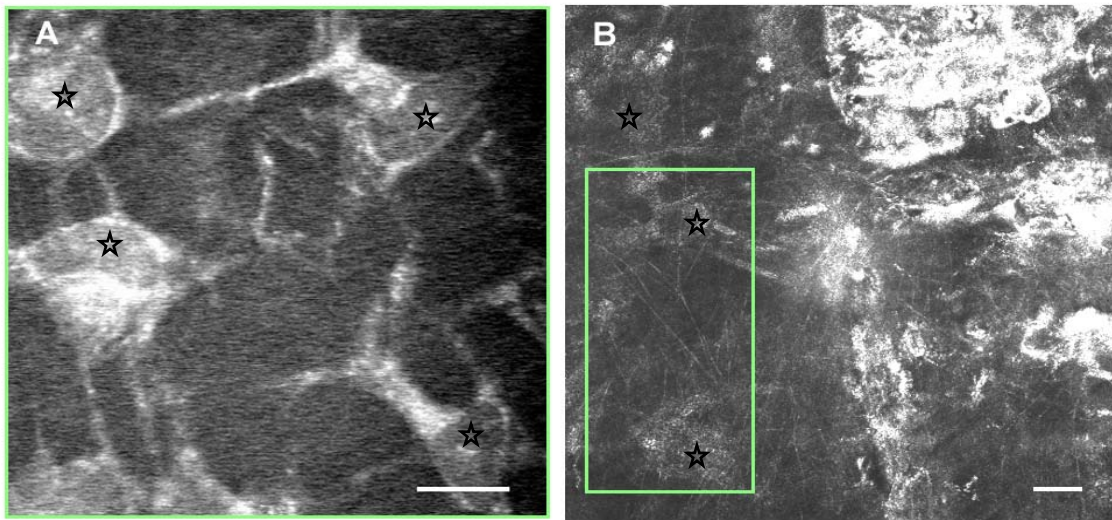


Fig.21_4 Optical detecting on emergence of myofibroblasts. **A:** In-vivo three-dimensional cellular nonlinear optical imaging based on 2PF at a wavelength of 760nm with subcellular high resolution. Magnified illustration of portion of figure B. **B:** Optical imaging of the treated cornea 24 hours postoperation showing the ablated area and the cell aggregates. Stars mark the activated keratocytes (in both figures). Scale bar: 20 μ m for both.

The corneas were examined again with the multiphoton microscope 24 hours postoperation. The treated cornea was clear. The luminescence in the ablated area observed under the microscope became weaker. Unexpectedly, cell aggregates in the surrounding region within 50 μ m far away from the lesion site were detected (Fig.21_4B). Due to their special morphology characterized by oval to round-shaped nuclei, 25-30 μ m-volume hypertrophic cell bodies (smaller than 20 μ m in physiological state Fig.18, 2.3/comparison of nonlinear optical imaging of keratocyte) and augmented cell processes (5-7 processes in physiological state), these cells suggest themselves to be the activated intrastromal keratocytes (myofibroblasts). The nuclei were surrounded by the intensified fluorescent NAD(P)H granular in mitochondria. In the control cornea, there was no such cell aggregates observed.

4. In-vivo multiphoton-mediated generation of corneal flap

4.1 Optical observations during performing corneal flaps

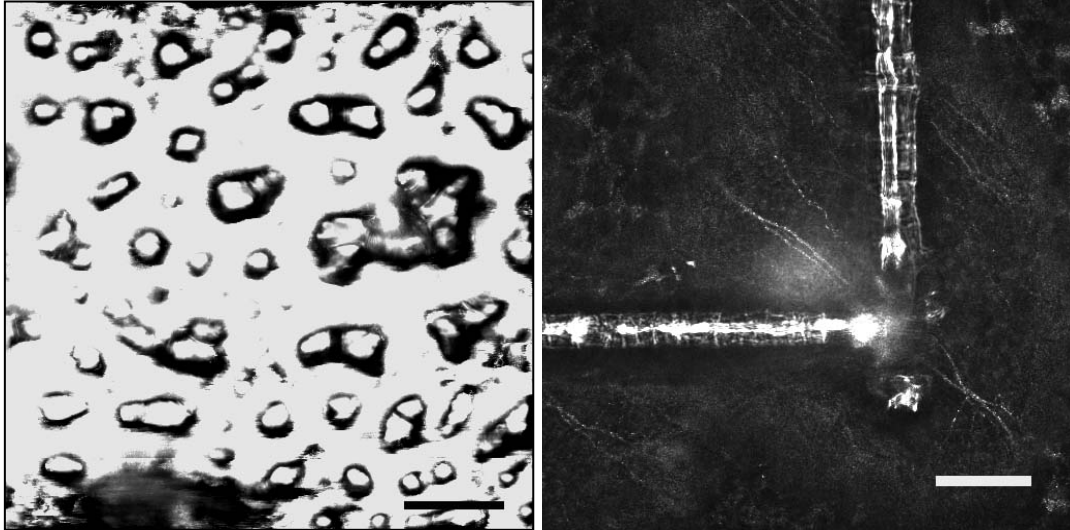


Fig.22_1 Optical images during flap generation at a depth of $120\mu\text{m}$ in cornea. **Left:** Horizontal flap bed performed with frame scanning. Scale bar: $10\mu\text{m}$. **Right:** Perpendicular cuts generated for cube walls of a corneal flap. Scale bar: $20\mu\text{m}$.

With the assistance of nonlinear optical tomography, the laser beam was directed on an intrastromal targeted region at a depth of $120\mu\text{m}$ to generate flap bed firstly. The mean laser power was enhanced to 188mW (mean power, corresponding to 2.35nJ pulse energy and 15.06KW peak power) to obtain a high focus light intensity at an order of TW/cm^2 , which induced intrastromal optical breakdown. The frame scan time was 16s with $\text{zoom}=1$ (full frame, Fig.22_1L). If large bed wished, this procedure should be iterative for numerous times according to the requirement. For example, the same 16 beds should be done for a flap with $1280\mu\text{m} \times 1280\mu\text{m}$. Secondly, the perpendicular walls were generated from $120\mu\text{m}$ to surface with different aforementioned laser powers and parameters correlating with corneal depth. Only three walls of the tissue cube were generated and the fourth was kept intact serving as flap hinge in this work. As shown on Fig.22_1R, there is virtually no perturbation in the surrounding tissue components since the formation of plasma is spatially confined to the focal volume.

4.2 Immediate outcomes of corneal flaps

With the above-mentioned procedures for generation of flap bed and walls, the two flaps in different depths were accomplished with two animals (Fig.22_2). With the

assistance of a mini-tweezers under a stereomicroscope, the flap with thickness of $120\mu\text{m}$ was tugged and lifted within 1 minute after laser operation. The lifted flap kept in a complete form is shown as on Fig.22_2. This corneal specimen with lifted flap was further treated for SEM (Fig.23) after photographing.



Fig.22_2 Photographs of corneal flaps taken immediately after the laser operation. **Left:** Unlifted flap with a volume of $1280\mu\text{m} \times 1280\mu\text{m} \times 60\mu\text{m}$ taken within 2 minutes postoperation ($60\mu\text{m}$ means the thickness of flap); **Right:** A lifted corneal flap with volume of $1280\mu\text{m} \times 1280\mu\text{m} \times 120\mu\text{m}$ taken after lifting within 3 minutes after laser operation ($120\mu\text{m}$ means the thickness of flap). Bar: 2mm.

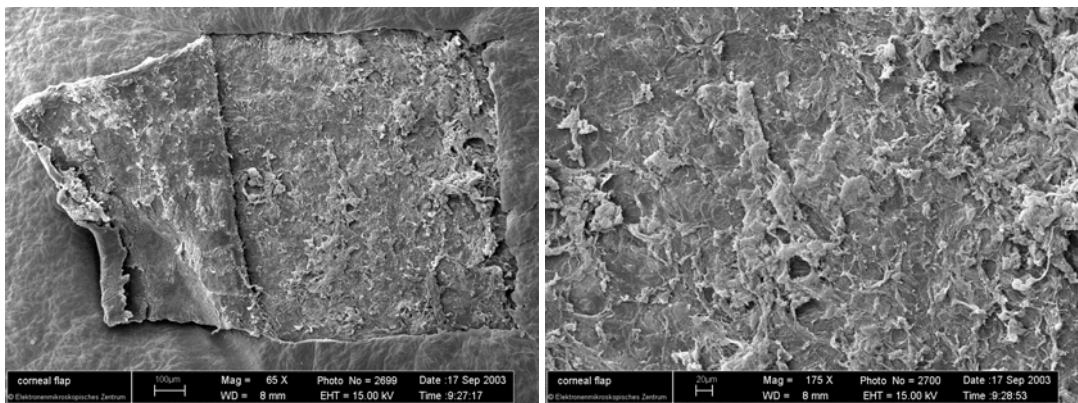


Fig.23 SEM of the lifted corneal flap shown on Fig.22_2R. **Left:** Overview of flap. Bar: $100\mu\text{m}$; **Right:** Magnification of flap bed with high resolution. Bar: $20\mu\text{m}$.

4.3 Following-up on wound repair of the unlifted corneal flaps

4.3.1 Flap at 1st day postoperation

The all flaps generated in this study were well kept in-situ through protection of the third lid during follow-up period. The treated eyes were much sensitive to light and the eye lids were in half-open-state. No significant corneal turbidity was observed. The perpendicular cuts can be still identified under the slit lamp and the stereomicroscope on 90th day postoperation.

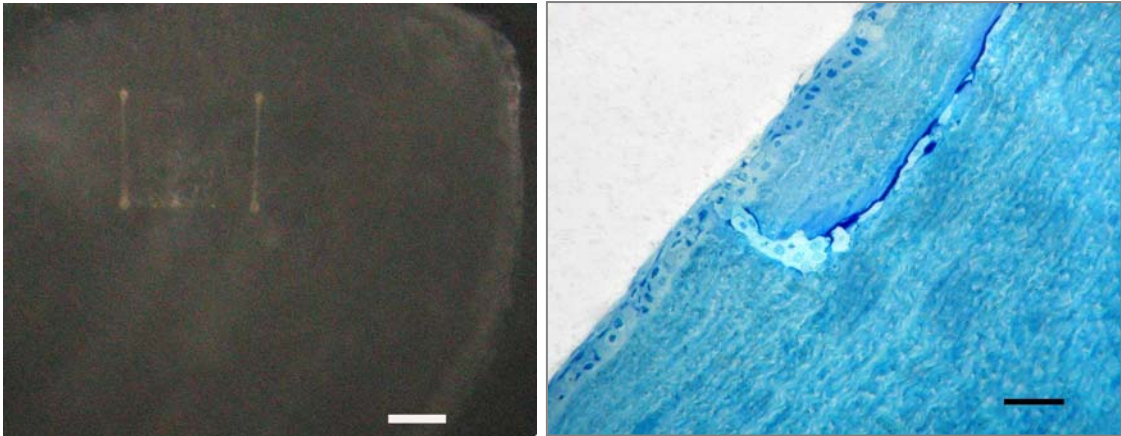


Fig.24 Observations on wound repair at 1st day. **Left:** Photograph of an unlifted flap scheduled for one-day follow-up preserved in 3% cacodylate-buffered glutaraldehyde for 24 hours. The three perpendicular cuts could be still identified. Bar: 500 μ m. **Right:** Light micrograph of a semi-thin cross-section stained by methylene blue of the left corneal specimen showing that the epithelial vertical incision healed totally. The migrating cells in the cut space are detailed in Fig.24_1. Bar: 40 μ m.

Epithelial and subepithelial layers as well as the adjacent region of intrastromal cuts were kept nicely intact on the histological sections (Fig.24R).

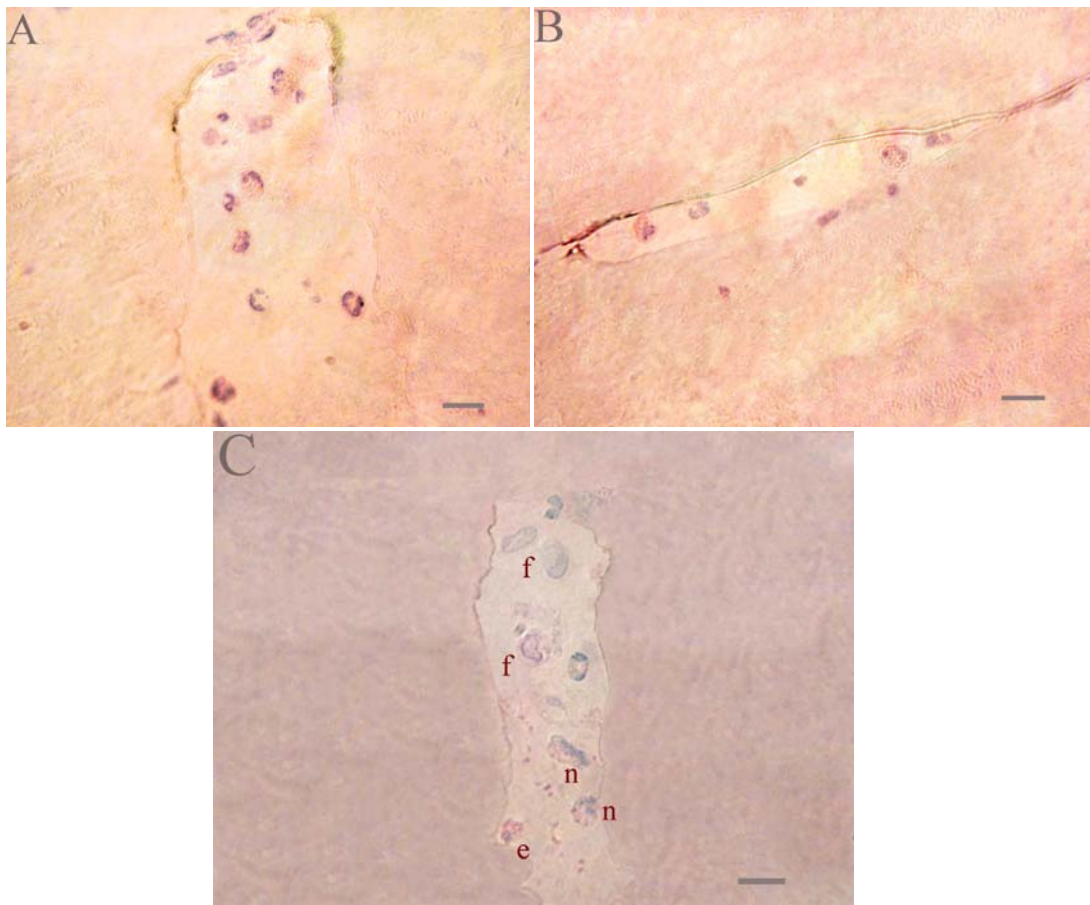


Fig.24_1 Histological observations on the migrating inflammatory cells at 1st day. HE-stained cross-sections of Fig.24 showing the inflammatory cells in the perpendicular and horizontal cut

spaces. **e**: eosinophils; **n**, neutrophils; **f**, fibroblasts. Scale bar: 20 μ m (three figures taken with 100x objective).

With the conventional HE-staining, the cells could be defined by characteristic cellular morphology as inflammatory cells, presumably including neutrophils and fibroblasts (section A and B). Eosinophilic cells also appeared on section C. The laser-effect at the cut edges could be still seen (section A and B).

The collateral effects including tissue streaks, thermal and mechanical effects could not be perceived in the adjacent tissue even with this high resolution (100x, oil).

4.3.2 Flap at 7th day postoperation

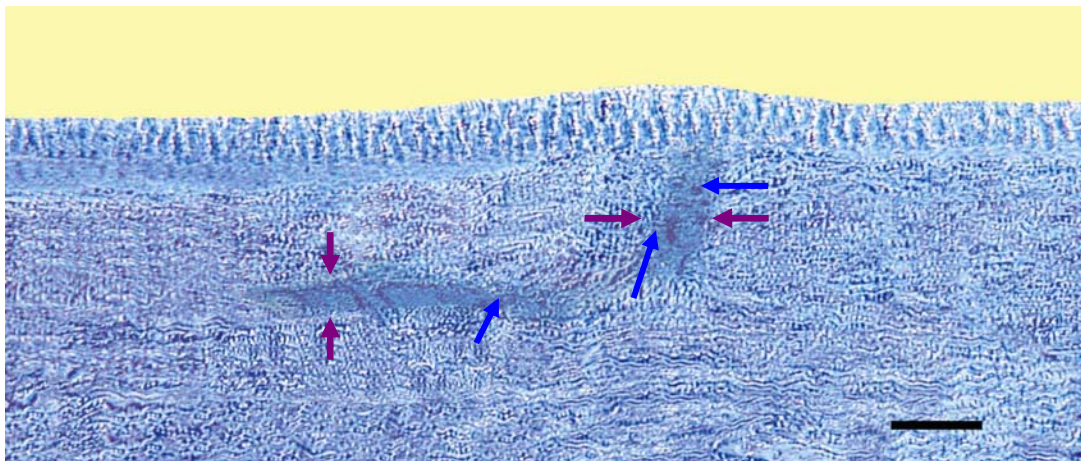


Fig.25_1 Histological observations of a flap at 7th day postoperation. Bar: 35 μ m.

The horizontal interface and perpendicular cut could be still identified with this light microscopic method. The spaces were filled with some migrating cells (blue arrows).

4.3.3 Flap at 16th day postoperation

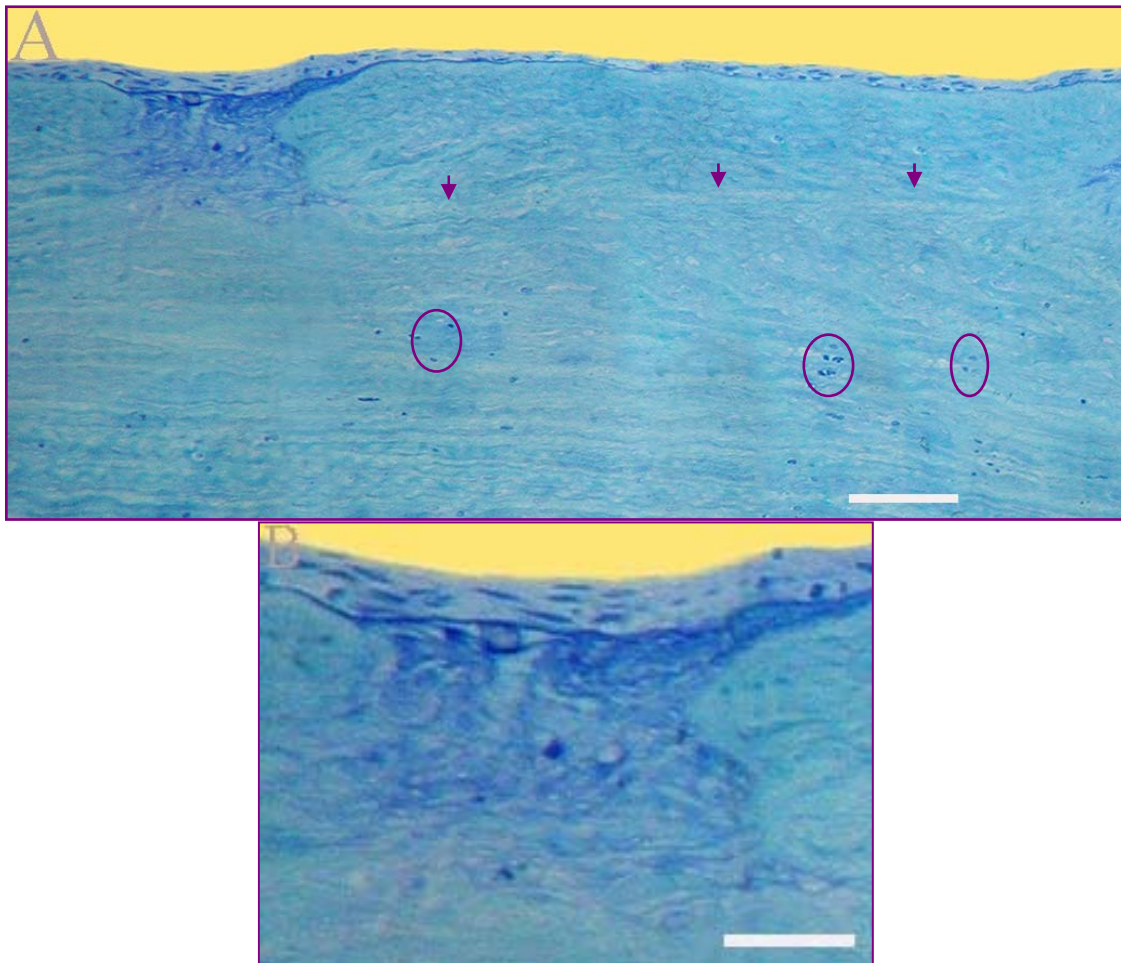


Fig.25_2 Flap at 16th day. **A:** Overview of vertical and horizontal interfaces; **B:** Magnification of the vertical cut depicting the regenerated collagens. Bar: 50 μ m.

In contrast to flap at 7th day, the wound repair in vertical cuts was significant. Collagen regeneration in this interface was just in process. Large amounts of migrating cells could be observed in the surrounding tissue (round). Horizontal interface could be no more observed (arrows mark the vestige of horizontal interface).

4.3.4 Flap at 28th day postoperation

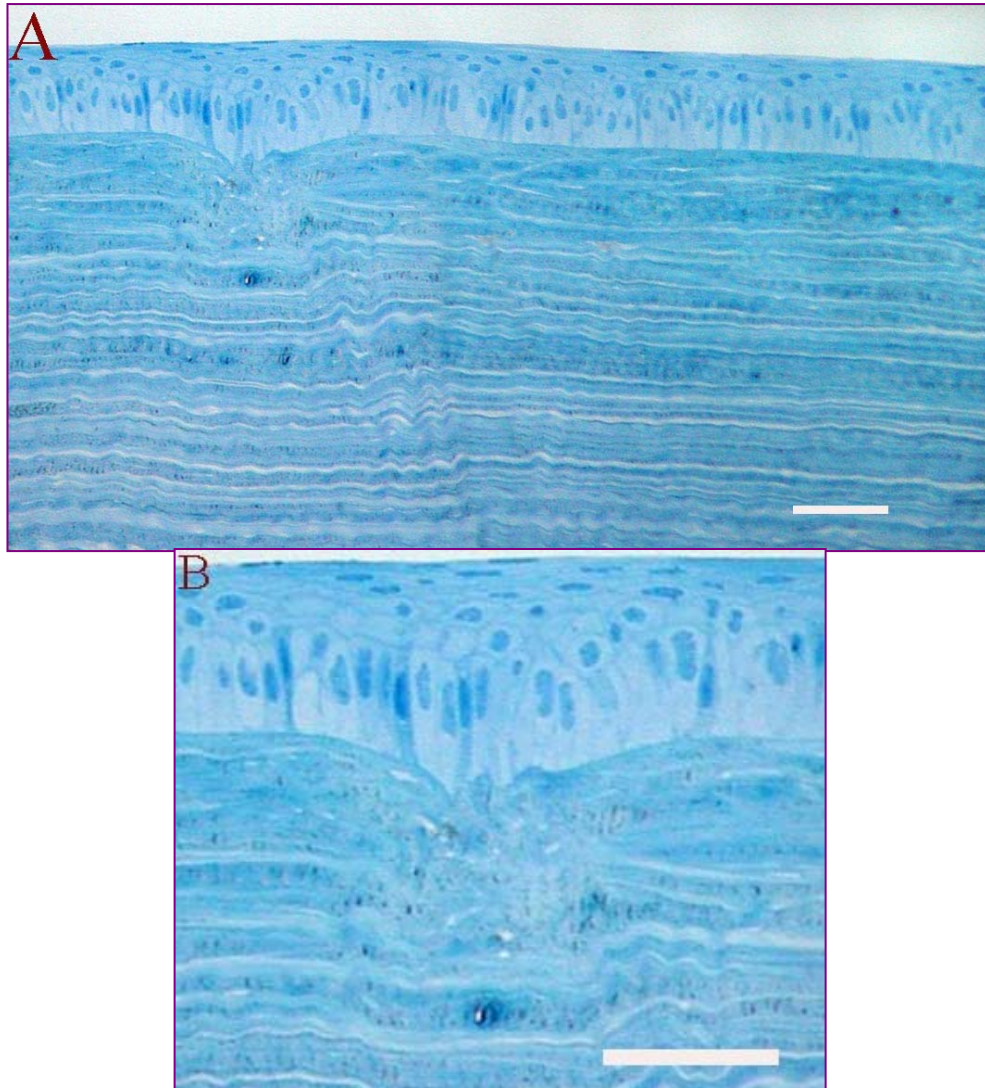


Fig.25_3 Flap at 28th day. **A:** Overview of vertical and horizontal interfaces; **B:** Magnification of the vertical interface. Scale bar: 30 μ m.

Vertical interface was further restored through collagen regeneration. Hyperplasia epithelial plug can be seen. The trace of horizontal cuts can hardly be observed with light microscopy.

4.3.5 Flap at 66th day postoperation

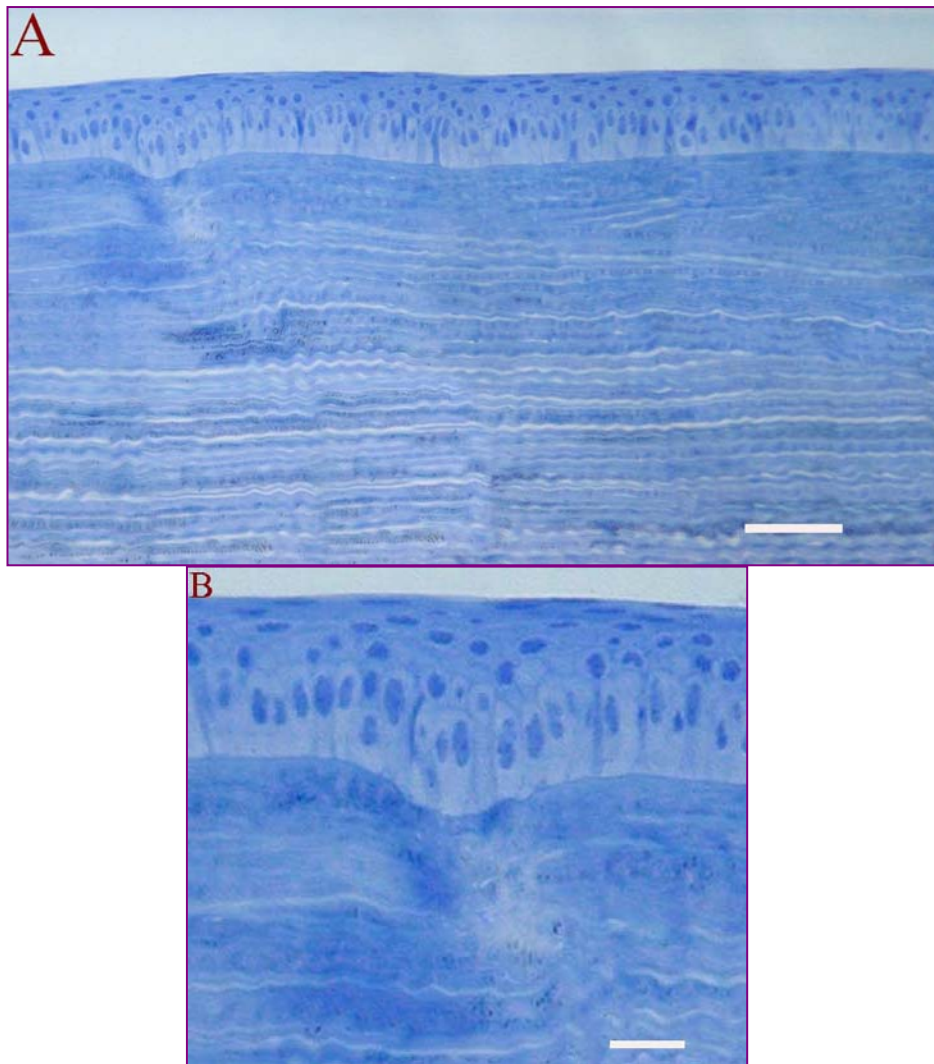


Fig.25_4 Flap at 66th day. **A:** Overview of vertical and horizontal interfaces; **B:** Magnification of vertical cut. Bar: A, 30 μ m; B, 20 μ m.

Compared with Fig.25_3, the epithelial plug reduced and the physiological state of epithelium and stroma restored gradually. However, the site of vertical cut could be still identified due to the confused collagen.

4.3.6 Corneal flap at 90th day postoperation

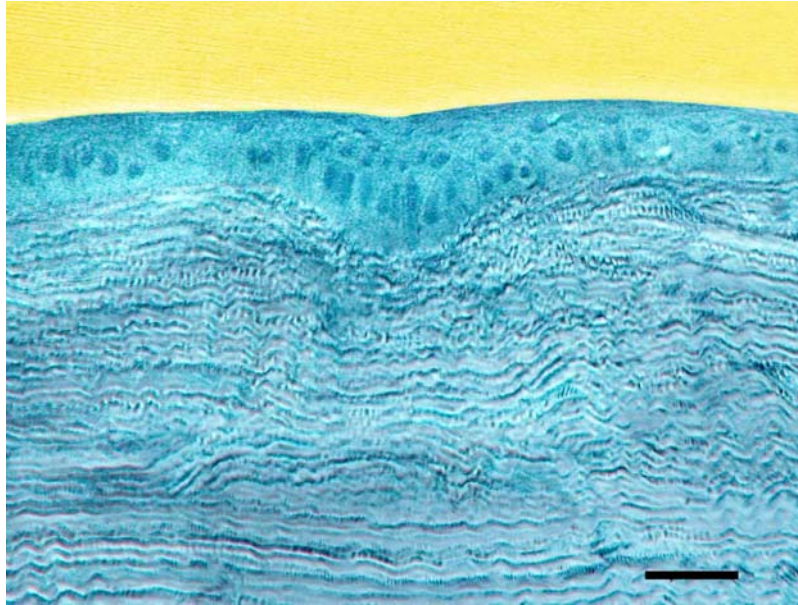


Fig.25_5 Flap at 90th day showing no significant improvement in comparison with Fig.25_4 on 66th day. The epithelial plug could be still seen. Scale bar: 35 μ m.

Summarizedly, the laser-generated horizontal bed can not be identified any more with the histological method from 16th day postoperation. At the vertical cuts, the laser-dissected collagen regenerated gradually and did not still stop at 90th day. Compared with untreated areas, the epithelial layer within this area of laser procedure became 30% thicker, presumably due to the epithelial ingrowths along the vertical cuts.

5. Simultaneous generation of corneal flap and stromal lenticule



Fig.26 Photograph showing simultaneous generation of corneal flap and intrastromal lenticule with porcine eye (Flap with a volume of $1280\mu\text{m} \times 1280\mu\text{m} \times 90\mu\text{m}$; Intrastromal lenticule with a volume of $1280\mu\text{m} \times 1280\mu\text{m} \times 50\mu\text{m}$ in the depth between $90\mu\text{m}$ and $140\mu\text{m}$).

Flap generation with lenticule has been accomplished with separate eye globes. In contrast to flap generation, a middle stage between the bottom and the surface of the flap must be created. By preparation of two intrastromal horizontal incisions, both the flap and the refractive lenticule can be generated in a single-step operation, fully replacing the microkeratome and the excimer laser used in LASIK and IntraLase.

Firstly, a deep intrastromal frame cut is set in order to separate the posterior interface of lenticule. Thereafter, a second scan is performed to determine the anterior interface of lenticule. Finally, third vertical cuts for the three cube walls will be done, allowing the opening of the corneal flap and the extraction of the lenticule. Consequently, a change of the corneal curvature and the refractive power could be achieved (Fig.26).

In details as shown on Fig.26, we focussed the femtosecond laser pulses at a depth of $140\mu\text{m}$ in cornea and performed the bottom in the x-y dimension with full frame scanning of $320\mu\text{m} \times 320\mu\text{m}$. In order to make a bottom with $1280\mu\text{m} \times 1280\mu\text{m}$, the same process was repeated 16 times. Then the vertical cuts in the z-dimension with steps of $2\mu\text{m}$ up to $90\mu\text{m}$ were done. And thereafter the anterior interface of lenticule was generated and finally the vertical cuts with z steps of $2\mu\text{m}$ up to corneal surface

were accomplished. The employed laser parameters correspond to those used for flap generation (4/in-vivo flap generation).

The lifting of flap and extraction of lenticule was performed with a mini-tweezers under a stereomicroscope and finished within 3 minutes. The lenticule was kept in one piece. It is worth mentioned that the intrastromal lenticule was separated with some surgical stress owing to its adherence to the bottom.

6. Observations on cells activation and migration in cornea during wound repair

6.1 Optical nonlinear tomography of activated keratocytes (myofibroblasts) during wound repair after corneal laser surgery.

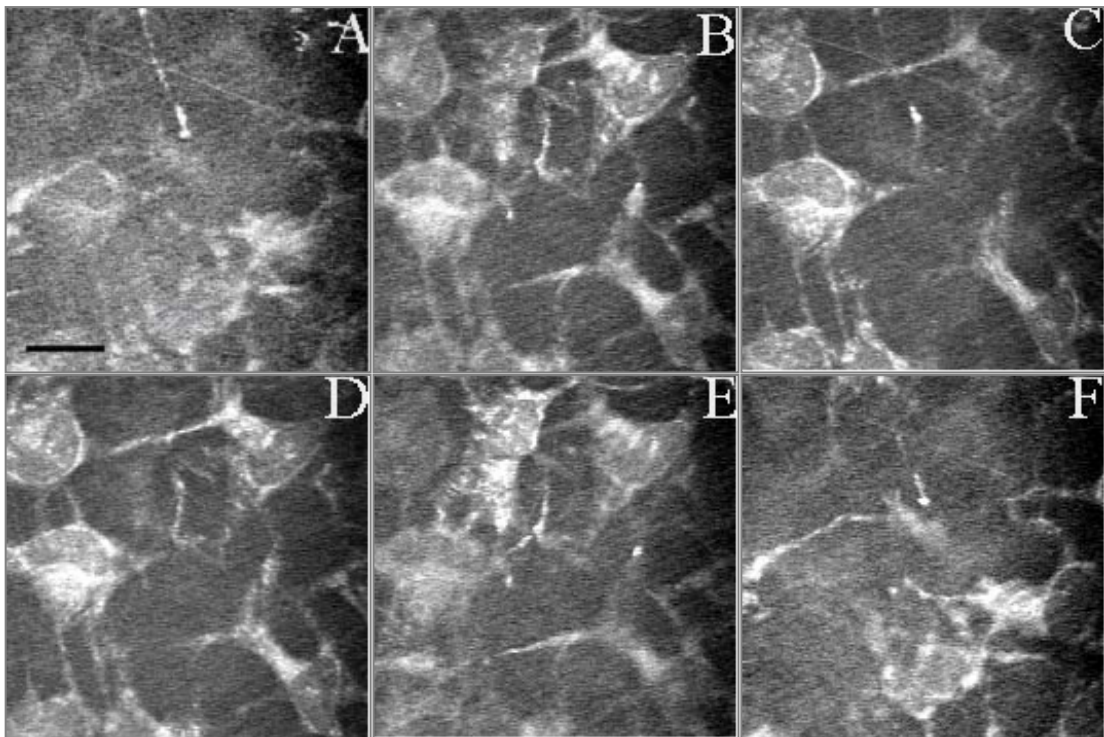


Fig.27 In-vivo cellular nonlinear optical tomography of myofibroblasts based on 2PF at wavelength of 760nm with z-interval of 2 μ m 24 hours after intrastromal surgery. **Fig.A** was taken at depth of 91 μ m. Scale bar: 35 μ m.

The surgery (Fig.27_1) was performed within the cornea at a depth between 90 μ m and 100 μ m with z-steps of 2 μ m using higher laser powers between 150mW (90 μ m) and 165mW (100 μ m) with the line scan. Observed 24 hours after treatment, the luminescence along the cut edges became much weaker than just after the laser-operation. The space between the cuts could be still observed where they were not filled

with the migrating inflammatory cells. The stuffing in cut space implied the migrating inflammatory cells which have been identified with histological section (Fig.24_1, Koenig *et al.* 2005). More interestingly, cell aggregates nearby the cut lines which don't exist in corneal physiological state were detected with this nonlinear imaging technique (Fig.27).

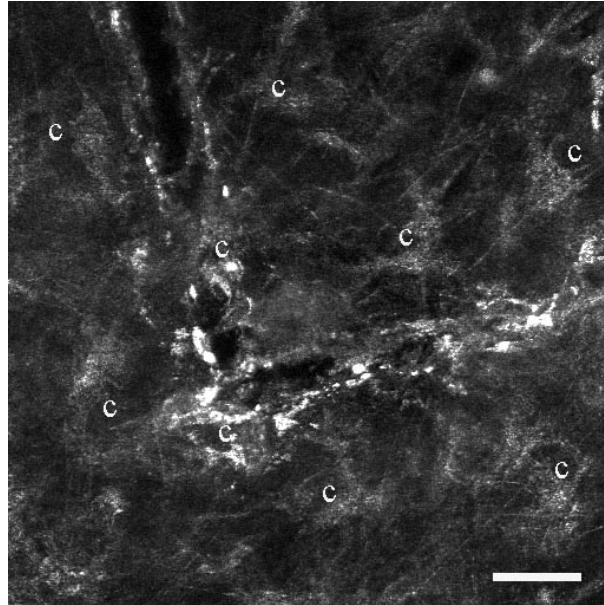


Fig.27_1 In-vivo optical imaging of the treated region 24 hours postoperation. c: activated keratocytes with hypertrophic cell bodies and augmented cell processes. Scale bar: 35 μ m.

As aforementioned, cell aggregates in the surrounding region (within 50 μ m of the lesion sites) were detected in the treated cornea 24 hours postoperation. Based on the cellular morphology of non-fluorescent nuclei round or oval in shape, hypertrophic cell bodies with volume of 25-30 μ m and appearance of cell processes, the cells were most likely activated hypertrophic keratocytes (myofibroblasts). Details and discussion about this observation were described (Wang *et al.* 2005).

6.2 Histological observations: migrating inflammatory cells and discrimination of eosinophils. The three sections stemmed from a same corneal specimen 28 days postoperation.

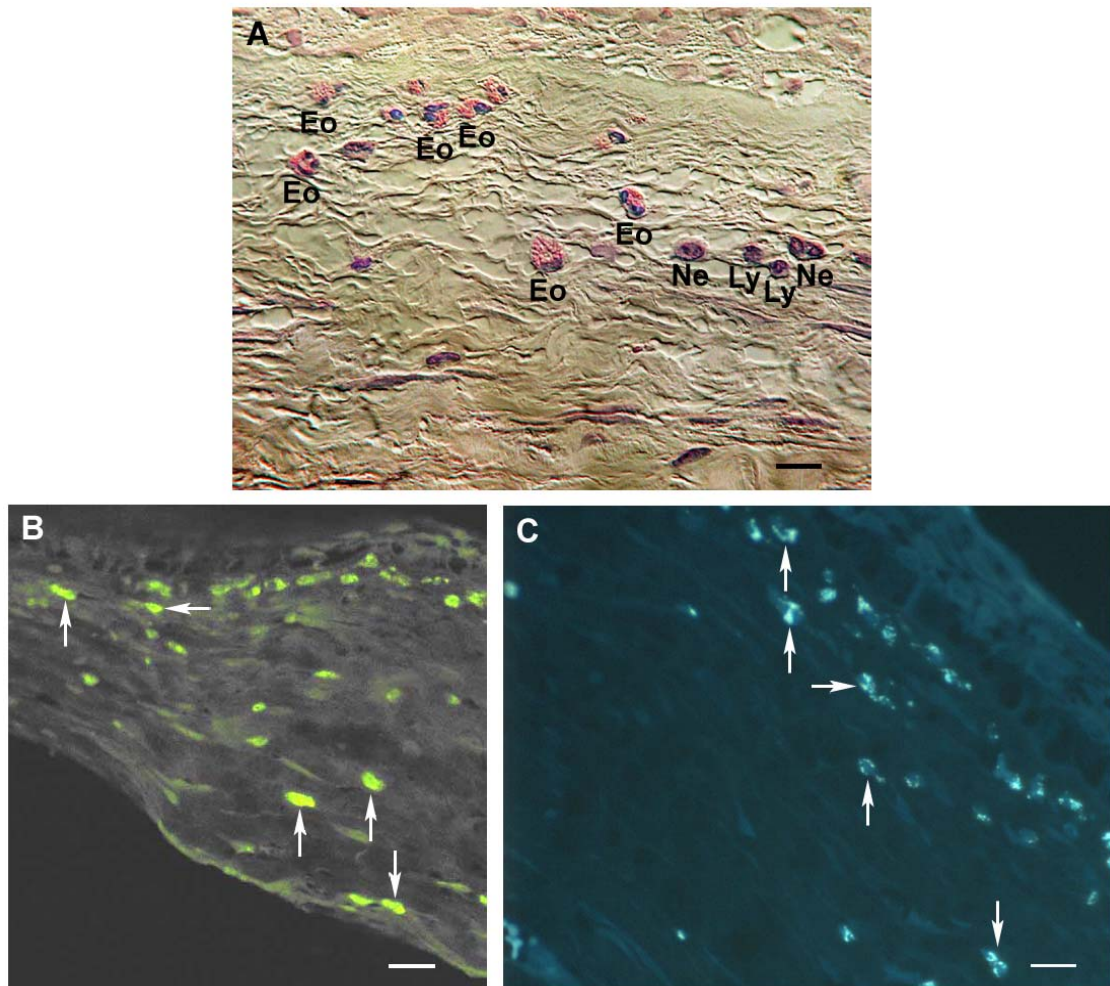


Fig.28 Histological observations on inflammatory cells and discrimination of eosinophils. **A:** Infiltration of inflammatory cells in the treated cornea at 28th day postoperation with haematoxylin-eosin- staining. Eo means eosinophils; Ne means neutrophils; Ly means lymphocytes (100x oil, Epon semi-thin section); **B:** Fluorescence microscopy stained with Eosin Y (pseudo-colour, 63x, LSM 310, excitation at 488nm, 2.5 μ m); **C:** Fluorescence microscopy of eosinophils stained with aniline blue (pseudo-colour, 63x, excitation at UVA, Epon 2.5 μ m section). The marked cells in B and C are some examples of strongly-fluorescent eosinophils. Scale bar: 15 μ m for A, B and C.

Unexpectedly, part of the migrating cells still remained in the treated cornea at 28th day postoperation. Fig.28A shows the semi-thin section stained with conventional HE method and reveals a vast majority of eosinophils, neutrophils and with comparatively fewer lymphocytes and other inflammatory cells.

Here, we tried to differentiate the eosinophils from the other cells such as neutrophils, lymphocytes and other inflammatory cells with eosin Y and aniline blue. Eosin can be excited at wavelength of 488nm and displays the cells with cytoplasmic eosinophilic

granules such as eosinophils (Fig.28B). Aniline blue can selectively stain the cytoplasmic granules in eosinophils (Berretty *et al.* 1978 and McCrone *et al.* 1988). The stained granules can be one-photon excited at a wavelength of UVA (Fig.28C). Using eosin Y and aniline blue, we have successfully confirmed that the migrating cells comprise eosinophils in this study. Eosinophils were also observed on 1st day with aniline blue-staining. The discrimination of other cells is subject to ongoing work with immunocytochemical methods in our group.

Summary

Animal Studies on Cornea Surgery and Multiphoton Microscopy with Nanojoule Femtosecond Near-infrared Laser Pulses

Three sub-theses **(i)** intracorneal multiphoton-mediated optical nanosurgery including flap-free non-invasive intrastromal ablation and flap generation; **(ii)** corneal nonlinear optical histology based on multiphoton microscopy; **(iii)** uses of multiphoton imaging in the femtosecond (fs) laser corneal nanosurgery (nJ) in this work have been studied based on the versatile 80MHz near-infrared (NIR) intense nJ fs lasers emitted from the solid-state Ti: Sapphire laser system with rabbits.

(i) The era of laser refractive surgery with the excimer lasers was heralded by the U.S. Food and Drug Administration's approval (FDA) in 1995. Conventional laser corneal refractive surgery (PRK, LASIK) for visual correction based on the high energy ultraviolet (UV) nanosecond excimer laser pulses is now just being challenged due to its disadvantages such as collateral damage outside the focal volume, UV mutation effects and induction of oxidative stress, and microkeratome-related complications. The NIR fs lasers have recently attracted amount attention due to its advantages such as no photon damage outside the focal femtoliter volume and multiphoton absorption without compromising viability. The nanodissection capability of the nJ fs laser pulses has been here confirmed through the histological outcomes of an intratissue fissure without any detrimental effects on overlying layers in the intratissue ablation procedure as well as corneal flap and intrastromal lenticule in the flap generation procedure. The encouraging surgical advances have potential in the treatment of the visual disorders as well as in the ultra-precise ablation of intratissue neoplasia, nanosurgical applications in the subcellular organelle and in developmental biology.

(ii) Multiphoton microscopy at a high light intensity of MW-GW/cm² based on the simultaneous absorption of more than one photon is one of the most exciting developments in biomedical imaging. So far, the anatomical micro- and nanostructures of corneal tissue have been extensively studied and reported with conventional histological and electron microscopical methods as well as the confocal one-photon laser scanning microscopy (CLSM). Based on the advantages of multiphoton microscopy such as in-vivo selective

displaying of tissue components with subcellular spatial resolution and high contrast, no requirement of cellular and tissue staining or slicing, no out-of-focus photobleaching, improved background discrimination, increased penetration through the biological bulk tissue with NIR light, and no need of pinhole aperture, the excitation of intracellular NAD(P)H/NAD(P)⁺ in the autofluorescence imaging and the SHG imaging of noncentrosymmetric collagen have been used in this work as novel diagnostic tools for in-vivo differentiation of corneal layers, for imaging of corneal cells such as epithelial cells, keratocytes and endothelial cells and collagen lamellas. The activated keratocytes (myofibroblasts) have been here as well detected in the wound repair of intrastromal surgery with this nonlinear optical imaging technique. This multiphoton optical imaging technique has potential to become a powerful means in advancing understanding of corneal biomechanics and even cellular reactions in term of laser lesions.

(iii) The uses of the multiphoton imaging technique has been also proved in this work to be essential for fs nJ cornea surgery such as to determine the surgical interest of region preoperation, to visualize and verify the outcomes of the laser surgery on line.

(Summary in German)

Kornea Laserchirurgie und Multiphoton Mikroskopie mittels Naher-Infrarot Nanojoule Femtosekunden Laser mit Kaninchen

Zusammenfassung

Basierend auf intensiven 80MHz Nanojoule (NJ) NIR-Femtosekunden (fs) Laserpulsen, die von Ti: Sa Lasersystemen ausgestrahlt wurden, wurden in der vorliegenden Arbeit drei Unterthemen mit Kaninchen bearbeitet: **(i)** intrakorneale multiphotonenvermittelte optische Femtosekunden-Nanochirurgie mit dem Ziel der Flap-freien non-invasiven intrastromalen Korneaablacion und der Flaperzeugung; **(ii)** nichtlineare optische Histologie der Kornea abbildet mit der Multiphotonen-Mikroskopie und **(iii)** Applikation des Multiphotonen-Imagings in der Femtosekunden-Nanochirurgie der Kornea.

(i) Die erste Applikation zur refraktiven Chirurgie mit Excimer Lasern zur Behandlung der Seherkrankungen wurde in 1995 durch die amerikanische FDA (Food and Drug Administration) genehmigt. Die konventionelle Laser refraktive Chirurgie wie Photorefraktive Keratektomie (PRK) und Laser In-Situ Keratomileusis (LASIK), die auf Nanosekunden Ultraviolett (UV)-Lasern hoher Energie basiert, besitzt entscheidende Nachteile wie kollaterale Schädigungen außerhalb des fokalen Volumens, UV-bedingte Mutationseffekte, die Verursachung von oxidativem Stress sowie mit Mikrokeratomen in Verbindung stehende Komplikationen. NIR fs Laser haben vor kurzem erhebliche Aufmerksamkeit erregt, da sie im Gegensatz zu UV-Lasern außerhalb des fokalen Volumens kaum Schädigungen verursachen und damit die Zell- und Gewebektivität nicht beeinträchtigen. Die Fähigkeit der NJ fs Laserpulse zur Nanodissektion wird hier durch die histologischen Resultate einer Fissure innerhalb des behandelten Gewebes ohne irgendwelche schädliche Effekte in benachbarten Schichten im Verfahren der intrastromalen Ablacion sowie in der Anfertigung eines Korneaflaps und einer intrastromalen Linse belegt. Diese laserchirurgischen Vorzüge haben ein großes Potential für die Methoden, welche die Korrektur von Sehfeldern zum Inhalt haben, sowie in der ultrapräzisen Entfernung von neoplastischem Gewebe, in nanochirurgischen Anwendungen an subzellulären Organellen und in der Entwicklungsbiologie.

(ii) Die Multiphotonen-Fluoreszenz-Mikroskopie, welche auf der simultanen Absorption von zwei oder mehr Photonen bei einer hohen Lichtintensität von MW-GW/cm² basiert, ist eine der herausragendsten neuen Entwicklungen bei biomedizinischen bildgebenden Verfahren. Bislang sind die Mikro- und Nanostrukturen des Korneagewebes weitgehend mit herkömmlichen Methoden der Histologie und Elektronmikroskopie sowie der konfokalen Laser-Scanning Mikroskop (CLSM) untersucht worden. Dank der Vorzüge der Multiphotonen-Mikroskopie wie der selektiven *in-vivo* Darstellung von Gewebestandteilen mit subzellulärer räumlicher Auflösung und hohem Kontrast ohne vorangehendes Anfärben und Schneiden des Präparates, kein Photobleaching außerhalb des Fokuses, dem hohen Signal/Hintergrund Verhältnis, der hohen Eindringtiefe von NIR-Licht in Gewebe und die Nutzung endogener intrazellulärer Fluorophore wie vor allem NAD(P)H/NAD(P)⁺ beim Autofluoreszenz Imaging machen in dieser Arbeit die Multiphotonenmikroskopie zu einem neuartigen Diagnosewerkzeug für die *in-vivo* Differenzierung von Korneaschichten, für die dreidimensionale optische Darstellung von Korneazellen wie Epithelzellen, Keratozyten und Endothelzellen sowie der Kollagenlamellen. Außerdem konnten aktivierte Keratozyten (Myofibroblasten) im Zusammenhang mit der Wundreparatur bei der intrastromalen Laseroperation mittels dieser nichtlinear optischen Mikroskopie detektiert werden.

(iii) Die Multiphotonenmikroskopie stellt somit ein leistungsfähiges Instrument beim vorrückenden Verständnis von 3-D Raumanalytik der Kornea und sogar von zellulären Reaktionen bei Laserläsion des Gewebes dar. Diese Imagingtechnologie ist auch, wie in dieser Arbeit bewiesen werden konnte, ein leistungsfähiges Hilfswerkzeug für die Femtosekunden-Nanochirurgie der Hornhaut wie die vor Ort Bestimmung des Operationsfeldes im Gewebe vor einer Operation, und abschließend dann die Resultate der Laserchirurgie online zu visualisieren und zu überprüfen.